

Graphene Quantum Dots as Imaging, Sensing, and Targeted Delivery Platform for Cancer  
Therapeutics

by

Elizabeth Campbell

Bachelor of Science in Physics May 2014

University of Dallas

Irving, Texas

Master of Science in Physics December 2018

Texas Christian University

Fort Worth, Texas

Submitted to the Graduate Faculty of the

College of Science and Engineering

Texas Christian University

in partial fulfillment of the requirements

for the degree of

Doctor of Philosophy

June 2021



## ACKNOWLEDGEMENTS

*I would like to first express my sincere gratitude to my advisor Dr. Anton V. Naumov for his guidance, support, and knowledge during my time at TCU. His patience, continued encouragement, and mentorship have helped me tackle any obstacle necessary to accomplish my research to date. I am also deeply grateful to Dr. Giridhar Akkaraju for teaching me how to work with cells, providing me with a deeper understanding of the biology behind this work, and guiding me to resources that helped develop this research. I would also like to thank Dr. Zygmunt (Karol) Gryczynski and Dr. Hana Dobrovolny for their time, suggestions, and advice to successfully complete this research and write this thesis. I have learned so much from each of my committee members and am a better researcher because of their guidance. I would also like to thank Md Tanvir Hasan and Roberto Gonzalez-Rodriguez for their support and patience as I learned so much from both during my time at TCU.*

*I am also thankful to all other staff, faculty members, and graduate students from the Department of Physics and Astronomy for all assistance and advice I asked of them. The support I received from this department has allowed me to be successful throughout the past five years, and I will be forever grateful for their willingness to help/work with me.*

*Lastly, I am beyond thankful to my mother, sisters, friends, my husband Trent and my daughters, Olivia and Violet, for their unending support and encouragement to pursue my education at TCU. Without you all, I certainly would not be where I am today.*

## Table of Contents

<b>ACKNOWLEDGEMENTS</b> .....	ii
<b>List of Figures</b> .....	v
<b>List of Tables</b> .....	x
<b>List of Abbreviations</b> .....	xi
<b>Chapter 1- Motivation</b> .....	1
<b>Significance/Merit</b> .....	1
<b>Impact</b> .....	3
<b>Questions to be Answered</b> .....	5
<b>Literature Review/Background Study</b> .....	6
<b>Cancer</b> .....	6
<b>Fluorescence</b> .....	7
<b>Graphene</b> .....	8
<b>Graphene Oxide</b> .....	9
<b>Graphene Quantum Dots</b> .....	10
<b>Introduction</b> .....	11
<b>Chapter 2- Experimental Methods and Procedures</b> .....	20
<b>Synthesis/Sample Prep</b> .....	20
<b>Optical Measurements and Characterization</b> .....	20
<b>Cell culture</b> .....	20
<b>MTT cytotoxicity assays</b> .....	21
<b>Imaging</b> .....	21
<b>Imaging Analysis</b> .....	22
<b>Synthesis of treatment formulation (Fc-GQD-HA)</b> .....	22
<b>Physical and Optical Characterization</b> .....	25
<b>Fluorescence Microscopy Measurements</b> .....	26
<b>Cell culture</b> .....	27
<b>Cellular Measurements of Oxidative Stress</b> .....	28
<b>Chapter 3- Are graphene quantum dots suitable for biomedical applications?</b> .....	30
<b>Results and Discussion</b> .....	30
<b>Size characterization/degradation</b> .....	30
<b>Absorbance</b> .....	34

Fluorescence .....	34
Cytotoxicity .....	36
Summary .....	39
<b>Chapter 4- Can Graphene Quantum Dots be used for imaging and delivery?.....</b>	<b>40</b>
<b>Results and Discussion .....</b>	<b>40</b>
<b>Internalization .....</b>	<b>40</b>
<b>Summary .....</b>	<b>50</b>
<b>Chapter 5- Do GQDs offer sensing capabilities? .....</b>	<b>52</b>
<b>Overview .....</b>	<b>52</b>
<b>Chapter 6- Can GQDs be used to create a targeted cancer treatment formulation suitable for biomedical applications?.....</b>	<b>60</b>
<b>Overview .....</b>	<b>60</b>
<b>Results and Discussion .....</b>	<b>61</b>
<b>Characterization .....</b>	<b>61</b>
<b>Summary .....</b>	<b>67</b>
<b>Chapter 7- Can the treatment formulation be used for imaging and delivery? .....</b>	<b>69</b>
<b>Results and Discussion .....</b>	<b>69</b>
<b>Fluorescence .....</b>	<b>69</b>
<b>Internalization.....</b>	<b>71</b>
<b>Summary .....</b>	<b>73</b>
<b>Chapter 8- Does the treatment formulation offer sensing capabilities? .....</b>	<b>74</b>
<b>Results and Discussion .....</b>	<b>74</b>
<b>Summary .....</b>	<b>75</b>
<b>Chapter 9- How does developing combined imaging/targeting/treatment formulation affect treatment efficacy and targeted accumulation? .....</b>	<b>76</b>
<b>Results and Discussion .....</b>	<b>76</b>
<b>Cytotoxicity .....</b>	<b>76</b>
<b>Summary .....</b>	<b>83</b>
<b>Chapter 10 Conclusions.....</b>	<b>85</b>
<b>Questions Answered.....</b>	<b>87</b>
<b>Future Works.....</b>	<b>90</b>
<b>References .....</b>	<b>92</b>

## List of Figures

FIGURE 1. SYNTHESIS DIAGRAM FOR THE PREPARATION OF THE FC-HA-GQD FORMULATION.	25
FIGURE 2. (A) TEM IMAGE SHOWING CRYSTALLINITY OF GQDS AND DISCERNABLE LATTICE DOMAIN STRUCTURE. (B) AND (C) TEM IMAGES OF N-GQDS AT VARYING MAGNIFICATIONS .....	31
FIGURE 3. AFM OF NITROGEN-DOPED GRAPHENE QUANTUM DOTS. MEAN HEIGHT= 1.82 NM..	32
FIGURE 4. FTIR SPECTRA OF N-GQDS, NS-GQDS, AND BN-GQDS. ....	33
FIGURE 5: ABSORBANCE SPECTRUM OF N-GQDS. ....	34
FIGURE 6. NORMALIZED FLUORESCENCE EMISSION SPECTRA IN THE VISIBLE (WITH 375 NM EXCITATION) AND NIR (WITH 700 NM EXCITATION) FOR N-GQDS (A), NS-GQDS (C), AND BN-GQDS (E) ALL MEASURED IN AQUEOUS DISPERSIONS AT pH ~7. MODEL STRUCTURES OF A SINGLE LAYER OF THE CORRESPONDING GQDS: N-GQDS (B), NS-GQDS (D), AND BN-GQDS (F). ....	35
FIGURE 7. TEM IMAGES OF N-GQDS FOR INCUBATED TIMES IN CELL MEDIA OF HEK-293 CELLS. SCALE BAR IS 5 NM. ....	37
FIGURE 8. CYTOTOXICITY OF BN-GQDS (BLACK), NS-GQDS (BLUE), AND N-GQDS (RED) IN HELA CELLS SHOWING PERCENT CELL VIABILITY WITH RESPECT TO THE GQD CONCENTRATION. ....	38
FIGURE 9. (A-E)-TEM IMAGES OF N-GQDS IN HELA CELL CULTURE AT VARYING TIMES WITH THE CORRESPONDING FFT IMAGE ANALYSIS, INDICATING THE CRYSTALLINITY OF THE STRUCTURE EXPOSED TO CELL MEDIA AT DIFFERENT TIMES; F- AVERAGE DIAMETER OF N- GQDS WITH RESPECT TO TIME, ANALYZED USING TEM IMAGES AT VARYING TIMES FOR	

OVER 100 N-GQDs IN HeLA CELL CULTURE, INDICATING DEGRADATION OF QUANTUM DOTS. ....	41
FIGURE 10. FLUORESCENCE MICROSCOPY. (A) OVERLAY OF GQD EMISSION WITH THE BRIGHT FIELD IMAGE OF HeLA CELLS TRANSFECTED WITH GQDs. (B)(C) – FLUORESCENCE AND BRIGHT FIELD IMAGES OF NON-TREATMENT CONTROL HeLA CELLS. ....	42
FIGURE 11. A) CELL INTERNALIZATION/EXCRETION TIMELINE ASSESSED THROUGH THE NORMALIZED GQD EMISSION INTENSITY PER UNIT AREA IN HeLA CELLS AT DIFFERENT TIME POINTS FOR N-GQDs (RED), NS-GQDs (BLUE), AND BN-GQDs (BLACK). ERROR BARS FOR SOME POINTS ARE WITHIN THEIR SIZE. B) FLUORESCENCE EMISSION OF VARIOUS QUANTUM DOT TYPES IN HeLA CELLS AT A NUMBER OF TREATMENT TIME POINTS. EXCITATION AND EMISSION FILTERS USED: $475\pm 25$ NM AND $535\pm 20$ NM. SCALE BAR= $10\mu\text{M}$ . ....	44
FIGURE 12: COLOCALIZATION IMAGE MATRIX SHOWING GQD LOCATION WITHIN THE CELLS FOR VARIOUS GQD TYPES AND FLUORESCENT STAINING. RED: LYSOTRACKER RED, EXCITATION AT 540 NM EMISSION RECORDED AT 600 NM; BLUE: DAPI, EXCITATION AT 375 NM EMISSION RECORDED AT 450 NM; GREEN: GQDs, EXCITATION AT 475 NM EMISSION RECORDED AT 535 NM. ....	45
FIGURE 13. FLUORESCENCE COLOCALIZATION IMAGES OF (A) N-GQDs, (B) NS-GQDs, AND (C) BN-GQDs EMISSION (GREEN) WITH DAPI (BLUE) AND LYSOTRACKER RED (RED) STAINING WITHIN HeLA CELLS. CONFOCAL COLOCALIZATION IMAGES OF (D) N-GQDs (SCALE BAR= $10\mu\text{M}$ ), (E) NS-GQDs (SCALE BAR= $10\mu\text{M}$ ), AND (F) BN-GQDs (SCALE BAR= $10\mu\text{M}$ ). ....	46
FIGURE 14: CONFOCAL OVERLAY IMAGE MATRIX INDICATING LOCALIZATION IN THE LYSOSOMES AND SOME IN THE NUCLEUS; TEXAS RED EXC.....	47

FIGURE 15: MICROSCOPY VIDEO OF GQDS FOR 420 SECONDS, SHOWING NO PHOTOBLEACHING DURING THAT TIME. IMAGED WITH 450 NM EXCITATION AND 535 NM EMISSION.....	48
FIGURE 16. MULTICOLOR IMAGING OF N-GQDS, NS-GQDS, AND BN-GQDS IN BLUE, GREEN, AND NEAR-IR. EXCITATION AND EMISSION FILTERS USED ARE BLUE- EXC: $375 \pm 14$ NM EM: $450 \pm 20$ NM; GREEN- EXC: $475 \pm 25$ NM EM: $535 \pm 20$ NM; NEAR-IR- EXC: $650 \pm 20$ NM EM: $750 \pm 20$ NM. ....	49
FIGURE 17. FLUORESCENCE SPECTRA OF N-GQDS AT VARYING PH LEVELS IN THE (A) VISIBLE AND (B) NIR AND NS-GQDS IN THE (C) VISIBLE AND (D) NIR. ....	53
FIGURE 18: IMAGES OF N-GQDS AT VARYING PH LEVELS. BLUE IMAGED WITH EXCITATION 375 NM, EMISSION AT 450 NM. GREEN IMAGED WITH EXCITATION 475 NM, EMISSION AT 535 NM. ....	54
FIGURE 19 (A) TEM IMAGE OF FC-GQD-HA FORMULATION (RED OUTLINE IS TO SERVE AS A GUIDE TO AN EYE) WITH (B) CORRESPONDING FFT ANALYSIS, VERIFYING THE CRYSTALLINE STRUCTURE AND THE GRAPHENE LATTICE OF THE QUANTUM DOTS. SCALE BAR = 5 NM. (C) PROPOSED CONNECTIVITY OF THE FC-GQD-HA FORMULATION. ....	62
FIGURE 20. TEM IMAGES OF SYNTHESIZED FC-GQD-HA FORMULATION. ....	63
FIGURE 21. TEM IMAGES OF FC-GQD-HA HYBRIDS WITH CORRESPONDING FFT ANALYSIS TO CONFIRM CRYSTALLINITY. ....	64
FIGURE 22. EDX MAPPING OF FC-GQD-HA AGGLOMERATES ON THE TEM GRID. ....	65
FIGURE 23. (A) TEM IMAGE OF FC-GQD-HA AGGLOMERATE. EDX ELEMENTAL MAPS OF THE SAME AREA FOR (B) CARBON, (C) OXYGEN, (D) CHLORINE, AND (E) IRON WITH THEIR AVERAGED ATOMIC WEIGHT PERCENTAGES LISTED IN THE TABLE.....	66
FIGURE 24. FTIR SPECTRA OF (A) PRISTINE N-GQDS AND (B) FREEZE-DRIED FC-GQD-HA FORMULATION. ....	67



FIGURE 25. (A) FLUORESCENCE SPECTRUM OF FC-GQD-HA FORMULATION (BLACK) AND PURIFIED N-GQDS (RED) IN THE VISIBLE WITH EXCITATION AT 400 NM, MEASURED IN AQUEOUS SUSPENSION; (B) ABSORBANCE SPECTRA OF FC-GQD-HA FORMULATION (BLACK) AND PRISTINE N-GQDS (RED)..... 69

FIGURE 26. NORMALIZED PEAK FLUORESCENCE AT 450 NM WITH 350 NM EXCITATION OF FC-HA-GQD FORMULATION IN BLOOD SERUM (BLUE), COMPLETE MEDIUM (ORANGE), AND HE LA CELL MEDIUM (GRAY) AT 1, 6, 12, 24, AND 48-HOUR TIMEPOINTS INDICATING FORMULATION STABILITY. .... 70

FIGURE 27. 3D FLUORESCENCE IMAGES OF FC-GQD-HAS IN HE LA CELLS BUILT BY Z-STACK ACCUMULATION OF CONFOCAL MICROSCOPY IMAGES OF GQD EMISSION AT DIFFERENT PLANES WITHIN THE CELLS COLLECTED WITH 480 NM EXCITATION AND 535 NM EMISSION. RIGHT AND LEFT IMAGES ARE RENDERED AT DIFFERENT ANGLES OF OBSERVATION. .... 71

FIGURE 28. FLUORESCENCE EMISSION OF 1 MG/ML OF THE FC-GQD-HA FORMULATION IN HE LA CELLS AND HEK-293 CELLS AT 1, 4, 12, 24, 48-HOUR TREATMENT TIME POINTS. 475  $\pm$  25 NM EXCITATION AND 535  $\pm$  20 NM EMISSION FILTERS USED. SCALE BAR = 20  $\mu$ M..... 72

FIGURE 29. NIR FLUORESCENCE SPECTRA OF FC-GQD-HA FORMULATION ..... 74

FIGURE 30. FLUORESCENCE SPECTRA OF FC-GQD-HA TREATMENT FORMULATION AT VARYING PH LEVELS. .... 75

FIGURE 31. CYTOTOXICITY OF FERROCENE IN MCF7 CELLS AND HEK-293 CELLS..... 78

FIGURE 32. FLUORESCENCE COLOCALIZATION IMAGES OF HE LA AND HEK-293 CELLS STAINED WITH DAPI (BLUE), LYSOTRACKER RED (RED) AND INTRODUCED TO FC-GQD-HAS (GREEN) FOR 12 H. .... 79

FIGURE 33. (A) MTT ASSAY FOR THE CYTOTOXICITY OF FC-GQD-HA FORMULATION AT VARYING CONCENTRATIONS IN HE LA (RED) AND HEK-293 (BLUE) CELLS. (B) MTT CELL

VIABILITY ASSAY OVER A PROLONGED TIMELINE. FC-GQD-HA FORMULATION IN HEK-293 CELLS (RED) AND HE LA CELLS (YELLOW) COMPARED TO FC-HA IN HEK-293 CELLS (GREEN) AND HE LA CELLS (BLUE). INTRODUCED AT A CONCENTRATION OF 1 MG/ML..... 80

FIGURE 34. DCFH-DA ASSAY OF FC-GQD-HA FORMULATION (GREY) AS COMPARED TO FERROCENE (ORANGE) AND N-GQDs (BLUE) IN HE LA CELLS..... 82

FIGURE 35. CELL INTERNALIZATION/EXCRETION TIMELINE ASSESSED THROUGH THE NORMALIZED INTRACELLULAR FC-GQD-HA EMISSION INTENSITY PER UNIT AREA IN HE LA (BLUE) AND HEK-293 (ORANGE) CELLS AT DIFFERENT TIME POINTS. ERROR BARS FOR SOME POINTS ARE WITHIN THEIR SIZE..... 83

## List of Tables

TABLE 1. N-GQD INTRACELLULAR AND EXTRACELLULAR GREEN/BLUE EMISSION INTENSITY RATIOS ACROSS HEALTHY (HEK-293) VERSUS CANCER (HELA AND MCF-7) CELL LINES, AND CORRESPONDING FLUORESCENCE IMAGES DEMONSTRATING EMISSION DIFFERENCES. SCALE BAR= 10 $\mu$ M. ....	56
TABLE 2. NS-GQD INTRACELLULAR AND EXTRACELLULAR GREEN/BLUE INTENSITY RATIOS ACROSS HEALTHY (HEK-293) VERSUS CANCER (HELA AND MCF-7) CELL LINES, AND CORRESPONDING FLUORESCENCE IMAGES DEMONSTRATING EMISSION DIFFERENCES. SCALE BAR= 10 $\mu$ M. ....	58

## **List of Abbreviations**

GO – Graphene oxide

GQD – Graphene quantum dot

N-GQD – Nitrogen doped graphene quantum dot

NS-GQD – Sulfur doped graphene quantum dot

BN-GQD – Boron-nitrogen doped graphene quantum dot

NIR – Near-infrared

AFM – Atomic force microscopy

SEM – Scanning electron microscopy

TEM- Transmission electron microscopy

FFT- Fast Fourier transform

CTCF – Corrected total cell fluorescence

Fc-Ferrocene

HA- Hyaluronic acid

ROS- Reactive oxygen species

EPR- Enhanced permeability and retention

## Chapter 1- Motivation

### Significance/Merit

Cancer remains a serious threat, considering that nearly 40% of men and women will be diagnosed in their lifetimes<sup>1</sup>. While existing therapies such as radiation, chemotherapy, and surgery can be successful<sup>2</sup>, they often affect both healthy and cancer cells, which is detrimental to a patients' health. Current cancer therapies are not deterministic and offer little to no information about the treatment pathways. Thus, more effective therapies that can improve cancer survival rates, detect cancer, and explain treatment pathways are desired. Nanomaterials are on the forefront of being utilized for biomedical applications, including their use in treatment and detection of cancer<sup>3</sup>, central nervous system (CNS) diseases<sup>4</sup>, sickle cell<sup>5</sup>, and autoimmune disorders<sup>6</sup>. Treatment of CNS diseases such as Parkinson disease and Alzheimer disease has also been improved via the use of nanoparticles<sup>4</sup>. Nanomaterials provide a platform that can be altered to address specific needs of the disease itself. Nanoparticles, for example, can be integrated into a system to either suppress or stimulate desired traits<sup>6</sup>, such as antitumor effects or treatment of inflammatory disorders. They can also help trace the treatment inside cancer cells in the visible and near-infrared (NIR) *in vitro* and *in vivo*<sup>7</sup> and be used for targeted delivery<sup>8</sup>.

The power of nanotechnology-based systems lies in their multi-functionality, offering both drug delivery and detection capabilities. The potential to perform multiple functions using one agent is the attractive force driving the integration of molecular therapeutics with nanomaterials-based drug or gene delivery vehicle systems. Although such nanoformulations significantly improve the capabilities of conventional therapeutics, there is still a challenge to expand the options for image and sensing guided therapy and improve targeting to multiple cancer types. Currently, no platform can carry out imaging, sensing, and delivery concurrently.

These gaps in functionality limit the capabilities of novel molecular therapeutics and restrict their utilization in cancer treatment. Nanomaterials possessing a number of exceptional properties are expected to fill this gap. One of such novel materials is graphene and its derivatives such as graphene oxide or graphene quantum dots.

Graphene oxide possesses unique properties that make it attractive for biomedical applications. It is water soluble, provides a large platform with a variety of addends for convenient functionalization-based drug attachment, and exhibits fluorescence in visible/near-infrared<sup>9</sup>. Nanoscale graphene oxide has already been adopted for the delivery of anticancer drugs into biological cells<sup>9-12</sup> aptamers for ATP probing in mouse epithelial cells, and protection and delivery of DNA for therapy<sup>13-15</sup>. For such applications, however, GO was modified and has only been utilized as a delivery agent or rarely as a fluorescent marker<sup>11, 16</sup> requiring either incorporation of external fluorophores<sup>17, 18</sup> and/or complementary covalent functionalization<sup>19</sup> with PEG for successful delivery. Additionally, many GO forms used in bio-applications fluoresce in the visible<sup>13, 20</sup>, which can be optimal for *in vitro* work but not for *in vivo* studies where near-IR emission in the water window is desired for deep autofluorescence-free tissue penetration. These complexities hamper the use of GO in biomedical applications.

Graphene quantum dots also have a variety of attributes that can be beneficial for biomedical applications. GQDs have desirable optical properties such as high quantum yield<sup>21</sup>, stability against photobleaching<sup>22</sup>, and some exhibit emission in the near-IR<sup>23</sup>. The current dilemma, however, is optimizing each of these desirable properties concurrently, such that quantum dots can be effectively imaged *in vitro* and *in vivo*<sup>24</sup>. The present study fills this gap by exploring the properties of novel GQDs developed in our laboratory as standalone multifunctional agents for imaging in red/near-IR, cellular internalization, and biosensing.

Cancer drug and gene therapeutics are currently lacking a multi-modal agent that can image, sense, and deliver therapies simultaneously. The **significant contribution** of this project is the development of several novel nanomaterials-based multifunctional formulations utilizing remarkable properties of GQDs to perform all the essential therapeutic functions: targeted delivery, imaging, and cancer sensing. Quantum dots can be made using fully biocompatible materials, while still maintaining desired properties such as considerably high quantum yield and stability across a large pH range<sup>25</sup>. They can be applied to a variety of biological applications, including disease detection, protein tracking, and intracellular reporting<sup>25, 26</sup>. In this project, I intend to use nitrogen-based graphene quantum dots (NQDs), sulfur-based graphene quantum dots, (SQDs) and boron-nitrate-based graphene quantum dots (BNQDs), as multifunctional imaging, sensing and delivery agents. The capabilities of the aforementioned nanomaterials will be assessed via cytotoxicity assays, imaging, cell analysis, and animal studies. I also intend to explore variations of these nanomaterials, including but not limited to quantum dots doped with rare earth metals due to their fluorescence in the near- IR range that can penetrate through layers of biological tissue.

### **Impact**

Currently, there are no multimodal agents that can be used as a delivery, imaging, and sensing moieties for applications in cancer therapeutics. There is an active development of nanoformulations possessing multifunctional properties approaching that ultimate goal and intended for drug transport and imaging<sup>27-29</sup> with, however, only a few having concomitant sensing capacity<sup>30, 31</sup>. I hypothesize that the properties of graphene quantum dots can be optimized and ultimately used for imaging, sensing, and delivery of individual cancer therapeutics and combination drug/gene delivery all together. The adaptability and variability

of medical conditions such as cancer requires both detection and treatment which can only be accomplished by such multimodal approach.

To provide impact on cancer therapeutics two areas; detection and treatment must be addressed in our work. Cancer detection is critical for effective therapeutics as it would allow for early treatment, development of the most effective therapeutic plans for patients, as well as for the opportunity to advance cancer research<sup>32-34</sup>. The development of new therapeutics is important and timely: current therapeutics can be quite toxic and detrimental to the patients offering no information about the pathways of the cancer therapies or the presence of the cancer sites. There are several advantages of the GQDs that we will impactfully utilize in this work to address both cancer treatment and detection: GQDs can be functionalized with molecular chemotherapy drugs in a variety of covalent and non-covalent approaches<sup>35</sup>, exhibit pH-dependent fluorescence in the red/near-IR<sup>36</sup> spectral region with reduced biological autofluorescence background, can even facilitate cell proliferation<sup>37</sup> and are suitable for photoluminescence sensing applications<sup>38</sup>. Thus, GQDs may offer a multifunctional alternative to improving cancer therapy and diagnostics.

The need to perform several therapeutic functions is imperative to successful drug development. The effective formulation must be accumulated in tumors following systemic administration, should exhibit anticancer effect, and at the same time provide no off-target toxicity or adverse immune response. At best, such formulation should also allow for imaging the location of the drug and sensing of cancerous environments to ensure accumulation in the tumor and possibly predict metastasized sites. Therefore, a new, more effective anticancer formulation than those existing currently should be developed to meet the needs of cancer therapeutics. A delivery platform (GQDs) will amplify the anticancer toxicity of the anticancer/gene delivery therapeutic by concentrating the amount delivered in cells and



provide fluorescence-based imaging of its delivery pathways and pH sensing of cancer environments. The intrinsic fluorescence response of such platforms makes them highly advantageous as imaging agents.

In the present GQD platform, fluorescence emission will be used to image the delivery pathways of the known redox cancer therapeutic and will be focused in cancer cells via the attached targeting agent. The multimodality of such therapeutic system, providing a unique opportunity for treating, detecting, and imaging several types of cancer is, therefore, expected to have a high impact on the advancement of multimodal treatment approaches and, therefore, on the field of cancer therapeutics in general. The approach is innovative as it utilizes unique properties of graphene quantum dots which are not yet used for the advantage of cancer therapeutics in order to simultaneously address multiple theranostic functions as opposed to conventional single-function therapies.

### **Questions to be Answered**

1. Are graphene quantum dots suitable for biomedical applications?
2. Can these nanomaterials be used for imaging and delivery?
3. Do they offer sensing capabilities?
4. Can these nanomaterials be used to create a targeted cancer treatment formulation?
5. Is the targeted cancer treatment formulation suitable for biomedical applications?
6. Can the targeted cancer treatment formulation be used for imaging and delivery?
7. Does the targeted cancer treatment formulation offer sensing capabilities?
8. How does developing combined imaging/targeting/treatment formulation affect treatment efficacy and targeted accumulation?

## **Literature Review/Background Study**

### **Cancer.**

Cancer is a group of diseases involving abnormal cell growth with the potential to spread. Understanding what leads to this abnormal growth can help the development of more effective therapies for the many different types of cancer. It is important to first understand that individual cells serve as the foundational components of tissue and organ structure and are both autonomous and versatile<sup>39</sup>. These individual cells, for the most part, contain a complete organismic genome which includes more information than any individual cell will ever need<sup>39</sup>. This allows for cellular maintenance throughout the lifetime of the organism. Unfortunately, however, this also allows for the possibility that cells may be able to obtain critical information within their genomes that they would typically not have access to and thus, assume roles that are detrimental to normal tissue activity<sup>39</sup>. Unlike their healthy counterparts, cancer cells are unable to regulate cell growth, which often results in a tumor. Cancer cells also lack adhesion molecules and can travel to other regions of the body, known as metastasis. These cells can grow and divide before they reach maturity and are able to evade growth suppressors present in the system. Additionally, many protein mutations have been associated with abnormal growth in cancer cells<sup>40</sup>. Identifying these irregularities can help with the successful development of treatment options for patients.

Currently, there are a variety of standard therapeutic approaches utilized to treat cancer. These include surgery, radiation therapy, chemotherapy, immunotherapy, targeted therapy, or biomarker testing<sup>41</sup>. While one therapy may be sufficient for some patients, many utilize a combination of therapeutic approaches to achieve the most effective treatment plan<sup>42</sup> and to account for the shortcomings of each individual method. For example, surgery is used to remove the tumor mass, but doesn't guarantee that all cancer cells have been removed<sup>41</sup>.

Therefore, patients often utilize a combination of surgery and chemotherapy. Chemotherapy is the use of cancer drugs to kill cancer cells in the body, but often impacts both cancer and non-cancer cell types, making it detrimental to patient health. There have also been a variety of immunotherapies developed to assist the immune system's response to cancer cells, including immune checkpoint inhibitors, T-cell transfer therapy, and monoclonal antibodies<sup>43</sup>. In addition to immunotherapy, with further development of molecular therapeutics<sup>44, 45</sup>, targeting approaches<sup>45, 46</sup> and nanotechnology<sup>47, 48</sup> new cancer treatment methods focused on affecting exclusively cancer tumors emerge. Many of these therapeutic approaches utilize fluorescence tracking to identify where the therapy goes, and potentially identify internalization pathways.

### **Fluorescence**

Fluorescence is the effect of light emission by an atom or molecule after a finite duration subsequent to the absorption of the excitation photon<sup>49</sup>. This phenomenon is observed when electron in a material in its ground (or lower energy) state is excited by a photon into an excited state. Once the electron reaches the excited state, it may undergo a non-radiative relaxation<sup>49</sup>, falling to the lowest excited state. The electrons in the lowest excited state can either further decay non-radiatively to the ground state or return to the ground state by radiatively releasing energy, which is known as fluorescence. The fluorescence process is characterized by the fluorescence quantum yield (QY) and fluorescence lifetime<sup>49</sup>. Fluorescence quantum yield is used to describe the efficiency of the fluorescence process<sup>50</sup>, and can be characterized using the following equation:  $QY = \frac{\text{number of photons emitted}}{\text{number of photons absorbed}}$ . These values, however, are often determined by comparing a sample to a known standard with similar excitation/emission wavelengths. Fluorescence lifetimes measure the amount of time a fluorophore spends in the excited state before emitting a photon to return to the ground state<sup>51</sup>. These values can be

determined through manipulation of the equation:  $I(t) = I_0 e^{-\frac{t}{\tau}}$  where  $I_0$  is the intensity at time  $t = 0$  s,  $t$  is the time after the absorption, and  $\tau$  is the fluorescence lifetime. A number of molecules exhibiting fluorescence, including such fluorophores as azadioxatriangulenium (ADOTA)<sup>52</sup>, citrazinic acid<sup>53</sup>, or rhodamine<sup>54</sup>, as well as more complex structures including emissive graphene derivatives<sup>55-58</sup> can be utilized in a variety of applications as fluorescence trackers<sup>59, 60</sup>.

## **Graphene**

Graphene is an allotrope of carbon serving as a parent structure to a multitude of materials, including graphene oxide, graphene quantum dots, and other derivatives. It has a hexagonal, crystal lattice structure composed of sp<sup>2</sup> hybridized carbon. Graphene is utilized in a number of applications, such as water desalination<sup>61</sup>, new age electronics<sup>62, 63</sup>, graphene-assisted laser desorption/ionization for mass spectrometry<sup>64</sup> and high resolution electron microscopy<sup>65</sup>, due to its uniquely high electrical<sup>66</sup> and thermal<sup>67</sup> conductivity, tensile strength<sup>68</sup> and transparency properties<sup>69</sup>. Although graphene has a number of remarkable properties, it is a zero-band gap semiconductor and is therefore unable to fluoresce. Unlike metals and semiconductors, where the valence band overlaps the conduction band or is separated by a small gap, respectively, the band structure of single-layer graphene must be explored further. Utilizing density functional theory (DFT), the electronic band structure can be shown to have conical structures formed by Dirac cones. The structure of graphene is what yields the remarkable properties desirable for electronic applications. While there is no fluorescence capability for graphene, graphene derivatives maintain the properties that are advantageous, allowing for it to be used in biomedical applications including DNA sequencing<sup>70</sup>, biosensor development<sup>71</sup>, and cell differentiation and growth<sup>71</sup>.

## Graphene Oxide

Graphene Oxide (GO) possesses unique properties which make it more attractive than graphene for optical and biomedical applications: it is water soluble, provides a large platform with a variety of addends for convenient functionalization-based drug attachment, and exhibits fluorescence in the visible/near-infrared. Graphene oxide is a 2-D material derived from graphene by introducing several oxygen functionalities that are covalently bonded to the carbon atoms. In aqueous solutions, GO flakes are negatively charged with the formation of an electrical double layer at the GO/water interface. This overall negative charge at physiological conditions governs water solubility of the nanomaterial. The chemical structure of GO depends on the synthetic process and can be altered via the protonation/deprotonation of the oxygen-containing groups on its surface. Reduction of the GO makes the material more hydrophobic and unstable<sup>72</sup>. The absorption spectrum is dominated by the  $\pi \rightarrow \pi^*$  transition of the carbon platform that usually occurs at approximately 230 nm. There are two theories regarding GO fluorescence. The first theory contributes fluorescence origins to the islands of graphitic carbon surrounded by oxygen-based functional groups<sup>73</sup>, and the second assumes that it originates from regions of confined electrostatic potential surrounding the functional groups<sup>74, 75</sup>. Each theory can be explained using the quantum mechanical example of a particle in a box, such that we see the splitting of the energy levels and therefore, the creation of the bandgap in otherwise gapless graphene, which is derived from a smaller size of the confined region. Using the first theory, it can be explained such that the confinement of the graphitic regions impacts the free electrons within graphitic islands, causing the quantization of the energy levels. Due to confinement, the gap between the conduction and valence bands is introduced with the energy of several eVs yielding the possibility of fluorescence in the visible<sup>73</sup>. The second theory also resembles the 2D particle in a box example, in which a confined region of

electrostatic potential is considered around certain functional groups and is thought to be inducing electronic confinement. As we expect both the regions of graphitic carbon and regions of electrostatic potential vary in size across GO platform, GO fluorescence feature is expected to consist of multiple emission peaks with different emission energies. It is important to note, however, that neither of these theories for the pathways of GO emission have been fully confirmed, although experimental evidence in ozone-driven oxidation of GO<sup>76</sup> points to the possibility of manipulation of the size of graphitic regions that leads to change in fluorescence emission energies. There are some drawbacks for GO, however, which include some cytotoxicity still setting a boundary for therapeutic concentrations, larger particle sizes inconvenient for internalization and tissue penetration, and also emission mostly in the visible only tailing into NIR, which inhibits its use for *in vivo* organ imaging, limiting applications only to intravital and *ex vivo*.

### **Graphene Quantum Dots**

The limitations of graphene platforms have a potential to be addressed through utilizing zero-dimensional graphene quantum dots (GQDs). GQDs share some desirable properties of graphene oxide including water solubility and fluorescence, but also have a variety of attributes such as small size and high biocompatibility that can enhance their use in biomedical applications. Those include their use as biological labels for stem cell research<sup>77</sup>, cellular and deep tissue imaging<sup>78</sup>, and photodynamic therapy<sup>79</sup>. GQD structures can be designed to exhibit higher quantum yields<sup>21</sup>, stability against photobleaching<sup>80</sup>, and some also possess emission in the near-IR<sup>81</sup>. NIR imaging modality has been hypothesized as an advantageous tool for *in vivo* imaging due to higher penetration depth and diminished scattering of near-infrared light in biological tissues. Similar to GO, the emission in the visible range is expected to be confinement-related, occurring due to the small size of quantum dots (3-5 nm) allowing for

band gaps in the visible<sup>73</sup>. This visible emission appears to be substantially excitation dependent<sup>82</sup>: broad distribution of QD sizes allows for exciting different-sized structures at different wavelengths thus resulting in wavelength-dependent confinement-governed emission<sup>82</sup>. The emission in the NIR, however, is potentially related to electronic states at the functional group-derived defects or their arrangements as was proposed in previous works<sup>82</sup> supported by the 10-fold lower NIR fluorescence life times. However, limiting toxicity observed in a few NIR-emissive QDs<sup>83</sup> hampers their further *in vivo* utilization, which results in biological applications of QDs, including bioimaging, being restricted to fluorescence in the visible<sup>84</sup>. Although more biocompatible, these novel nanomaterials still face significant obstacles preventing their large scale fabrication and biomedical imaging applications: widespread top-down QD synthesis has generally poor reproducibility<sup>85</sup> while bottom-up approach tends to produce QDs with lower quantum yields<sup>82, 86</sup>. Attempts to improve quantum yields<sup>87</sup> and broaden the emission range<sup>83</sup> typically increase QD toxicity due to the introduction of additional chemical components. Combined, all the aforementioned drawbacks hamper translational studies, diminishing the value of QDs for therapeutic applications and requiring for new QD structures with more advantageous properties.

## **Introduction**

Cancer is one of the leading causes of death worldwide, with a staggering death toll of over 609,000 in the United States alone in 2018<sup>88</sup>. Nearly 40 % of all people will be diagnosed with cancer at some point<sup>89</sup>. While existing therapies such as radiation, and chemotherapy can be successful<sup>2</sup> and non-invasive, they often affect both healthy and cancer tissues, posing a threat to patients' health. Some of these health concerns include nausea, vomiting, gastrointestinal and/or oral mucositis, and increased risk of cardiovascular disease are a few of the commonly cited issues with use of a variety of current chemotherapeutics<sup>90</sup>. Another major drawback of

modern chemotherapies is the inability to provide information about the treatment pathways, hampering the optimization and advancement of the treatment. While current therapeutics have efficiently increased survival rates, there is still need for improved treatment options. Effective therapeutic strategies must address several issues simultaneously, such as imaging, targeting, treatment, and sensing due to the variability and adaptability of the range of cancer types known to date. Thus, image-guided therapies are needed to explain treatment pathways and provide cancer detection leading to the improved treatment of cancer.

Development of a multifunctional imaging, targeted delivery, and treatment agent would address a multitude of critical issues. Poor delivery of the drugs to cancer tumors hinders the efficacy of cancer treatment regimens, and often leads to longer or more aggressive treatments for patients<sup>91</sup>. Furthermore, since cancer therapeutics are often not focused on the tumor, their accumulation in healthy tissues causes unnecessary offsite toxicity<sup>92, 93</sup>. One step towards improving cancer therapeutic efficacy by using multidrug treatment agents is being currently developed to overcome potential drug resistance in tumor issues<sup>94</sup>. Creating a treatment platform that can account for the need to attach and deliver multiple drugs simultaneously would optimize treatment options for multiple cancer types, improving the delivery and allowing for focusing delivery to tumors by specific cancer-binding targeting agents<sup>95, 96</sup>. Targeted delivery can boost efficacy of a multimodal treatment agent and prevent non-selective toxicity<sup>97</sup>. Finally, there is a critical need for image-guided approaches. Currently, there are a variety of therapeutic imaging techniques, including CT, MRI, PET, ultrasound as well as visible, and near-infrared (NIR) fluorescence imaging. NIR fluorescence imaging does not require complex equipment as CT, MRI and PED do, but offers deeper tissue imaging than that available to visible fluorophores due to lowered absorption and scattering of near-infrared light by the biological tissue<sup>98</sup>. However, there are few NIR emitters known to



date and conventional fluorophores, both visible and infrared suffer from the issues of biotoxicity and low photostability.

New technologies and materials are actively being developed to address a number of aforementioned therapeutic and imaging issues. For instance, a novel class of structures, nanomaterials, are currently utilized in a variety of bioapplications, including imaging<sup>99</sup>, disease and cancer detection<sup>3, 100</sup>, drug delivery<sup>101</sup>, photodynamic<sup>102</sup> and photothermal therapy<sup>103</sup>. Nanotechnology provides multiple platforms that can be altered via chemical synthesis to address a specific condition's treatment needs<sup>104</sup> and stimulate or suppress biological responses<sup>105</sup>, facilitating antitumor effects<sup>106</sup> or treatment of inflammatory effects<sup>107</sup>. The ability of nanomaterials to meet the needs of these applications, by the means of drug<sup>108</sup>, targeting agent<sup>109</sup> or fluorophore<sup>110</sup> attachment, gives them an advantage to become a platform for desired multimodal therapeutics. Drug delivery with nanomaterials can be beneficial as delivery agents may protect the healthy tissue from adverse effects of chemotherapeutics encapsulating them, or enable safe transport of gene therapeutics prone to degradation and water-insoluble drugs to cancer tumor sites and cells. Additionally, nanomaterials can provide imaging in cancer cells and tissues in the visible and near-infrared (NIR)<sup>7</sup> with high photostability<sup>111</sup> and enable targeted delivery<sup>112, 113</sup>. Thus, nanotechnology-based systems are advantageous due to their multifunctionality, offering both drug delivery and detection capabilities.

Although such nanoformulations significantly improve the capabilities of conventional therapeutics, there is still a challenge to expand the options for image- and sensing-guided therapy and improve targeting to multiple cancer types. Currently, very few nanomaterial systems can carry out imaging, sensing, and delivery concurrently<sup>114</sup>, while none are used in clinic due to low biocompatibility<sup>115</sup>, complex fabrication<sup>116, 117</sup>, issues with body clearance,

and unknown decomposition routes<sup>118</sup>. Biocompatible nanomaterials exhibiting environment-dependent electronic and/or structural properties are expected to fill this gap with a promise of utilization as molecular sensors as well as for imaging and drug delivery. As a result, the leading modern approaches in cancer therapeutics are now directed toward both molecular and nanomaterials-based formulations performing several functions at once. Those formulations, however, are still often restricted by non-specific toxicity<sup>114, 119</sup>, lack of sensing capabilities<sup>120</sup> or drawbacks of structural complexity<sup>121, 122</sup>. New multimodal theranostic approaches combining targeted<sup>123,124</sup> and image-guided delivery with cancer-selective treatment<sup>125</sup> and diagnostics are required to fully meet the demanding needs of cancer therapeutics.

Carbon-based materials can often be more versatile and offer some outstanding properties unlike other nanoplatforms, which can be further advantageously utilized in biotechnology. Graphitic nanomaterials, in particular, such as carbon nanotubes or graphene, are also becoming competitive contenders for bioapplications. Single-walled carbon nanotubes have been utilized as delivery and imaging agents with the potential to address antibiotic resistance<sup>126</sup> and perform drug<sup>127</sup> and gene delivery<sup>128</sup> as well as photothermal therapy<sup>128</sup>. Reduced graphene oxide has been utilized in nanoscale sensors of glucose<sup>129</sup> and as carriers for magnetic resonance imaging (MRI) agents<sup>130</sup>. These graphitic nanomaterials offer distinct advantages such as remarkable optoelectronic properties for some including an ease in covalent/non-covalent functionalization. Unfortunately, however, multiple carbon nanomaterials are limited in further translation to the clinic due to the insolubility of some of those in water<sup>131</sup>, potential toxicity<sup>131</sup>, or complex synthetic processes<sup>129</sup>. To further utilize the advantages of carbon-based formulations in cancer therapeutics, the nanomaterial would need to address all the desired theranostic functions including targeting, cancer-selective treatment, high biocompatibility, image-tracking detection and be simple/cost-effective to produce.

Significant development was recently made to utilize nanocarbon vehicles for a variety of multimodal biomedical applications, including the use of nanodiamonds for targeted delivery and imaging of cancer therapeutics<sup>132</sup>, modified carbon nanotubes for imaging and targeted therapy of a brain glioma<sup>133</sup> or graphene oxide devices for electrochemical biosensing of four DNA bases<sup>134</sup> or sensing of biomolecules such as dopamine or cholesterol<sup>135</sup>. However, to date, none that have been engineered address all the aforementioned capabilities and many still exhibit some toxic or biologically incompatible responses<sup>136</sup>. Graphene is one of such materials that, having a plethora of applications in science and engineering<sup>137, 138</sup>, cannot be utilized as a therapeutic carrier due to its insolubility in water, cytotoxic biological profile and lack of fluorescence imaging capabilities. On the other hand, more biocompatible graphene derivatives<sup>139, 140</sup>, including graphene quantum dots, graphene oxide<sup>141</sup> and an assortment of graphene-based nanoparticles<sup>142, 143</sup>, provide water-soluble platforms that can be in principle optimized for imaging and drug/gene therapeutic transport. So far these materials have been used for targeted delivery<sup>113,144, 145</sup>, imaging<sup>144, 145</sup> and chemical sensing<sup>146</sup>. In many of these applications, however, carbon nanomaterials have to be modified, via PEG conjugation for imaging, biocompatibility and therapy<sup>147, 148</sup> or require the use of additional fluorescent dyes for detection<sup>17, 77, 149</sup>. Such formulations again still may exhibit significant non-specific toxicity via off-site accumulation<sup>113,144, 145</sup>, and many of them do not possess desired capabilities for cancer detection.

Among the carbon-based platforms, graphene oxide (GO) possesses some of the properties more attractive for biotechnology: it is water soluble, provides a large platform for functionalization with targeting, therapeutic or diagnostic agents<sup>150, 151</sup>, and exhibits fluorescence in the visible range tailing into near-infrared<sup>76, 141, 152</sup>. GO is often used in cancer targeting approaches due to the enhanced permeability and retention (EPR) effect. Our work

shows that graphene oxide is non-toxic in the cells up to the imaging concentrations of ~15  $\mu\text{g/mL}$ , rapidly internalizes and functions as a ratiometric pH sensor due to its pH-specific emission<sup>141</sup>. GO offers the benefit of a large platform for attachment of functional groups including targeting moieties, MRI agents and anticancer drugs<sup>153</sup>, and possesses imaging capabilities due to its fluorescence in the visible and NIR, as well as a pH-dependent electronic transitions<sup>154</sup>. GO pH-specific emission is beneficial for non-invasive optical sensing as it offers the capabilities to detect small shifts in the spectra depending on the environment and can therefore quantify its acidity. Given that cancer environments are generally more acidic than the healthy ones due to the excretion of lactic acid by cancer cells<sup>155</sup> GO can be used for cancer detection. Although in our previous work<sup>141</sup> GO was successfully utilized for simultaneous imaging, cancer sensing, and delivery, we still encountered limitations to its use *in vivo*. Drawbacks include some cytotoxicity still setting low maximum boundary for therapeutic concentrations, and the size of ~200-300 nm inconvenient for cell internalization and tissue penetration, and emission mostly in the visible only tailing into NIR and not suitable for even low depth tissue imaging.

The restrictions of graphene platforms can be overcome by the use of graphene quantum dots. GQDs maintain the desirable properties, such as water solubility and fluorescence, but have additional properties that can be used to enhance their use in biomedical applications. For example, GQDs can be synthesized having different sizes<sup>156</sup>, optical properties with fluorescence in multiple spectral regions<sup>157, 158</sup> and different addend structures on their surface<sup>159</sup> yielding a platform with a variety of water solubility and biocompatibility levels<sup>160, 161</sup>. GQDs have an advantage of being produced by a variety of synthetic methods that can be readily adjusted to fit particular applications. These can be prepared via a plethora of different synthetic approaches including top-down and bottom up routes<sup>162, 163</sup> and a variety

of precursor materials, which allows for a range of properties, some more advantageous for bioapplications. GQDs can be synthesized having different sizes<sup>156</sup>, optical properties with fluorescence in multiple spectral regions<sup>157, 158</sup> and different addend structures on their surface<sup>159</sup> yielding a platform with a variety of water solubility and biocompatibility levels<sup>160, 161</sup>.

GQD structures can be designed to exhibit higher quantum yields<sup>21</sup>, stability against photobleaching<sup>80</sup>, and some possess emission in the near-IR<sup>81</sup>. NIR imaging modality has been hypothesized as an advantageous tool for *in vivo* imaging due to higher penetration depth and diminished scattering of near-infrared light in biological tissues. There are very few NIR-emissive materials compatible for biological use, thus developing a new one is a significant step forward in that field. Limiting toxicity observed in a few NIR-emissive QDs<sup>83</sup> developed to date impacts potential for *in vivo* utilization, which results in biological applications of GQDs, including bioimaging, being restricted to fluorescence tracking *in vitro* with mostly GQDs fluorescing in the visible used.<sup>84</sup> Such GQDs with fluorescence in the visible, although more robust, still face significant obstacles preventing their large scale fabrication and biomedical imaging applications: top-down GQD synthesis has generally poor reproducibility<sup>85</sup>, whereas bottom-up synthesis often produces QDs with lower quantum yields<sup>82, 86</sup>. Attempts to improve quantum yields<sup>87</sup> and broaden the emission range<sup>83</sup> typically increase QD toxicity due to the introduction of additional chemical components. Combined, these drawbacks hamper translational studies, diminishing the value of GQDs for therapeutic applications.

To address biocompatibility, reproducibility in fabrication and the need for high-yield fluorescence capabilities along with near-IR imaging, we develop novel doped graphene quantum dots with advantageously modified optical properties. Nitrogen-doped (N-GQDs),

sulfur-doped (NS-GQDs), and boron-nitrogen codoped (BN-GQDs) graphene quantum dots are synthesized via a simplistic, scalable and reproducible 1-step hydrothermal route, and tested for biological imaging in the visible and near-IR as well as for pH-based cancer detection *in vitro*. These GQDs with high biocompatibility, and high-yield visible emission along with near-IR fluorescence in NIR demonstrate the capacity to become non-toxic, standalone, multifunctional agents for multicolor imaging, effective cellular internalization, and biosensing. Of these, nitrogen-doped graphene quantum dots are found to be the most promising candidates with highest biocompatibility, fluorescence-based pH response and simplest synthetic process.

As a platform with a variety of oxygen and nitrogen-containing functional groups, N-GQDs exhibit the potential for the attachment and delivery of multiple cancer therapeutics. Here we not only synthesize the GQDs as an imaging platform but go all the way to test those in novel anticancer therapeutic transport. The lack of specificity of current chemotherapeutics calls for utilizing novel cancer-selective treatment avenues. A strategy selected in this work is based on the reducing environment of cancer cells, which leads to the production of reactive oxygen species (ROS) due to their high metabolic rate and mitochondrial dysfunction. This reducing environment of cancer cells is caused by the production of superoxide, which is prevalent in cell signaling for tumor proliferation<sup>164</sup>. This is less prominent in non-cancer cells, where reactive oxygen species (ROS) are more easily mitigated<sup>165</sup>. Excessive ROS generation in cancer cells by the therapeutic is therefore expected to create a toxic effect<sup>166</sup>, that is aimed to be used as a cancer-selective therapeutic approach. Ferrocene (Fc) is a known reducing agent generating a cytotoxic response specifically in the reducing environments of cancer cells linked to the production of reactive oxygen species (ROS) during the redox cycle of iron<sup>167, 168</sup>. The attachment of Fc to the electron-rich N-GQD platform may facilitate enhancement of its redox-

based toxicity to cancer cells. In addition to cancer-selective treatment, targeting utilized currently in a variety of nanoformulations can aid to further focus the treatment to cancer cells only. Our work utilizes one of the common and highly effective approaches involving the use of hyaluronic acid (HA) to target CD44, a receptor overexpressed in cancer cells<sup>169</sup>. While the functional roles of CD44 are not fully understood<sup>169-171</sup>, CD44 and its variants play a role in cancer development and progression<sup>171</sup>. HA is able to target and activate the CD44 receptors, which induces both cell proliferation and cell survival<sup>171</sup>. HA functionalization of the therapeutic Fc unit will allow targeting a variety of cancer cell lines known to overexpress these CD44 receptors, including cervical cancer (HeLa) cells<sup>170, 171</sup> used in this work.

## **Chapter 2- Experimental Methods and Procedures**

### **Synthesis/Sample Prep**

Graphene quantum dots are synthesized using a hydrothermal microwave-assisted treatment using a commercial microwave. A 0.14 M aqueous glucosamine-HCl solution is placed in a microwave and treated for 40 minutes at a power setting of 450 W. Different dopant precursors (sulfur thiourea or benzenboronic acid) is also added prior to the synthesis to achieve a variety of quantum dot types (N-GQDs, NS-GQDs, and BN-GQDs). GQDs produced using this method are then purified from the smaller-sized molecular starting materials via bag dialysis with 500-1000 Da membranes for seven days. A substantial synthetic yield of 15-20% is achieved after purification<sup>82</sup>.

### **Optical Measurements and Characterization**

Fluorescence spectra were measured using SPEX NanoLog, Horiba Scientific spectrofluorometer in the regions of 300 to 1000 nm with the excitation in the visible at 400 nm and excitation in the NIR at 800 nm. Different types of GQDs show different quantum efficiencies due to doping-related fluorescence quenching or enhancement.

### **Cell culture**

Two cancer cell lines (HeLa –Human cervical carcinoma, and MCF-7 – Human breast cancer) were used in this work, as well as one non-cancer cell line (HEK-293, Human embryonic kidney fibroblast). Cells were maintained in a Thermo-Scientific Midi 40 CO<sub>2</sub> Incubator at 37.1°C with 5% carbon dioxide, 95% air. For microscopy, cells were plated onto the glass coverslips which were placed at the bottom of 6-well plates. A minimum of 6 hours was allowed for cell attachment to the coverslips before the addition of quantum dot samples. N-GQDs and NS-GQDs were introduced to the wells at a final concentration of 1 mg/mL in each well, while BN-GQDs were introduced at a lower concentration of 0.1 mg/mL per well. The



cells for the internalization experiments follow the initial procedure listed in ‘Graphene Quantum Dots, Cell Culture’ section. The cells were then washed with 0.5 mL of PBS to remove extracellular GQDs and prepare cells for imaging. For the cell internalization/excretion experiment, 0.5, 1, 3, 12, and 24 hours were used as treatment time points. For the pH study, cells were imaged without a washing step, to maintain GQD presence both in the intra- and extracellular environments for pH detection in both.

### **MTT cytotoxicity assays**

An MTT cytotoxicity assay is conducted with several GQD samples (NS-GQDs, N-GQDs, and BN-GQDs), at the concentrations from (0-2mg/mL). Each sample is prepared via serial dilutions at the testing concentrations ranging from the maximum concentration. After incubation for 12 hours, an MTT solution is introduced and incubated for 4 hours, as the reduction of the MTT is dependent on cellular metabolic activity. Absorbance values below the measured control indicate a decrease in the rate of cell viability, as only living cells are able to metabolize and convert the MTT into a highly absorbing purple colored formazan product<sup>172</sup>. The absorbance, serving as an indication of cell viability, is then measured using the FLUOstar Omega microplate reader, and analyzed via Omega software.

### **Imaging**

Samples were sealed and imaged via visible/near-IR spectrally-resolved microscopy setup. It includes Olympus IX73 microscope with 60x IR-corrected Olympus Plan Apo objective coupled to Photometrics Prime 95B CMOS camera through a filter wheel with emission filters covering the visible part of the spectrum. An optimal configuration of filters selected based on GQD emission spectra including  $375 \pm 14$  nm and  $475 \pm 25$  nm excitation and  $450 \pm 20$  nm and  $535 \pm 20$  nm emission filters is utilized for visible imaging, while a  $650 \pm 20$  nm excitation and  $750 \pm 20$  nm emission filters are used for NIR imaging. Appropriate exposure time and

illumination levels for each filter set were determined using control cells with no QDs present, ensuring zero autofluorescence background both in the visible and NIR for control samples.

### **Imaging Analysis**

Image analysis was performed using ImageJ software. Background-subtracted emission per unit area for each biological cell was calculated by taking the integrated fluorescence intensity and subtracting a product of an average (over ~10 cells per cell type) mean gray value of the background intensity per unit area and the area of each measured section. This was done for multiple regions to account for any variation in the background. The corrected total cell fluorescence (CTCF) was determined by subtracting out the average background intensity from the integrated intensity over the whole cell. pH analysis statistics comparing cancer versus healthy cells were obtained by comparing emission intensity in green (550 nm) and blue (450 nm) for over 100 cells. The images compared were of the same regions, allowing for the analysis of the emission from the same cells or extracellular environments in both green and blue. The CTCF for both emission wavelengths were determined and then compared, allowing for the quantification of the green to blue emission ratios utilized for pH sensing.

### **Synthesis of treatment formulation (Fc-QD-HA)**

Nitrogen-doped graphene quantum dots (N-GQDs) are synthesized using a low cost, simple, hydrothermal route<sup>159, 173</sup>. Aqueous glucosamine-HCl solution (a glucosamine precursor) (0.14 M) is suspended in water and subjected to hydrothermal microwave-assisted treatment at 400 watts for 60 min. Microwave irradiation facilitates polymerization and nucleation of carbon clusters<sup>173</sup> ultimately leading to the formation of graphene quantum dots decorated with nitrogen- and oxygen-containing functional groups. Upon completion, N-

GQDs are purified via bag dialysis with 500-1000 Da Molecular Weight Cut-off (MWCO) membrane for 24 hours to remove unreacted precursor.

The synthesis of the GQD-Fc-HA formulation is schematically represented in Figure 1. In preparation for covalent functionalization in organic solvent, purified N-GQDs are initially freeze-dried in a Labconco, FreeZone 4.5 freeze-dryer. Further, they are complexed with HA and Fc via the following reaction steps. Chemical modifications are carried out in a fritted syringe. Step 1: 95.3 mg ethylene diamine and fluorenylmethyloxycarbonyl (Fmoc) (0.3 mmol) are added to a coupling cocktail of diisopropylcarbodiimide (DIC) (37.1  $\mu$ L, 0.3 mmol), diisopropylethylamine (DIPEA) (38.0  $\mu$ L, 0.3 mmol), and hexafluorophosphate benzotriazole tetramethyl uronium (HBTU) (113.8 mg, 0.3 mmol) in dichloromethane ( $\text{CH}_2\text{Cl}_2$ ). This solution is then added to 250 mg dry N-GQD (0.1 mmol) powder, which is loaded to a fritted syringe. The reagents are mixed thoroughly for 4 hours at room temperature, which is then followed by a sequence of 6 washing steps in dichloromethane to remove any remnants of the coupling cocktail. Each wash is performed by submerging the product in  $\sim$  5 mL dichloromethane, inverting the syringe, and filtering the liquid through a 0.45  $\mu$ m disk filter. Step 2: The washed product is then mixed with a 20% piperidine/ $\text{CH}_2\text{Cl}_2$  solution for 20 minutes at room temperature, to remove the Fmoc group and leave the free  $\text{NH}_2$  group. This is repeated a total of two times. The insoluble materials are separated from the piperidine/ $\text{CH}_2\text{Cl}_2$  solution through syringe filtration. Further, the product is again subjected to 6 washing steps in dichloromethane as in step 1. This yields N-GQDs with amine groups suitable to react with the carboxyl groups of the hyaluronic acid. Step 3: the product of step 2 is mixed with hyaluronic acid (367.7 mg, 0.3 mmol), the same coupling cocktail of DIC (37.1  $\mu$ L, 0.3 mmol), DIPEA (38.0  $\mu$ L, 0.3 mmol), and HBTU (113.8 mg, 0.3 mmol) in dichloromethane ( $\text{CH}_2\text{Cl}_2$ ). The reaction is stirred for 4 hours and the resulting GQD-HA

compound is washed 6 times with dichloromethane to remove the remaining coupling cocktail. An excess of the amine groups on GQDs allows for further reaction of the remaining ones with Fc-COOH in Step 4. Step 4: the product is mixed with ferrocene monocarboxylic acid, dichloromethane, and the coupling cocktail. After shaking for 4 hours, it is again washed 6 times in dichloromethane as described previously. Upon completion, the Fc-GQD-HA formulation is dispersed in 5 mL DI water and subjected to centrifugal filtration in a 3 kDa centrifugal filter at 10,000 x g's for 3 minutes to remove smaller constituent reagents leaving larger (over 3 kDa) Fc-GQD-HA formulation. A diagram of synthesis can be found in Figure 1. A concentration of 1 mg/mL is used for the Fc-GQD-HA formulation in all further experiments, while comparable concentrations (based on the iron content assessed via the EDX analysis) are utilized for the HA-ferrocene, prepared via serial dilutions from the stock solutions.

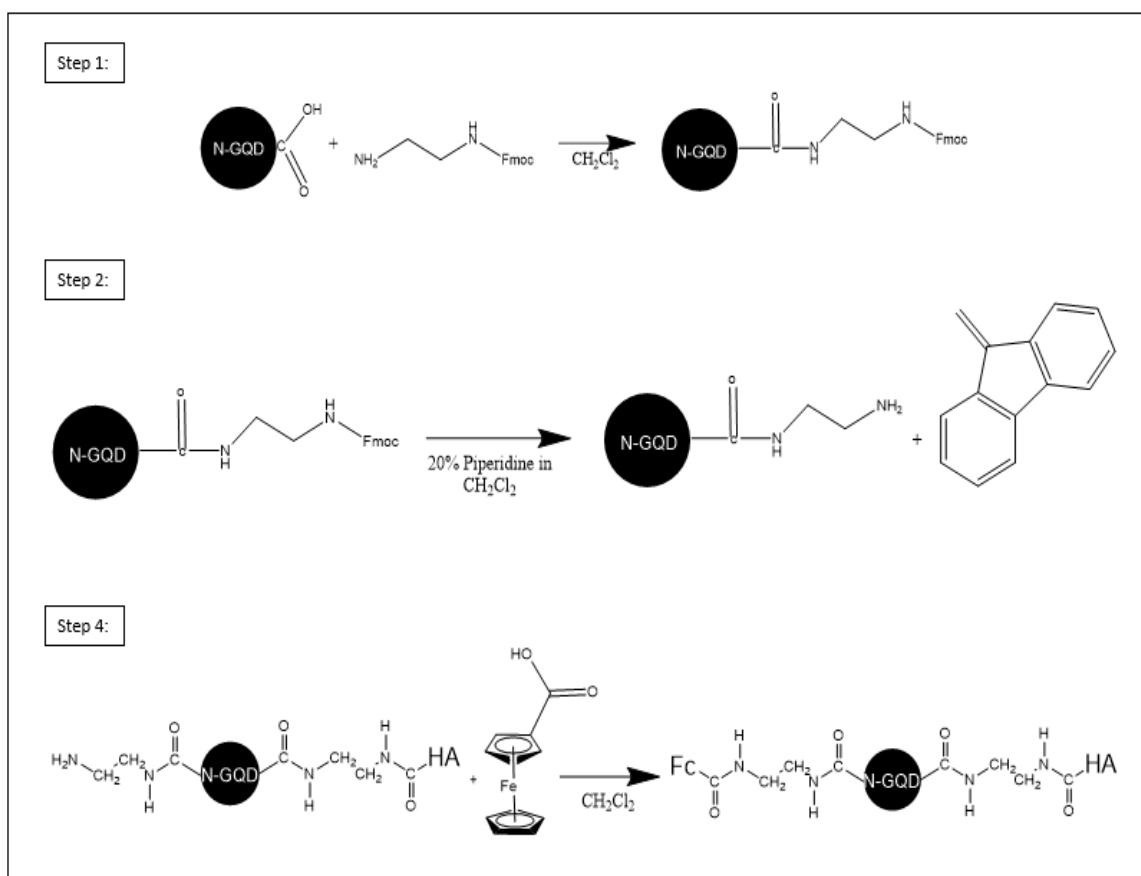


Figure 1. Synthesis diagram for the preparation of the Fc-HA-GQD formulation.

### Physical and Optical Characterization

In order to assess the synthesis of Fc-GQD-HA formulation, we perform several characterization procedures. The morphology of Fc-GQD-HA hybrid deposited on the carbon-coated 200 mesh copper grid under ambient conditions is characterized using transmission electron microscopy (TEM JEOL JEM-2100). Fast-Fourier-transform (FFT) analysis of TEM images indicates crystalline graphitic structure present in the Fc-GQD-HA formulation. Energy dispersive X-ray spectroscopy (EDX) analysis is performed to determine the presence of expected elements, while Fourier Transform Infrared Spectroscopy (FTIR) in the ATR mode of Thermo Nicolet Nexus, 670 FTIR, is used to qualitatively assess the presence of expected functional groups and thus, success of the synthesis. A change in optical properties due to

alteration of the electronic structure of the GQDs is assessed via absorption and fluorescence spectroscopy. The absorbance is measured using Agilent Technologies, Cary 60 UV-vis spectrophotometer in the range of 200-1100 nm, while SPEX NanoLog, Horiba Scientific spectrofluorometer is used to measure the fluorescence spectra of the hybrid in the region of 365 to 700 nm with 350 nm excitation.

### **Fluorescence Microscopy Measurements**

Cover slips with treated cells are sealed and imaged using a visible/near-IR spectrally resolved microscopy setup. This setup is composed of Olympus IX73 microscope with 60x IR-corrected Olympus Plan Apo objective, using Photometrics Prime 95B CMOS camera coupled to Olympus DSU (disk-spinning unit) confocal system for visible imaging with excitation/emission filter wheels enabling spectrally resolved image acquisition. An optimal configuration of filters is selected based on GQD emission spectra (475 ± 25 nm excitation and 535 ± 20 nm emission filters). Appropriate exposure time and illumination levels for each filter set are determined using control cells with no GQDs present, ensuring zero autofluorescence from control cells. Spinning disc confocal microscopy utilizes the DSU, which eliminates the light emitted at image planes other than that in focus, allowing for collecting the confocal image. Z-stacking of confocal images from different planes is further used to create 3-D images. Colocalization images are acquired based on optimal exposure and contrast settings for each staining, determined using non-treated control cell slides to ensure zero autofluorescence. The following filter combinations are utilized: DAPI excitation filter: 375 ± 14 nm, DAPI emission filter 450 ± 20 nm; LysoTracker Red excitation filter: 540 ± 10 nm LysoTracker Red emission filter: 600 ± 20 nm; Fc-GQD-HA formulation excitation filter: 475 ± 25 nm, Fc-GQD-HA formulation emission filter: 535 ± 20 nm.

## Cell culture

In this study, one cancer cell line (HeLa, Human cervical carcinoma) and one non-cancer cell line (HEK-293, Human embryonic kidney fibroblast) are used for *in vitro* work. One more cancer cell line (MCF-7, Breast cancer cells) is used specifically for DCFHDA experiments with ferrocene. Cells are maintained at 37 °C with 5% carbon dioxide and 95% air using a Thermo-Scientific Midi 40 CO<sub>2</sub> Incubator. *In vitro* fluorescence microscopy is performed on cells on glass coverslips mounted on microscope slides. The slides are prepared for cell plating by soaking in 1M HCl for a minimum of 6 hours at 50-60 °C. Coverslips are then washed twice with DI water and stored in a 70% ethanol solution. These coverslips are used when plating HeLa or MCF-7 cells, however, for HEK-293 cells, an additional collagen treatment is performed ensuring better cellular adhesion. For the collagen treatment, 1 mL sterilized 1M NaOH is added to 1 mL sterilized 10X PBS in a falcon tube, followed by the addition of 2 mL of collagen (5 mg/mL suspension in 0.02 N acetic acid). PBS formulation includes 80 g NaCl (1.37 M), 2 g KCl (27 mM), 17.8 g Na<sub>2</sub>HPO<sub>4</sub> · 2H<sub>2</sub>O (100 mM) and 2.4 g KH<sub>2</sub>PO<sub>4</sub> (18 mM) in distilled water. The final volume is then brought to 10 mL using sterile DI water. The coverslips are submerged in the collagen solution for at least 12h. The collagen coating is solidified as the cover slips are placed in a 6-well plate in the 37°C incubator overnight. The collagen coating is then equilibrated with complete medium and allowed to sit for 30 minutes at room temperature prior to use. After the medium is removed, the coverslips are washed once using 0.5 mL of 1X PBS. For microscopy, cells are plated onto respective glass coverslips which are placed at the bottom of 6-well plates. A minimum of 12 hours is allowed for cell attachment to the coverslips before the addition of the quantum dot samples. The Fc-GQD-HA formulation is further introduced to the wells at a final concentration of 1 mg/mL in each well. Prior to imaging, the cells are washed twice with 0.5 mL of PBS helping to remove

extracellular quantum dots by replacing the cell medium. To fix the cells, coverslips are washed with 0.5 mL 1X PBS and treated with 0.5 mL of 4% paraformaldehyde. After 30 minutes of exposure to 4% paraformaldehyde, coverslips are washed again with 0.5 mL 1X PBS. A drop of mounting solution, Fluoromount, is then placed in the center of the slide prior to placing the coverslip cell-side down. The coverslip is finally sealed to the microscope slide in preparation for imaging. Additional colocalization study is also performed to determine the location of Fc-GQD-HA formulation within the cells. Cells are stained with two different fluorophores blue nuclear (DAPI) and red lysosomal (Lysotracker red (ThermoFisher)) stain added to each well containing HeLa cells for 10 minutes and 30 minutes, respectively. Upon completion, the wells are washed once using 0.5 mL of 1X PBS and then fixed for imaging.

### **Cellular Measurements of Oxidative Stress**

To compare the reactive oxygen species (ROS) generated by N-GQDs, ferrocene-COOH, and Fc-GQD-HAs in biological environments, a DCFDA (Dichlorofluorescein diacetate) assay is performed in HeLa cells. Samples are prepared via serial dilutions at the testing concentrations in serum-free medium and added to the cells. After a minimum of 12 hours of incubation, cell media is removed from the 96-well plate, and DCFDA is introduced at a concentration of 25 $\mu$ M and incubated in the plate for 45 minutes. Once the DCFDA has diffused into the cells, it is deacetylated into a non-fluorescent compound<sup>174</sup>. This compound can then be oxidized by ROS, resulting in the production of DCF (dichlorofluorescein), which is highly fluorescent<sup>174</sup>. The DCFDA solution is further removed and replaced with complete medium. Serial dilutions-based of sample volumes are then introduced to each well, and those are incubated for 12 hours to yield the production of the DCF. After that, the fluorescence of DCF is measured using the FLUOstar Omega microplate reader with 485 nm excitation and 520 nm emission wavelength



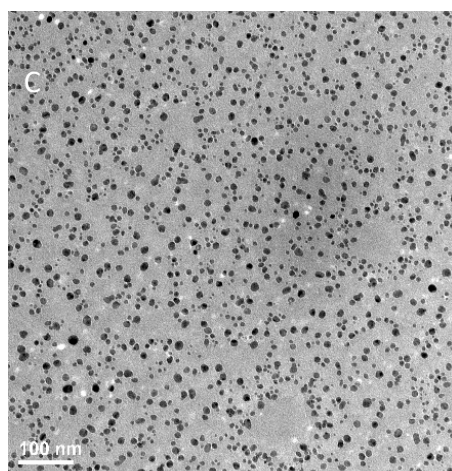
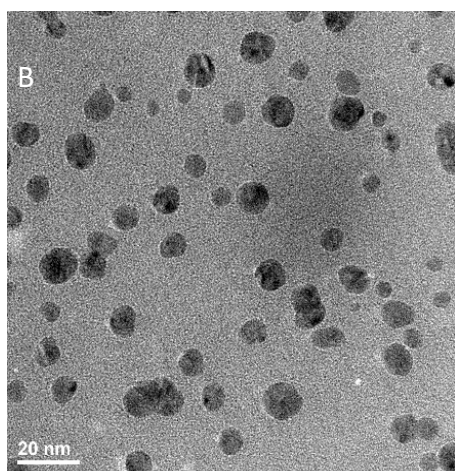
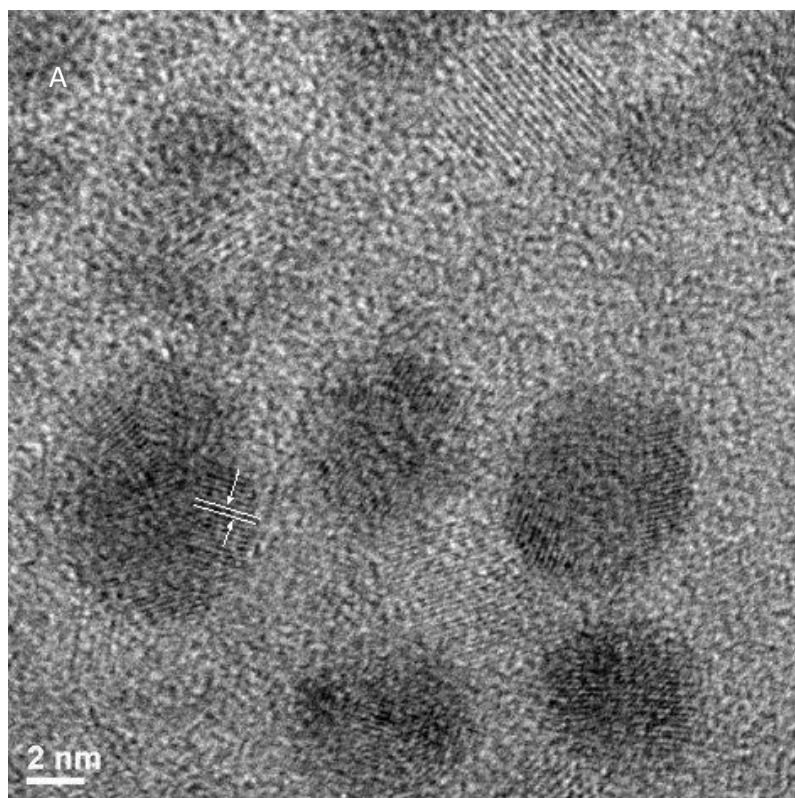
settings and further analyzed with Omega software. The same procedure was used to assess ROS generated by ferrocene in MCF-7 cells.

## **Chapter 3- Are graphene quantum dots suitable for biomedical applications?**

### **Results and Discussion**

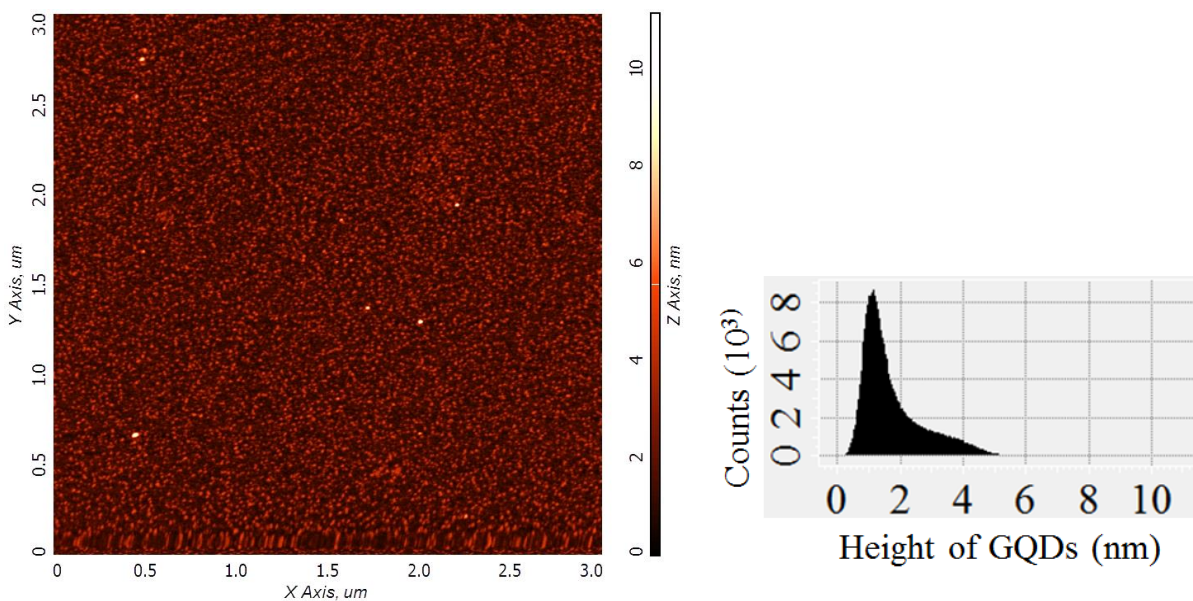
#### **Size characterization/degradation**

In this work, we synthesize several types of quantum dots with different dopants to determine which are most suitable for internalization, sensing, and imaging. GQDs are produced via a simple one-step hydrothermal route: a single glucosamine precursor is subjected to a microwave treatment in water suspension in a household microwave. This allows for scalable low-cost production of GQDs for biotechnology applications. As-synthesized nitrogen-doped graphene quantum dots were characterized as well as in our previous studies<sup>82, 175</sup>, confirming their size, structure and composition. GQDs show crystallinity signifying a presence of graphene lattice and have the sizes of 3-5 nm derived from TEM images (Figure 2, Figure 7) that are potentially suitable for cell internalization.



*Figure 2. (a) TEM image showing crystallinity of GQDs and discernable lattice domain structure. (b) and (c) TEM images of N-GQDs at varying magnifications*

Their structure is likely to contain few layers as assessed by the AFM height profile analysis (Figure 3) showing the GQD height distribution with 1.82 nm mean.



*Figure 3. AFM of nitrogen-doped graphene quantum dots. Mean height= 1.82 nm.*

FTIR of each quantum dot type indicates the presence of the respective dopants and a variety of oxygen-containing functional groups beneficial for GQD solubility and potential active agent attachment. (Figure 4). Each quantum dot type shows an O-H peak and N-H peak at  $3275\text{ cm}^{-1}$  and  $3090\text{ cm}^{-1}$ , respectively. Additionally, there is the expected COOH peak at  $1600\text{ cm}^{-1}$ . For each of the graphene quantum dot types, the stretching vibrations of C-N/N-H/C-H are present at  $1330$ ,  $1240$ , and  $1021\text{ cm}^{-1}$  respectively, which are common for each type<sup>82</sup>. The C-S stretching peak at  $1020\text{ cm}^{-1}$  and S-H shoulder at  $2560\text{ cm}^{-1}$ , are common for NS-GQDs, and a B-N peak observed at  $1380\text{ cm}^{-1}$  is common for BN-GQDs. The existence of these functional groups indicates the successful doping of each quantum dot type.

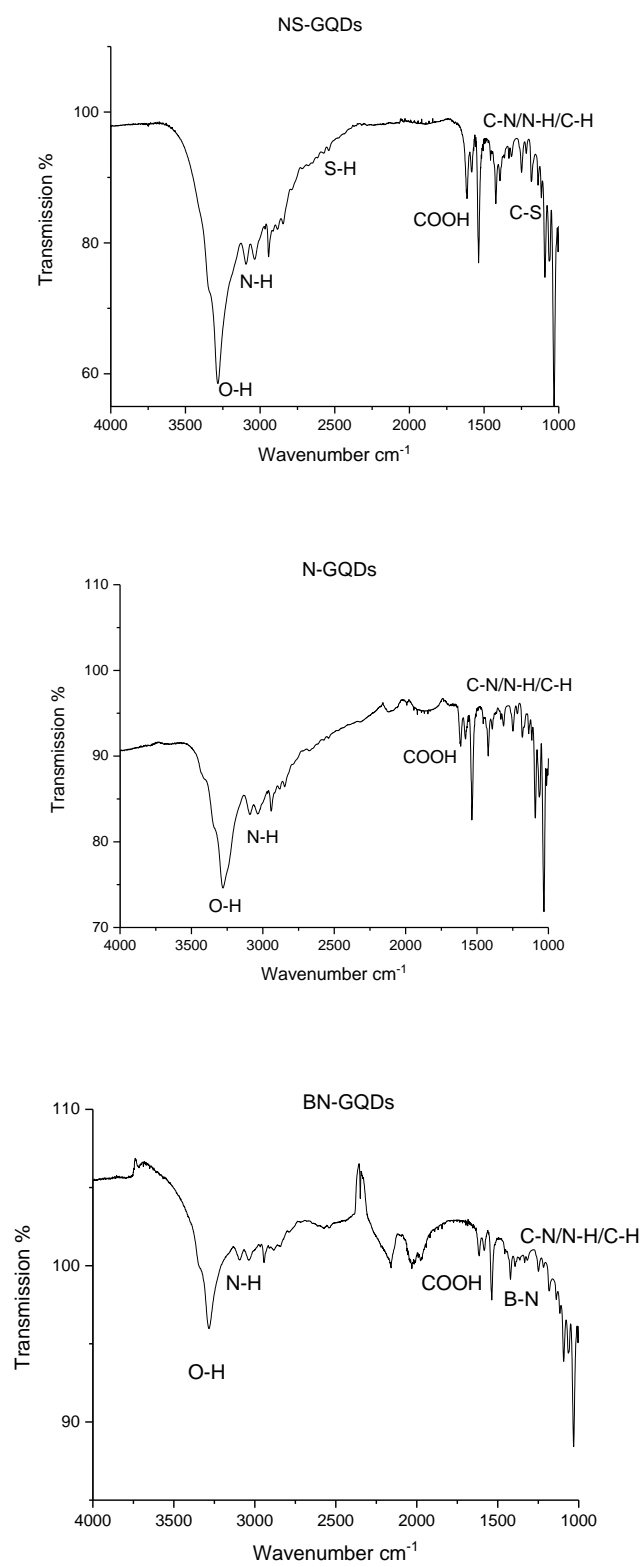


Figure 4. FTIR spectra of N-GQDs, NS-GQDs, and BN-GQDs.

## Absorbance

The absorbance spectrum of the N-GQDs is measured from 200-1100nm and shows absorbance in the visible region (Figure 5).

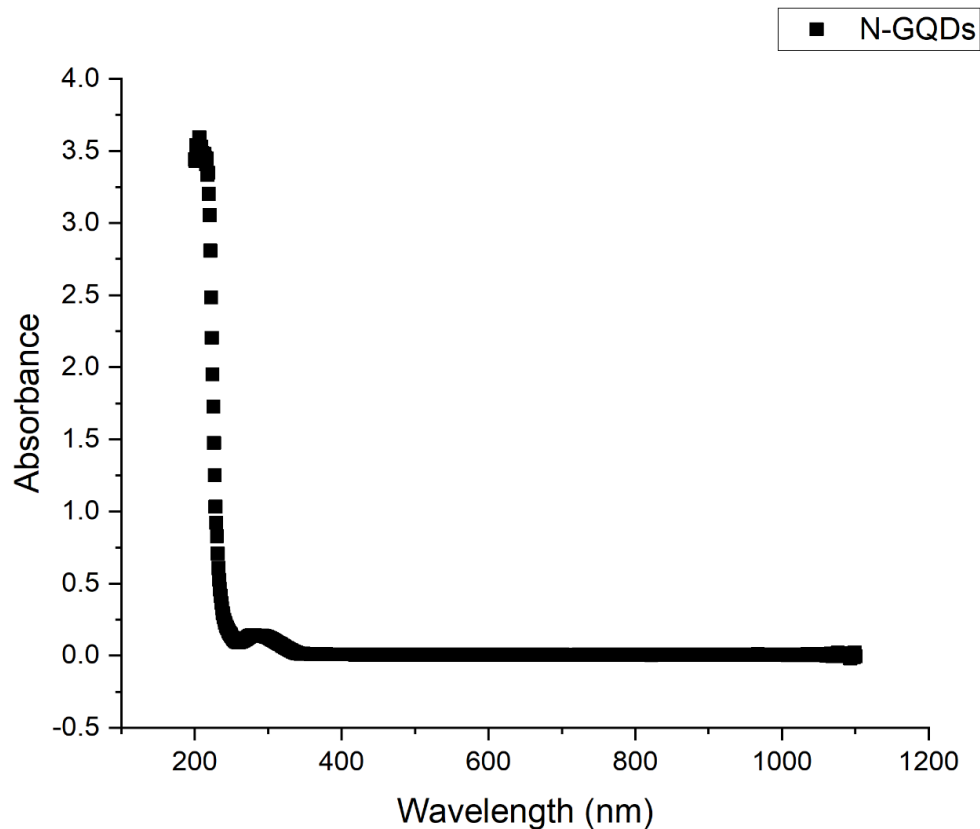


Figure 5: Absorbance spectrum of N-GQDs.

## Fluorescence

The differences in chemical structure of quantum dots doped with nitrogen (N-GQDs), sulfur (NS-GQDs), and boron and nitrogen (BN-GQDs) alter the emission spectra (Figure 6), providing some variations in spectral peak positions and their relative intensities that may be beneficial for the aforementioned applications. These fluorescence properties possessed by GQDs make them promising materials for potential use in biological applications, as unlike most conventional fluorophores and nanomaterials, they exhibit bright emission both in the

visible and near-IR (NIR) with quantum yields from 22 to 60% measured via a comparative method in our previous work<sup>82</sup>. The emission in the visible range is expected to be confinement-related occurring due to the small size of quantum dots (3-5 nm) allowing for band gaps in the visible<sup>73</sup>.

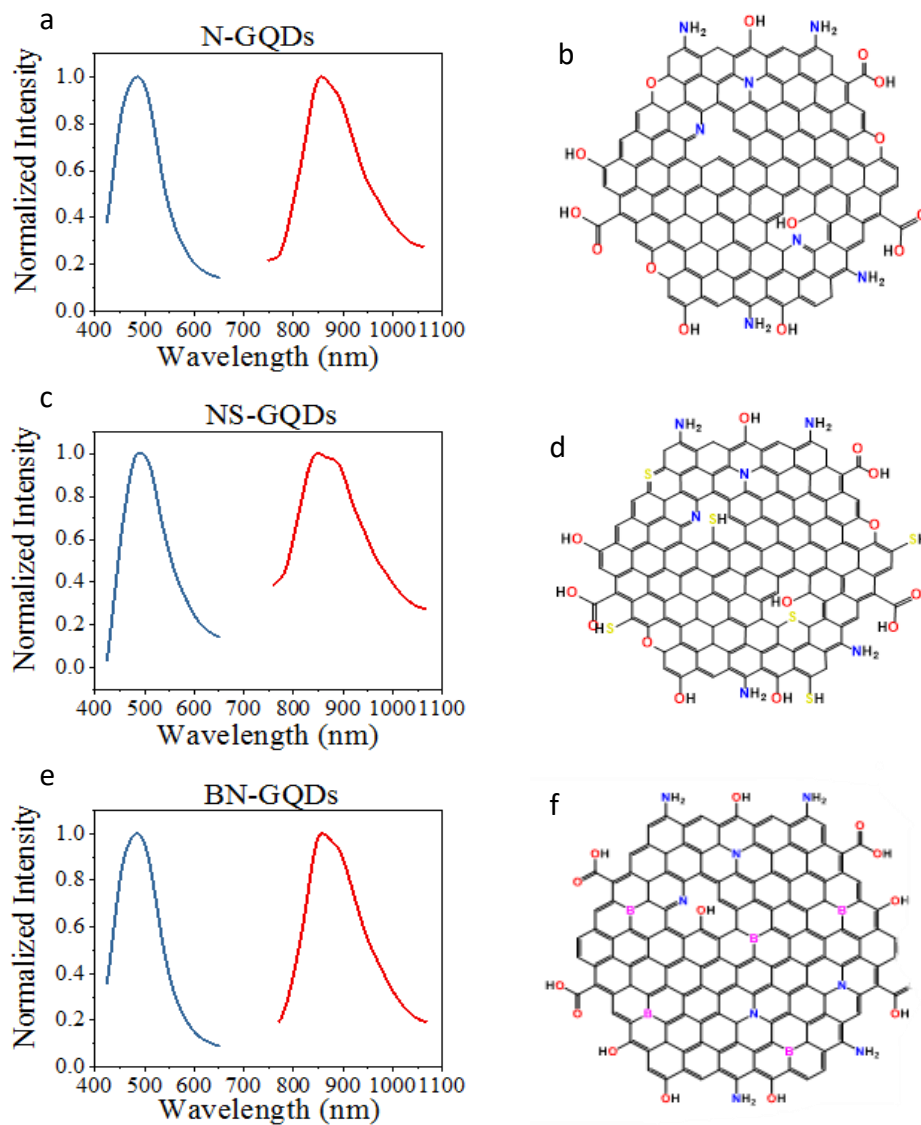


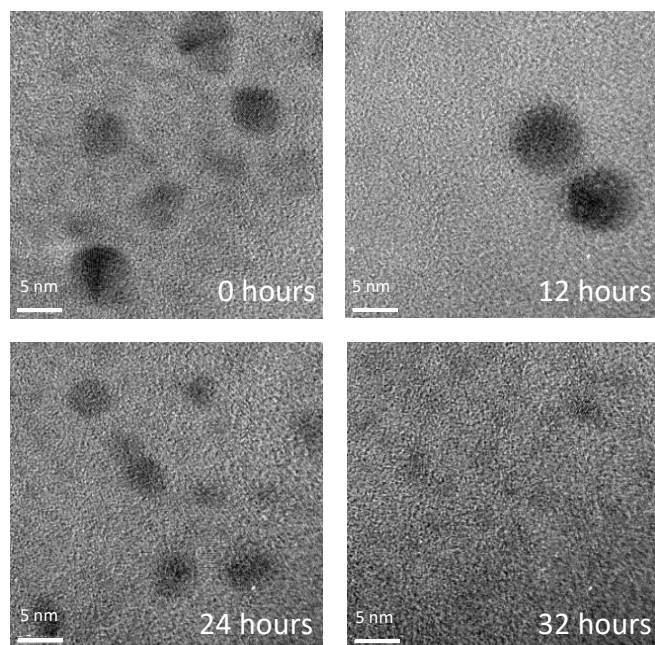
Figure 6. Normalized fluorescence emission spectra in the visible (with 375 nm excitation) and NIR (with 700 nm excitation) for N-GQDs (a), NS-GQDs (c), and BN-GQDs (e) all measured in aqueous dispersions at pH ~7. Model structures of a single layer of the corresponding GQDs: N-GQDs (b), NS-GQDs (d), and BN-GQDs (f).

This visible emission appears to be substantially excitation dependent<sup>82</sup>: broad distribution of GQD sizes allows for exciting different-sized structures at different wavelengths thus resulting into wavelength-dependent confinement-governed emission<sup>82</sup>. The emission in the NIR, however, is potentially related to electronic states at the functional group-derived defects or their arrangements as was proposed in previous works<sup>82</sup> supported by the 10-fold lower NIR fluorescence life times. These fluorescence properties possessed by GQDs make them promising materials for potential use in biological applications, including multicolor imaging. Due to its higher tissue penetration depth up to several centimeters,<sup>176</sup> NIR capabilities may allow for *in vivo* imaging. High quantum yield<sup>82</sup> visible emission from GQDs on the other hand can be advantageously utilized for *in vitro* studies. A capability of imaging across a variety of visible wavelengths makes quantum dots even more versatile for potential applications utilizing image-guided therapy.

### **Cytotoxicity**

Quick and efficient delivery is desirable in order to be compatible for biological studies, while the clearance of the platform from the cells is critical to avoid cytotoxicity and cell damage associated with accumulation of the large amounts of nanomaterials. GQD sizes of 3-5 nm are more advantageous for internalization as opposed to other larger graphitic platforms.





*Figure 7. TEM images of N-GQDs for incubated times in cell media of HEK-293 cells. Scale bar is 5 nm.*

The issue of non-specific toxicity in healthy tissues is one of the major drawbacks for the use of nanomaterial-based platforms, preventing their translation into clinic. Therefore, both the toxicity and internalization must be evaluated to assess the feasibility of graphene quantum dots for *in vitro* studies. MTT cytotoxicity assay performed with HeLa cells treated with each quantum dot type up to maximum concentrations allowed by the synthetic procedure shows no significant cytotoxic response for NS-GQDs and N-GQDs.

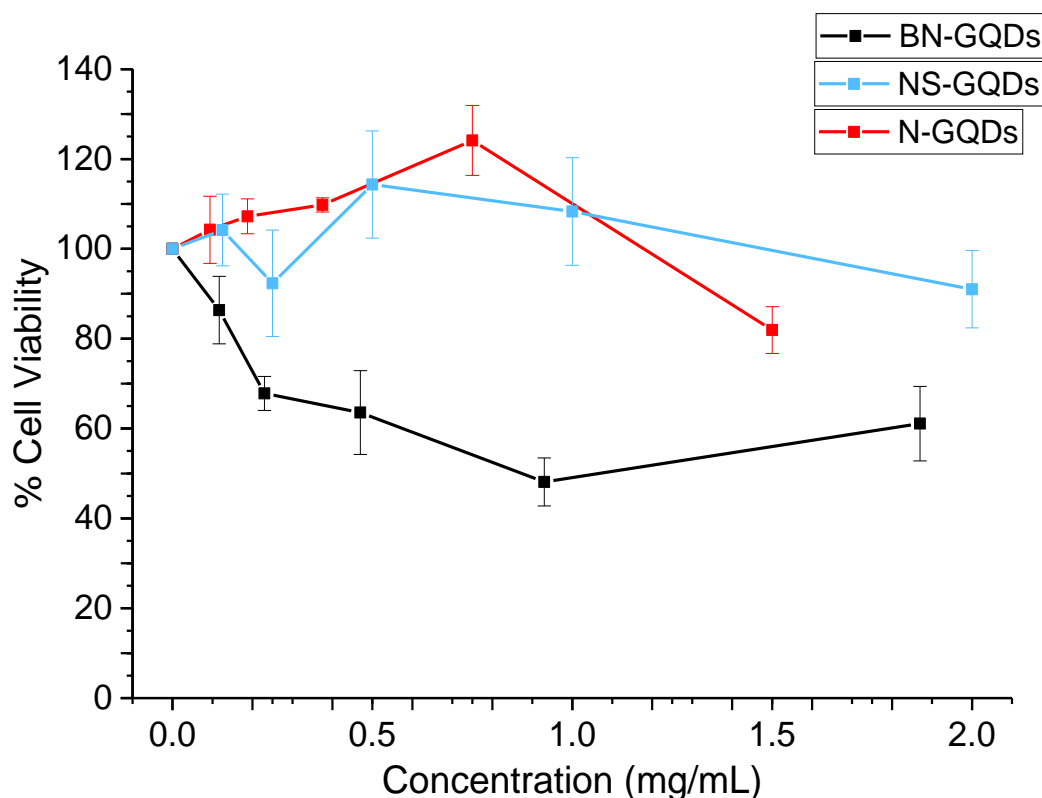


Figure 8. Cytotoxicity of BN-GQDs (black), NS-GQDs (blue), and N-GQDs (red) in HeLa cells showing percent cell viability with respect to the GQD concentration.

Both NS-GQDs and N-GQDs result in exceptional, ~100% cell viability at the imaging concentrations of 1 mg/mL (Figure 8). The apparent increase in cell viability at lower doses could be potentially explained by the metabolizing of either GQDs or any remaining glucosamine impurities by cells. The absence of significant cytotoxic response of the cells to high concentrations of these quantum dots shows that unlike many other nanomaterials they have the potential to be used in biological *in vitro* applications at high doses. However, a significantly greater cytotoxic response is displayed for BN-GQDs with less than 60% cell viability at the 1 mg/mL doses, thus limiting their future applications to the concentrations below 0.1 mg/mL that yield over 80% cell viability. The higher toxicity of BN-GQDs could in part originate from the reducing effects of boron-based addends.

## **Summary**

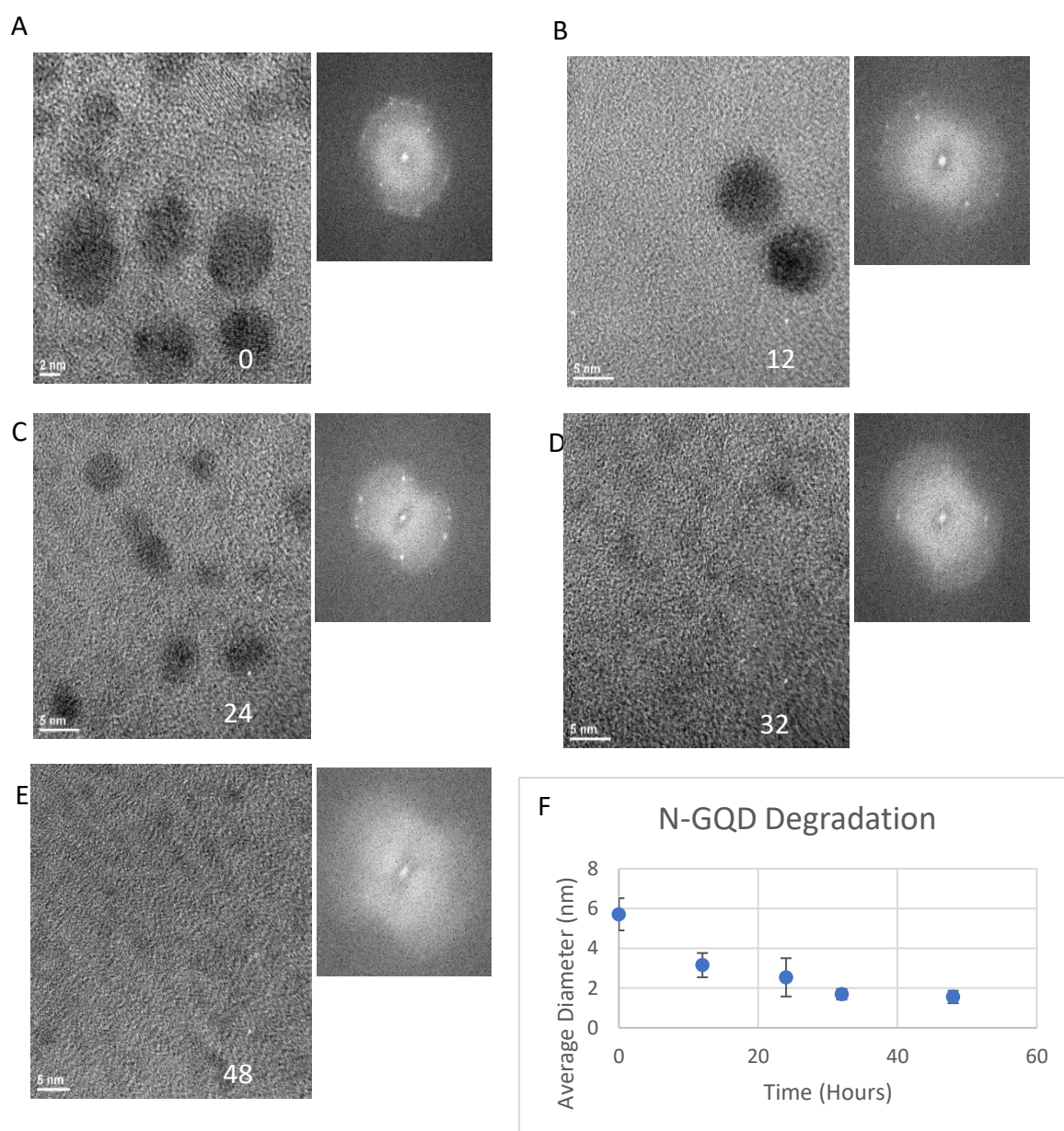
This chapter evaluates the use of graphene quantum dots in biomedical applications. Three different quantum dot types were analyzed (nitrogen-doped, boron-nitrogen-doped, and nitrogen-sulfur doped) and characterized. The crystalline structure of the quantum dots was verified through TEM analysis, suggesting that the quantum dots maintained their advantageous properties. Additionally, the average height of the nitrogen-doped graphene quantum dots was shown to be 1.82 nm, making them suitable for cellular internalization. Through FTIR analysis, it appears as if the dopants are consistent with expected peaks, indicating the successful doping of each quantum dot type. Each quantum dot shows a fluorescence signal in both the visible and NIR and degrade within 24 hours. N-GQDs and NS-GQDs show a minimal cytotoxic response, while the BN-GQDs have a slightly higher cytotoxic response. Overall, the graphene quantum dot types tested appear to be suitable for their use in biomedical applications.

## **Chapter 4- Can Graphene Quantum Dots be used for imaging and delivery?**

### **Results and Discussion**

#### **Internalization**

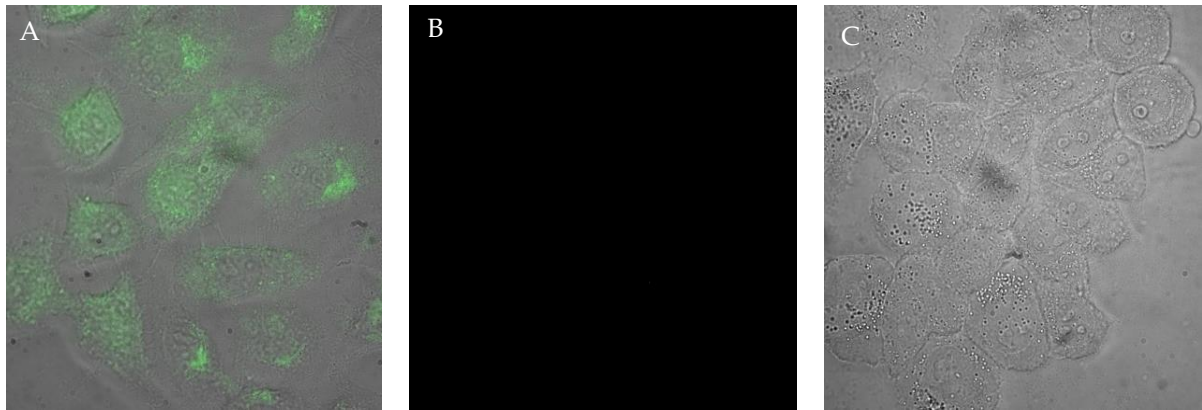
In addition to low cytotoxicity for two types of GQDs, their potential for biodegradation and cellular internalization must be investigated as major factors enabling their utilization in biomedical applications. The lack of biodegradability yielding to offsite accumulation and over time acquired toxicity is by far one of the major drawbacks for utilizing nanomaterials-based delivery vehicles <sup>2, 177</sup>. To ensure full biocompatibility, we image GQDs in HeLa cell culture over time with TEM tracing the QD shapes in the extracellular environments. Images of the GQDs at the incubation times up to 12 hours indicate stable structures and QD sizes. However, further incubation results in significant decrease in size and deterioration of QD structures (Figure 7): at 24 hours, GQD sizes tend to become smaller and they lose their circular shape; by 32 hours, the quantum dots appear to be partially - to fully degraded into monomeric or smaller polymeric structures. This process is verified by the apparent loss of crystallinity of GQDs with incubation time assessed by FFT analysis of transmission electron images (Figure 9) and the flake size analysis performed on over 100 flakes in TEM images showing monotonic GQD size decrease with incubation time.



*Figure 9. (A-E)-TEM images of N-GQDs in HeLa cell culture at varying times with the corresponding FFT image analysis, indicating the crystallinity of the structure exposed to cell media at different times; F- Average diameter of N-GQDs with respect to time, analyzed using TEM images at varying times for over 100 N-GQDs in HeLa cell culture, indicating degradation of quantum dots.*

Such time-dependent biodegradation is rare among carbon platforms and provides a critical advantage making GQDs unique biocompatible nanovehicles for therapeutic transport.

Optically assessed internalization study in HeLa cells is further utilized to evaluate the pathways of different GQD types in biological cells. We use 475 nm excitation known to yield a green emission from these GQDs imaged with 535 nm filter and ensure no autofluorescence (Figure 10) by using lower accumulation and excitation intensity settings providing zero autofluorescence background from control cells.



*Figure 10. Fluorescence microscopy. (a) overlay of GQD emission with the bright field image of HeLa cells transfected with GQDs. (b)(c) – Fluorescence and bright field images of non-treatment control HeLa cells.*

Since these GQDs show remarkable photostability<sup>82</sup>, the maximum integral fluorescence intensity detected intracellularly is assumed to occur at the maximum internalization point. Additionally, extracellular GO is removed by the washing of HeLa cells prior to imaging, leaving only the emission from internalized GQDs. As a result, GQD emission could be used as a measure of their internalization. Such intracellular GQD detection at different time points shows increased accumulation (Figure 11a) for up to 12 hours after which for all GQD types, intracellular emission is diminished.

Since extracellular GQDs were removed, the integrated emission signal calculated per unit cell area and averaged over ~200 cells is deemed to be proportional to the amount of

GQDs internalized into cells helping to assess the most efficient internalization time frame (*Figure 11*). Similar internalization trend holds for all GQD types and agrees with images of individual cells and cell clusters (*Figure 11*). This is expected as the GQDs tested in this work have similar structures and sizes only varying in doping types and levels affecting so far only the cytotoxicity. Emission decrease at 24 hours for all quantum dot types is indicative of potential excretion of GQDs from the cells or, possibly, their partial degradation.

A colocalization study undertaken with regular fluorescence (*Figure 13 (a-c)*) and confocal microscopy imaging (*Figure 13 (d-f)*) helps to assess GQD potential for drug and gene delivery by compartmentalizing green GQD emission with blue nuclear (DAPI) and red (Lysotracker Red) lysosomal staining. Each fluorophore's emission is also assessed individually to verify GQD location within the cells (*Figure 12*).

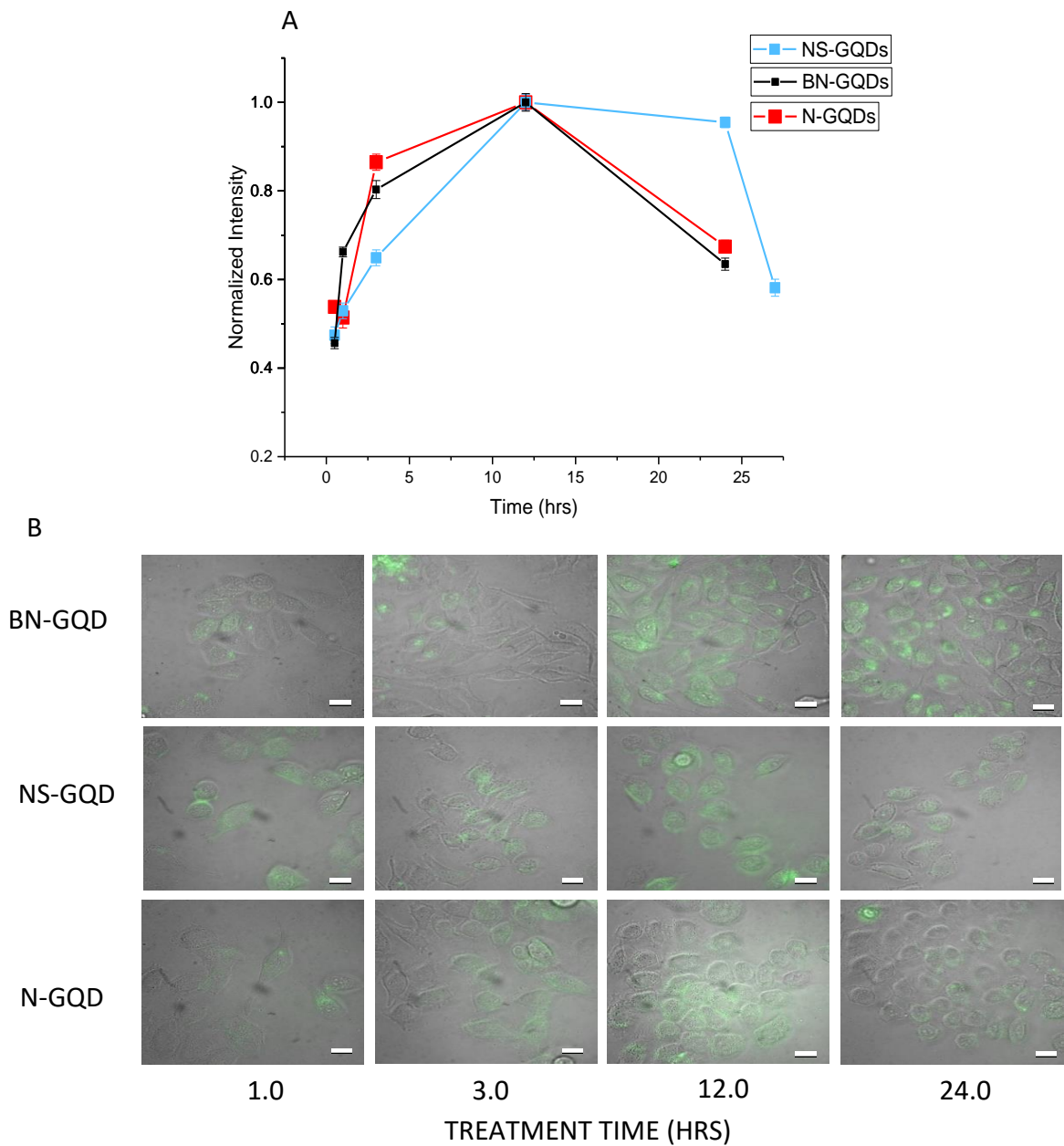


Figure 11. a) Cell internalization/excretion timeline assessed through the normalized GQD emission intensity per unit area in HeLa cells at different time points for N-GQDs (red), NS-GQDs (blue), and BN-GQDs (black). Error bars for some points are within their size. b) Fluorescence emission of various quantum dot types in HeLa cells at a number of treatment time points. Excitation and emission filters used:  $475 \pm 25$  nm and  $535 \pm 20$  nm. Scale bar =  $10 \mu\text{m}$ .



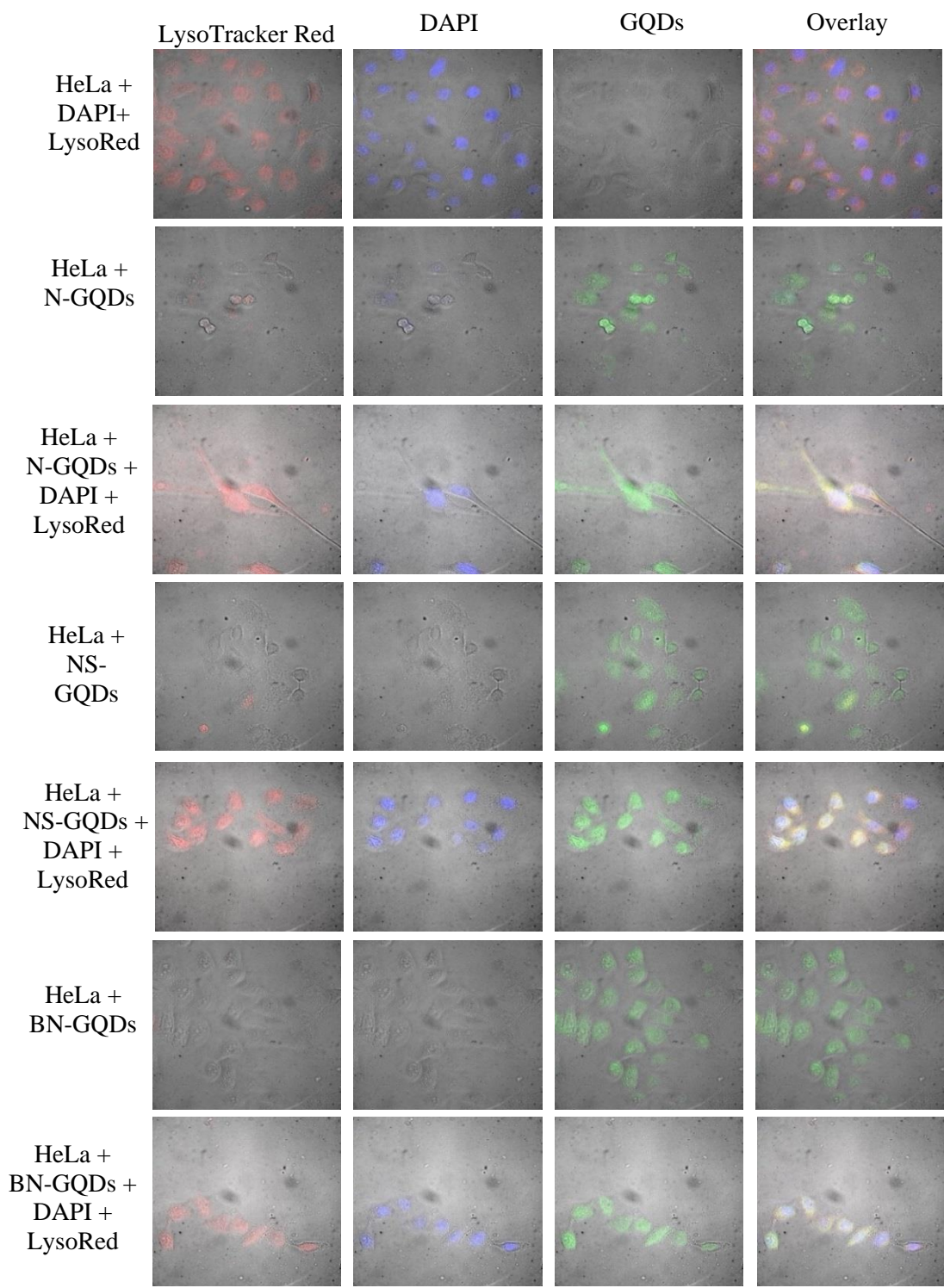
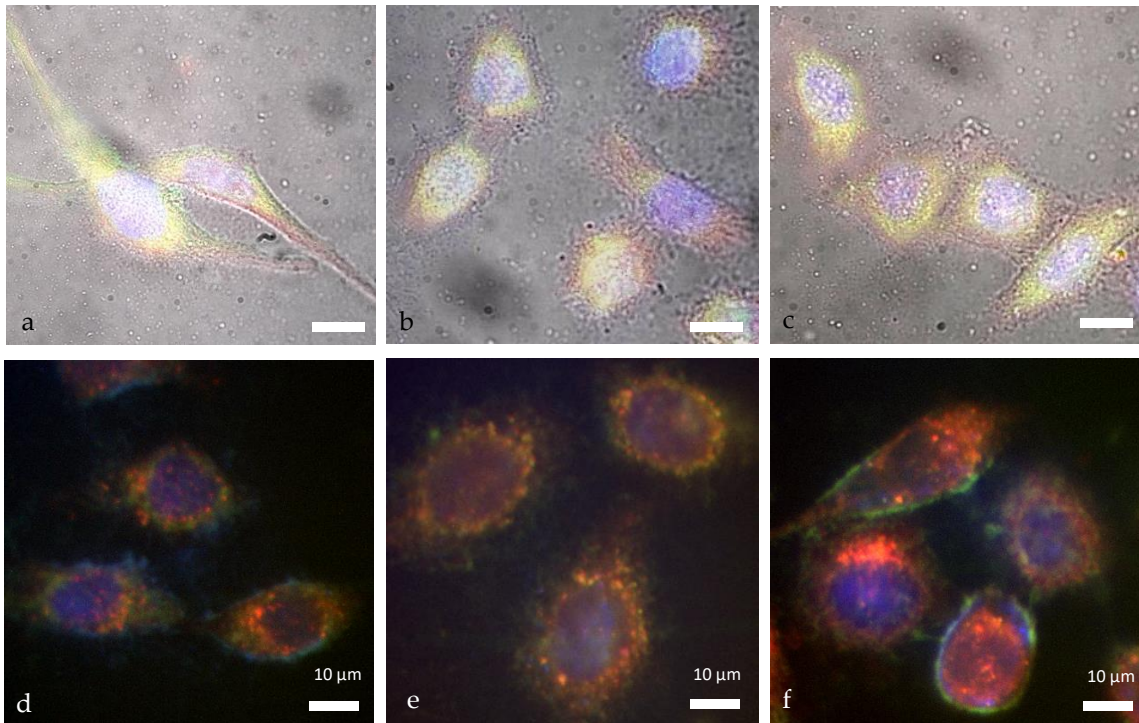
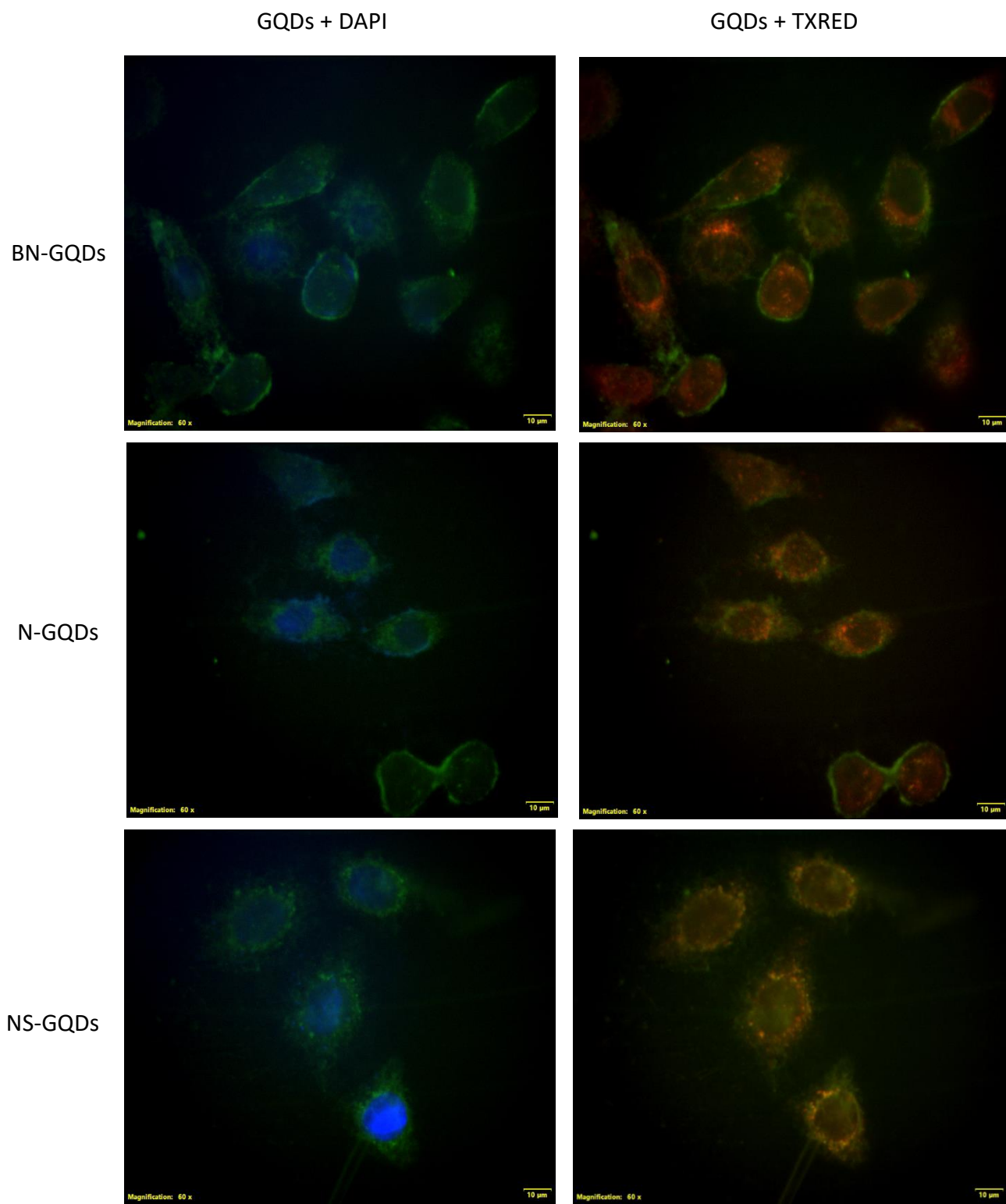


Figure 12: Colocalization image matrix showing GQD location within the cells for various GQD types and fluorescent staining. Red: LysoTracker Red, excitation at 540 nm emission recorded at 600 nm; Blue: DAPI, excitation at 375 nm emission recorded at 450 nm; Green: GQDs, excitation at 475 nm emission recorded at 535 nm.

Confocal images taken at the variety of focal planes throughout the cells indicate that all GQD types appear to at least partially localize with lysosomes as their fluorescence coincides with lysotracker emission (Figure 13 (d-f) and Figure 14 right panel) indicating endocytosis as one of the potential entry pathways, and mostly reside in the cytoplasm.



*Figure 13. Fluorescence colocalization images of (a) N-GQDs, (b) NS-GQDs, and (c) BN-GQDs emission (green) with DAPI (blue) and Lysotracker Red (red) staining within HeLa cells. Confocal colocalization images of (d) N-GQDs (scale bar=10 $\mu$ m), (e) NS-GQDs (scale bar=10 $\mu$ m), and (f) BN-GQDs (scale bar=10 $\mu$ m).*



*Figure 14: Confocal overlay image matrix indicating localization in the lysosomes and some in the nucleus; Texas Red exc.*

Some GQD emission in the cytoplasm is not localized within endosomes suggesting either their endosomal escape or other entry mechanisms. GQDs as opposed to many other graphitic materials<sup>141</sup> show some co-localization with nuclei best seen in the fluorescence overlays of only DAPI and GQD emission (Figure 14). This suggests that GQDs may serve as delivery agents into cytoplasm and may have potential for reaching the cell nucleus.

### **Multicolor Fluorescence Imaging**

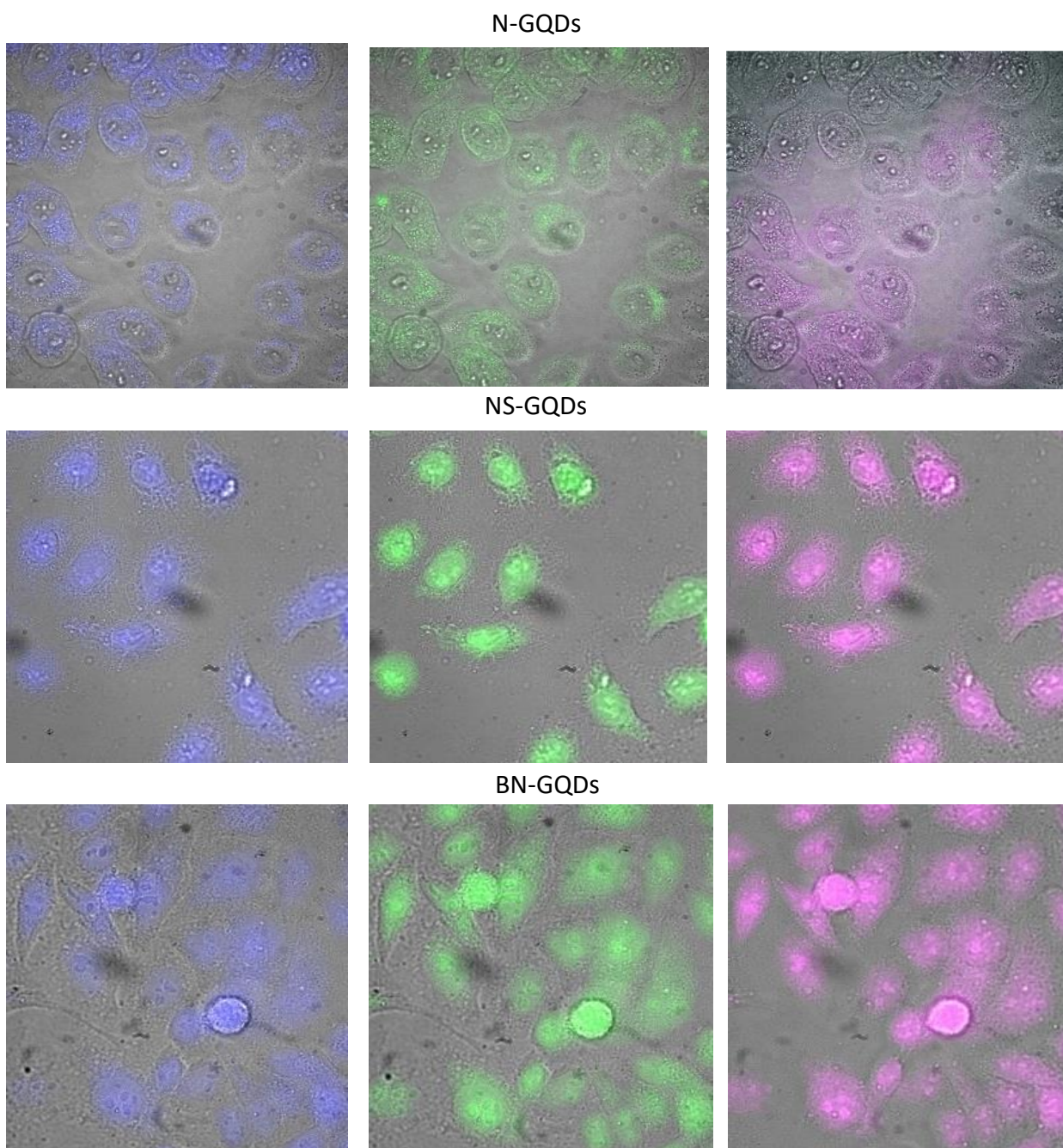
Unlike a single fluorophore exhibiting fluorescence emission in a particular spectral range, GQDs also offer multicolor imaging capabilities in the visible as well as the near-infrared due to the excitation dependence of their fluorescence. Each quantum dot type is imaged at a variety of excitation and emission wavelengths, and shows emission as it is internalized into HeLa cells in blue (450 nm), green (535 nm), and NIR (750 nm) (Figure 16). These nanomaterials have stable fluorescence that does not show detectable fluctuation with prolonged irradiation (Figure 15) and thus allows for intracellular imaging both in the visible and the near-IR.



stack-3\_MMStack\_Pos0.ome\_xvid.avi

*Figure 15: Microscopy video of GQDs for 420 seconds, showing no photobleaching during that time. Imaged with 450 nm excitation and 535 nm emission.*

Capability of multi-wavelength imaging suggests the versatility of GQDs as an imaging platform that can be combined with many other visible biological fluorescence markers in vitro: there will always be spectral areas where GQD emission is not overlapped with the dyes.



*Figure 16. Multicolor imaging of N-GQDs, NS-GQDs, and BN-GQDs in blue, green, and near-IR. Excitation and Emission filters used are Blue- exc:  $375 \pm 14$  nm em:  $450 \pm 20$  nm; Green- exc:  $475 \pm 25$  nm em:  $535 \pm 20$  nm; near-IR- exc:  $650 \pm 20$  nm em:  $750 \pm 20$  nm.*

Additionally, GQD near-infrared emission can be potentially utilized for imaging in vivo, as near-IR yields deeper penetration into biological tissues. If successful, this could allow for non-

invasive optical imaging of the therapeutic pathways simultaneously with drug delivery in small animal models.

As a multifunctional delivery/imaging/sensing platform, GQDs provide a variety of advantages over other nanomaterials-based systems. Many imaging and drug delivery nanoparticle systems, such as aptamer-conjugated GNPs for DOX transport<sup>145</sup> or metal-organic nanocomposites for delivery and imaging of therapeutic agents<sup>178</sup>, generate systemic toxicity, which is still a limiting issue. Graphene quantum dots, on the other hand, present a modifiable platform for drug attachment that provides effective imaging and cellular internalization with a 100% cell viability at substantially higher concentrations reaching 1 g/mL for N-GQDs and NS-GQDs. GQDs are simple and inexpensive in preparation as opposed to many nanoscale therapeutic delivery systems that require elaborate multistep synthesis<sup>117</sup>. High quantum yield (over 60% for N-GQDs<sup>82</sup>) intrinsic fluorescence of GQDs allows for imaging without the attachment of additional fluorophores, often used to track many other nanoparticles<sup>179, 180</sup> and adding to their toxicity profile. GQDs show substantial biodegradability within 36 hours that sets them ahead of all non-biodegradable nanoscale platforms, accumulation of which in the cells and tissues may hinder their long term use<sup>177, 178, 181</sup>. In addition, GQDs offer multicolor visible and visible and near-IR imaging capabilities for both in vitro and in vivo detection unlike the majority of nanoscale drug delivery platforms, or even other graphene quantum dots<sup>182, 183</sup>, which only offer imaging in the visible.

## **Summary**

GQDs utilized in this work have for the first time been developed in our lab to provide unique capabilities not present in other current GQD platforms. We also propose graphene quantum dots as imaging and delivery agents for cancer therapeutics, as they have superior properties of smaller size, no cytotoxicity, ease in preparation and apparent biodegradability.

Toxicity analyses show that within the imaging concentrations used throughout the study, N-GQDs and NS-GQDs are essentially harmless to the cells, while BN-GQDs offer some cytotoxic response and should be restricted to lower concentrations of  $\sim 0.1$  mg/mL. Each quantum dot type is approximately 3-5 nm in size, therefore making them easily internalized by the cells, with their maximum internalization occurring at 12 hours. This is verified both visually and analytically, indicating that the GQDs are also excreted within 24 hours, making them suitable for drug delivery as they are not expected to accumulate in cells for an indefinite time as many current delivery vehicles do. Additionally, GQDs studied here are biodegradable with over 36h degradation period allowing time for drug release and at the same time making them safe to use in living organisms as they are not expected to accumulate and are hypothesized to degrade in glucose-based monomers. N-GQDs, NS-GQDs, and BN-GQDS all exhibit fluorescent emission that peaks both in the visible to the near-IR, suggesting their imaging capabilities are superior to other nanomaterials used in biomedical applications only exhibiting visible fluorescence. These GQDs can be used for multicolor imaging, indicating the possibility of imaging in cells via visible fluorescence and in tissues via NIR emission.

## Chapter 5- Do GQDs offer sensing capabilities?

### Overview

For GQDs to be used also as a sensing platform, we explore their ability to optically detect the difference in pH of the biological environments. GQD fluorescence exhibits substantial response to pH that can be potentially derived from protonation/deprotonation of oxygen-containing functional groups similarly to that observed for graphene oxide<sup>154</sup>. This effect can be beneficially utilized for biosensing of cancerous environments as those typically have lower pH<sup>184, 185</sup> due to excretion of lactic acid<sup>186</sup>. Fortunately, the significant variation of N-GQDS and NS-GQD spectra falls within the biological pH (6-8) range suggesting a promise for a deterministic spectral sensing. At the basic pH – blue (469 nm) and at the acidic pH – green (500 nm) shoulders of GQD spectra become more dominant (Figure 17 (a), (c)) yielding intensity ratios of approximately 1.7 for N-GQDs and 1.6 for NS-GQDs.



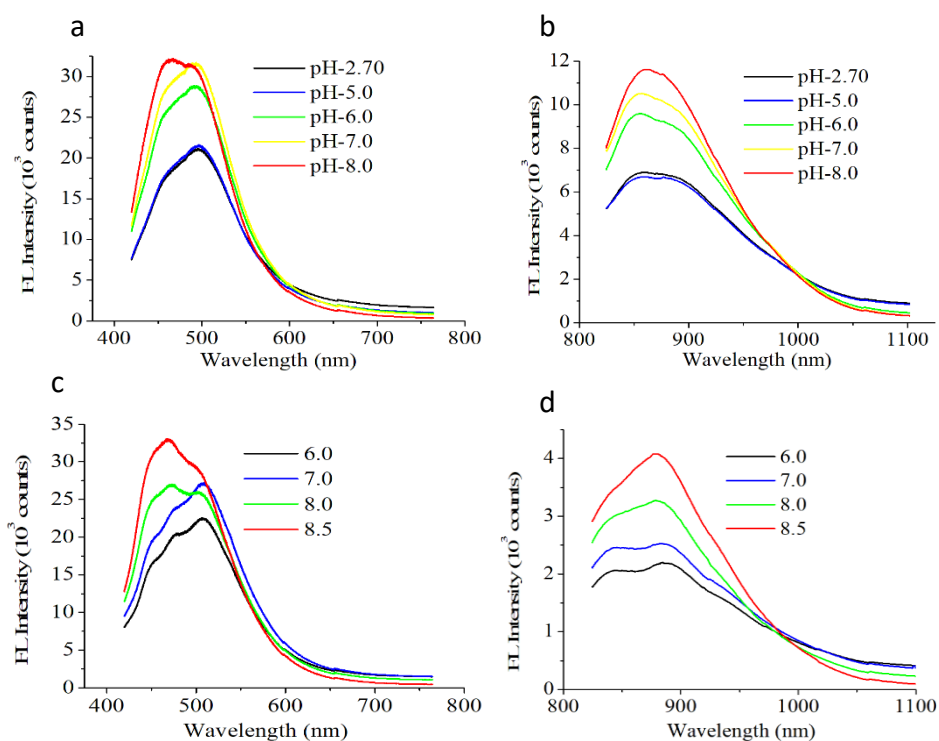
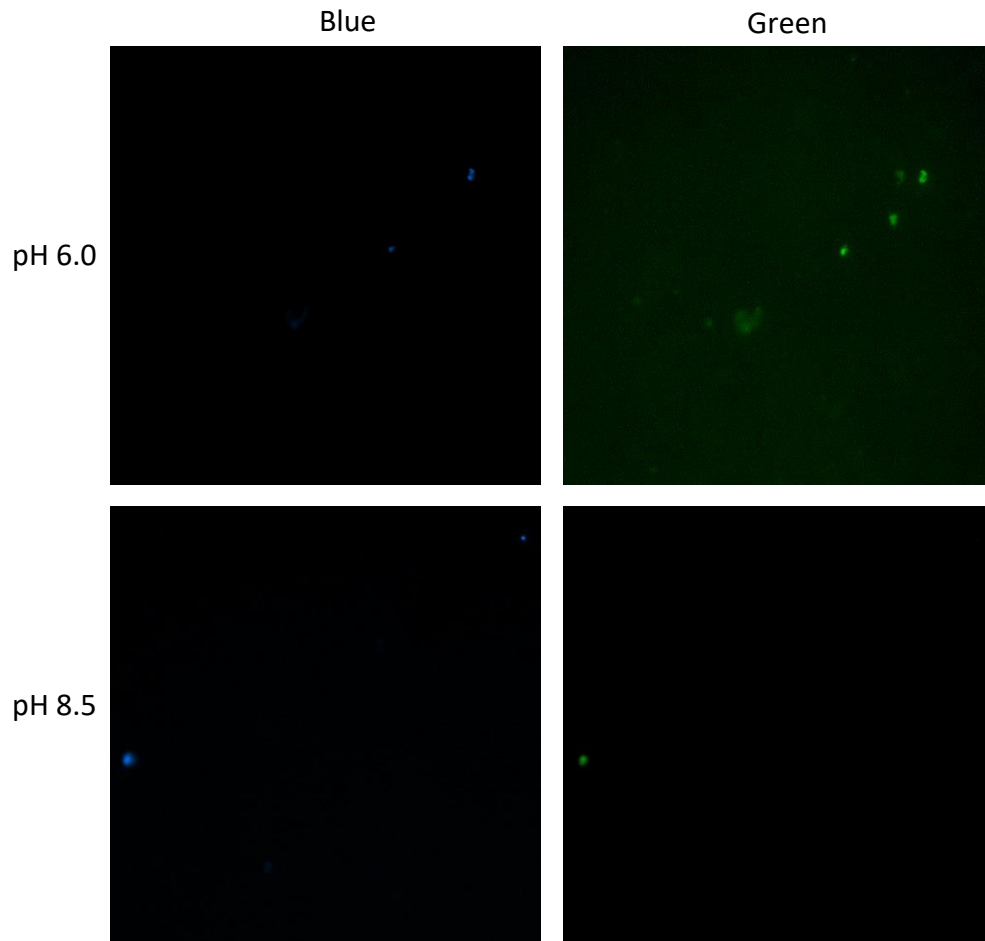


Figure 17. Fluorescence spectra of N-GQDs at varying pH levels in the (a) visible and (b) NIR and NS-GQDs in the (c) visible and (d) NIR.

Although this effect is less significant than intensity variations observed for pH-sensor visible fluorophores<sup>187, 188</sup>, the ability to vary spectral signature rather than emission intensity that can be quenched by a number of extrinsic factors may allow for a more deterministic and reliable pH sensing. The emission spectra for BN-GQDs show no spectral variation with pH, potentially due to the passivation of a number of functional groups by boron dopants and their electronic environments. pH-induced spectral changes are also observed in the NIR spectra for both N-GQDs and NS-GQDs (Figure 17 (b), (d)) suggesting a potential for pH sensing in the NIR with superior penetration depth in biological tissue. However, initial sensing feasibility studies in this work focus on pH sensing via GQD emission in the visible, as it exhibits spectral

changes that can be more conveniently discriminated with spectral filters utilized in the present microcopy system.

Prior to cell studies pH-sensitivity of GQDs is first assessed on microscopic level imaging those on a cover slip at various pH levels (Figure 18).


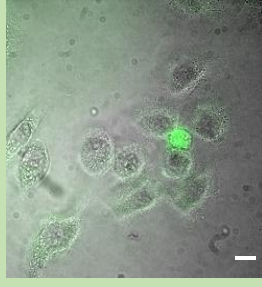
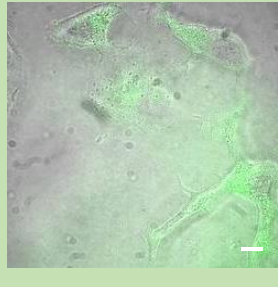

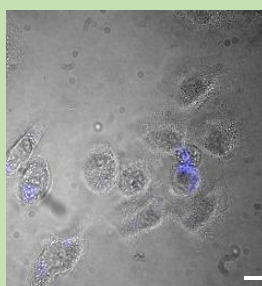
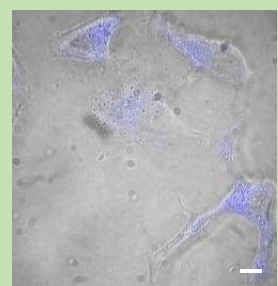


*Figure 18: Images of N-GQDs at varying pH levels. Blue imaged with excitation 375 nm, emission at 450 nm. Green imaged with excitation 475 nm, emission at 535 nm.*

This simple test shows qualitative apparent difference in GQD blue to green emission between acidic and basic pH environments (green emission is brighter in acidic rather than basic conditions) further suggesting GQD potential for pH-sensing of microenvironments. To verify the *in vitro* sensing capabilities of the N-GQDs and NS-GQDs, we introduce suspension of

each quantum dot type to two cancer and one healthy cell lines (HeLa, MCF7, and HEK-293). Here the cells are imaged without a washing step so that the extracellular quantum dots will remain: the pH sensing of extracellular environments could be an important marker of high extracellular lactic acid levels in cancer cells. Based on pH-induced variation of the spectral features (Figure 17), we propose using green/blue emission ratios as quantitative assessment of pH-induced GQD emission changes. Fluorescence imaging at two wavelengths, in green (535nm) and blue (450nm) also allows better visualization of the difference in GQD blue versus green emission between cancer and healthy cell lines. For N-GQDs (Table 1 images) and NS-GQDs (Table 2 images) it is evident that the emission in green is more significant in cancer versus healthy cellular environments.

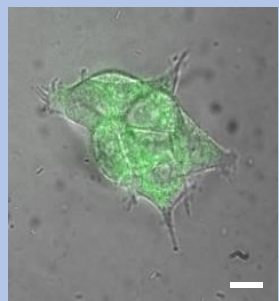
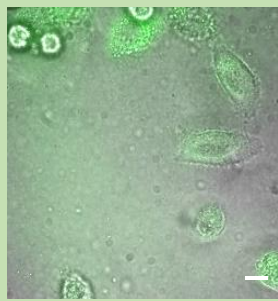


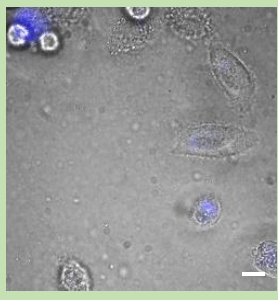
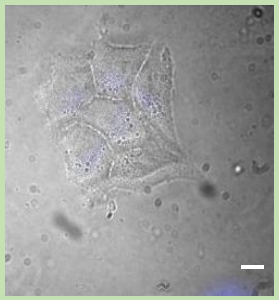
Table 1. N-GQD intracellular and extracellular green/blue emission intensity ratios across healthy (HEK-293) versus cancer (HeLa and MCF-7) cell lines, and corresponding fluorescence images demonstrating emission differences. Scale bar= 10 $\mu$ m.

535/450 nm Intensity Ratios Across Cell Lines N-GQDs			
	HEK-293	HELA	MCF-7
INTRACELLULAR	1.73 $\pm$ 0.49	2.56 $\pm$ 0.05	2.27 $\pm$ 0.63
EXTRACELLULAR	1.22 $\pm$ 0.01	8.27 $\pm$ 0.05	8.38 $\pm$ 0.63
Green (535 nm)			
Blue (450 nm)			

Green to blue ratios of background-subtracted average fluorescence intensities per unit area for each cell further provide quantitative estimates of pH variations between cancer and healthy environments (Table 1, Table 2) indicating significant extracellular variations of GQD emission between healthy (HEK-293) and cancer (HeLa, MCF-7) cell lines. Green to blue emission ratios calculated for NS-GQDs and N-GQDs in extracellular cancer cell environments are significantly higher than those assessed in healthy cell environments by the

factors of 1.6 to 6.8 respectively, suggesting a capability of deterministic ratiometric spectral cancer pH detection by the GQDs in vitro. A less pronounced trend was observed among the intracellular ratios. This could be explained by intracellular pH buffering by cell proteins and phosphate buffers maintaining cell pH within a narrow biological range<sup>189, 190</sup>. Thus, mainly extracellular GQD emission is considered in this work as a potential mechanism of pH sensing of cancerous environments. The emission of BN-GQDs does not indicate pH-dependence spectrally and therefore was not analyzed in vitro for pH-based cancer detection. The ratios observed in the in vitro study are generally larger than those expected from the variation of GQD spectral signatures with pH. Such a dissimilarity can be caused by either the effects of complex biological redox environments not present in aqueous suspensions, and/or by integration of the emission intensity over the whole spectral range permitted by the microscopy filters in the in vitro studies. In these studies GQDs were also generally imaged near the cells, assessing the significantly lower pH microenvironments in the vicinity of cells where the lactic acid is excreted<sup>191, 192</sup> and thus yielding more significant intensity variations.

Table 2. NS-GQD intracellular and extracellular green/blue intensity ratios across healthy (HEK-293) versus cancer (HeLa and MCF-7) cell lines, and corresponding fluorescence images demonstrating emission differences. Scale bar= 10 $\mu$ m.

535/450 nm Intensity Ratios Across Cell Lines NS-GQDs			
	HEK-293	HELA	MCF-7
INTRACELLULAR	1.09 $\pm$ 0.01	2.18 $\pm$ 0.35	1.73 $\pm$ 0.09
EXTRACELLULAR	1.50 $\pm$ 0.01	4.96 $\pm$ 0.35	3.57 $\pm$ 0.09
Green (535 nm)			
Blue (450 nm)			

### Summary

This fluorescence signal of graphene quantum dots is pH-dependent, allowing the GQDs to detect a difference between cancerous (HeLa and MCF-7 cells) and healthy (HEK-293 cells) environments. *In vitro* data derived from over 200 cell and extracellular environments statistics reveals an efficient cancer sensing that provides a promise of using GQDs as nanoscale pH sensors. Furthermore, pH-dependence of NIR emission indicates the potential for GQDs to be applied as sensors of low depth cancerous environments *in vivo* or *ex vivo*. GQDs are

affordable, easy to produce, and agents possessing the properties that could help revolutionize cancer treatment detection and potentially aid in detecting tumor boundaries for surgical tumor removal. However, the main novelty of doped GQDs tested in this work is their multimodality: GQDs can simultaneously perform several desired theranostic functions: being a biocompatible/degradable platform for imaging, delivery, and cancer detection.

## **Chapter 6- Can GQDs be used to create a targeted cancer treatment formulation suitable for biomedical applications?**

### **Overview**

As a platform with a variety of oxygen and nitrogen-containing functional groups, N-GQDs exhibit the potential for the attachment and delivery of multiple cancer therapeutics. The lack of specificity of current chemotherapeutics calls for utilizing novel cancer-selective treatment avenues. A strategy selected in this work is based on the reducing environment of cancer cells, which leads to the production of reactive oxygen species (ROS) due to their high metabolic rate and mitochondrial dysfunction. This reducing environment of cancer cells is caused by the production of superoxide, which is prevalent in cell signaling for tumor proliferation<sup>164</sup>. This is less prominent in non-cancer cells, where reactive oxygen species are more easily mitigated<sup>165</sup>. Excessive ROS generation in cancer cells by the therapeutic is therefore expected to create a toxic effect<sup>166</sup>, that is aimed to be used as a cancer-selective therapeutic approach. Ferrocene (Fc) is a known reducing agent generating a cytotoxic response specifically in the reducing environments of cancer cells linked to the production of reactive oxygen species during the redox cycle of iron<sup>167, 168</sup>. The attachment of ferrocene to the electron-rich N-GQD platform may facilitate enhancement of its redox-based toxicity to cancer cells. In addition to cancer-selective treatment, targeting utilized currently in a variety of nanoformulations can aid to further focus the treatment to cancer cells only. This work utilizes one of the common and highly effective approaches involving the use of hyaluronic acid (HA) to target CD44, a receptor overexpressed in cancer cells<sup>169</sup>. While the functional roles of CD44 are not fully understood<sup>169-171</sup>, CD44 and its variants play a role in cancer development and progression<sup>171</sup>. HA is able to target and activate the CD44 receptors, which induces both cell proliferation and



cell survival<sup>171</sup>. HA functionalization of the therapeutic Fc unit will allow targeting a variety of cancer cell lines known to overexpress these CD44 receptors, including cervical cancer (HeLa) cells<sup>170, 171</sup> used in this work. Additional to the HA targeting, the nanoscale size of the N-GQDs will also facilitate the preferential accumulation in cancer tissues via enhanced permeation retention (EPR) effect.

In the present therapeutic platform, GQD emission will be used to image the delivery pathways of Fc-HA without the need of additional fluorophores, HA will provide targeting and Fc will provide cancer-selective treatment. As opposed to the aforementioned therapeutic nanoformulations performing only a few of those functions, the proposed model will be fully multifunctional and, therefore, more versatile, ultimately providing a new solution for safer cancer-selective and targeted diagnostics.

## **Results and Discussion**

### **Characterization**

Nitrogen-doped graphene quantum dots developed in our previous work<sup>159</sup> are chosen as convenient multifunctional delivery/imaging agents for the Fc-based therapeutic model. These GQDs have an advantage of high biocompatibility, exhibit intrinsic fluorescence for image-based tracking and can be effectively internalized and excreted/degraded by cells. Most importantly, GQDs have both carboxyl and amino groups, which we utilize for the attachment of targeting and treatment moieties leading to the synthesis of Fc-GQD-HA formulation. Hyaluronic acid is used as the targeting agent, as it preferentially binds to the overexpressed CD44 receptors on several cancer cell types<sup>193, 194</sup>, including HeLa cells. This provides a versatile mechanism of achieving preferential accumulation of the therapeutic in a variety of cancers. The formulation synthesis can be separated in 3 critical steps. In step 1 of the

synthesis, carboxylic acid moieties of the quantum dots are modified to yield amine functionalized N-GQDs primed for further functionalization. In step 2, carboxylic acid groups of HA are covalently attached to the amine groups, now present on the N-GQDs. In step 3, ferrocene-COOH, selected as an oxidative stress-based therapeutic<sup>195</sup>, is linked to the remaining NH<sub>2</sub> groups on the GQDs, to serve as a therapeutic part of the joint formulation. In this procedure, centrifugal filtration and washing steps ensure the purity of the final formulation (Figure 19 C).

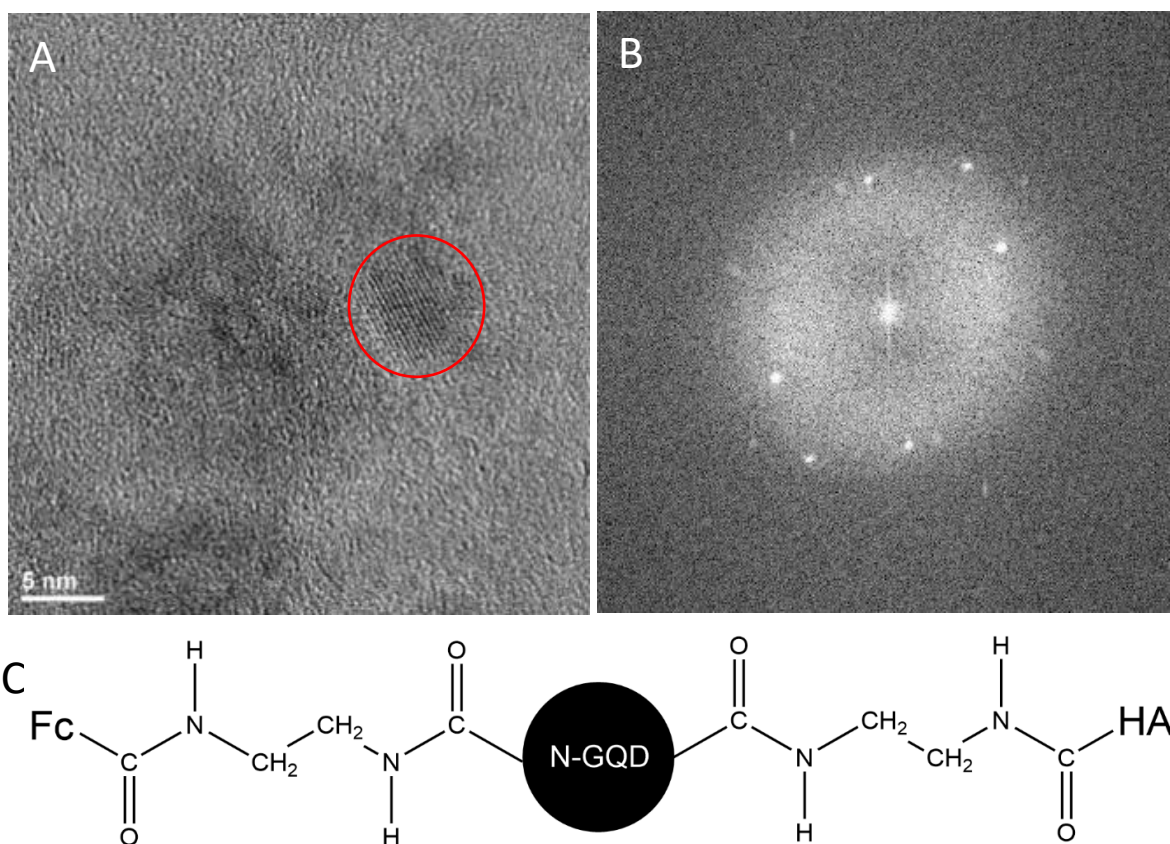
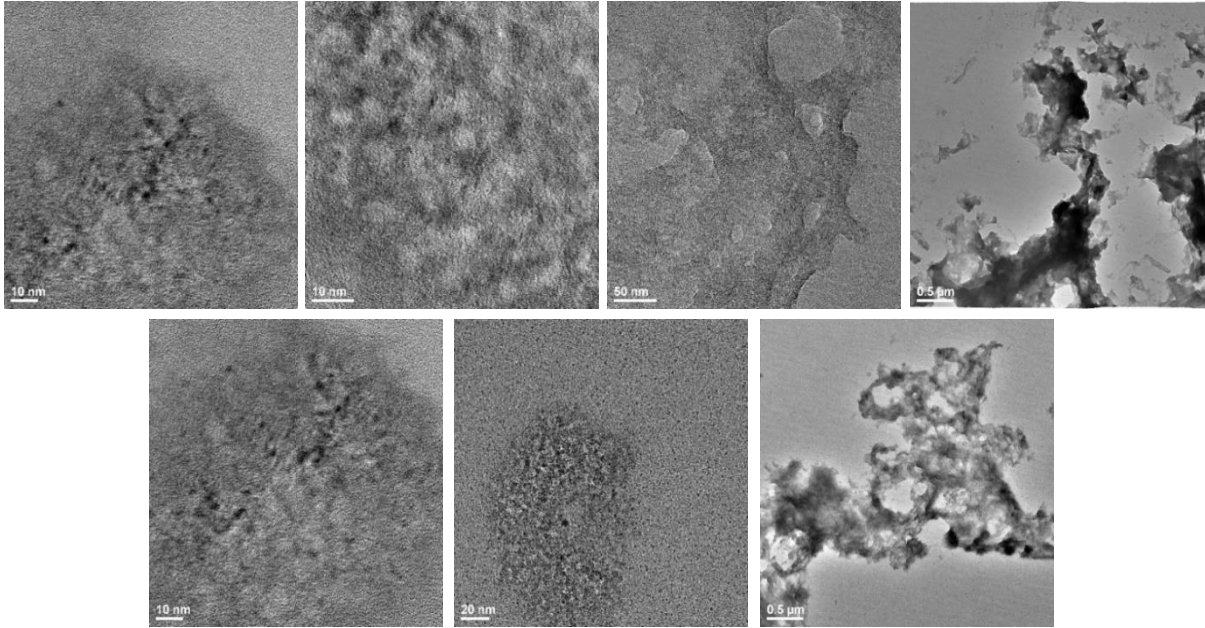


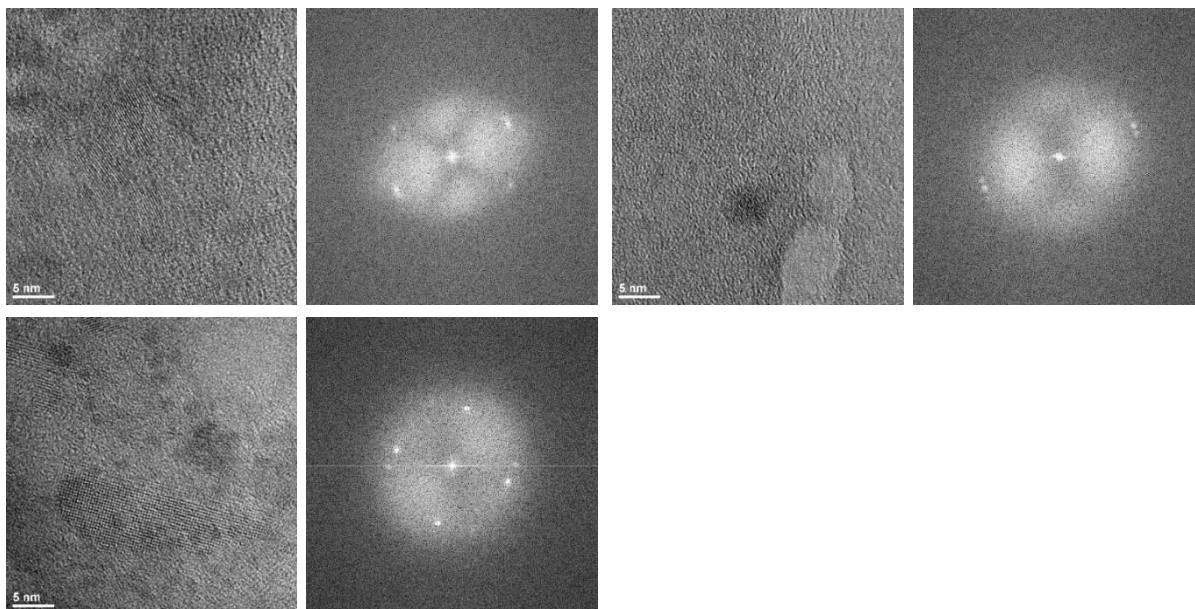
Figure 19 (A) TEM image of Fc-GQD-HA formulation (red outline is to serve as a guide to an eye) with (B) corresponding FFT analysis, verifying the crystalline structure and the graphene lattice of the quantum dots. Scale bar = 5 nm. (C) Proposed connectivity of the Fc-GQD-HA formulation.

The synthesized hybrid is analyzed via Transmission Electron Microscopy (TEM) to confirm the size, composition, and the crystalline structure of the N-GQD platform.



*Figure 20. TEM images of synthesized Fc-GQD-HA formulation.*

TEM scans (Figure 19(A), Figure 20) depict the discernable graphitic lattice fringes of GQDs, while the FFT images (Figure 19(B), Figure 21) verify their crystallinity, indicating that the integrity of the GQD platform in the Fc-GQD-HA formulation is not affected by chemical functionalization.



*Figure 21. TEM images of Fc-GQD-HA hybrids with corresponding FFT analysis to confirm crystallinity.*

EDX analysis is further used to confirm weight/atomic percentage of expected elements (Figure 23, Figure 22) including carbon, oxygen, chlorine, nitrogen, and iron averaging those over several sample areas.

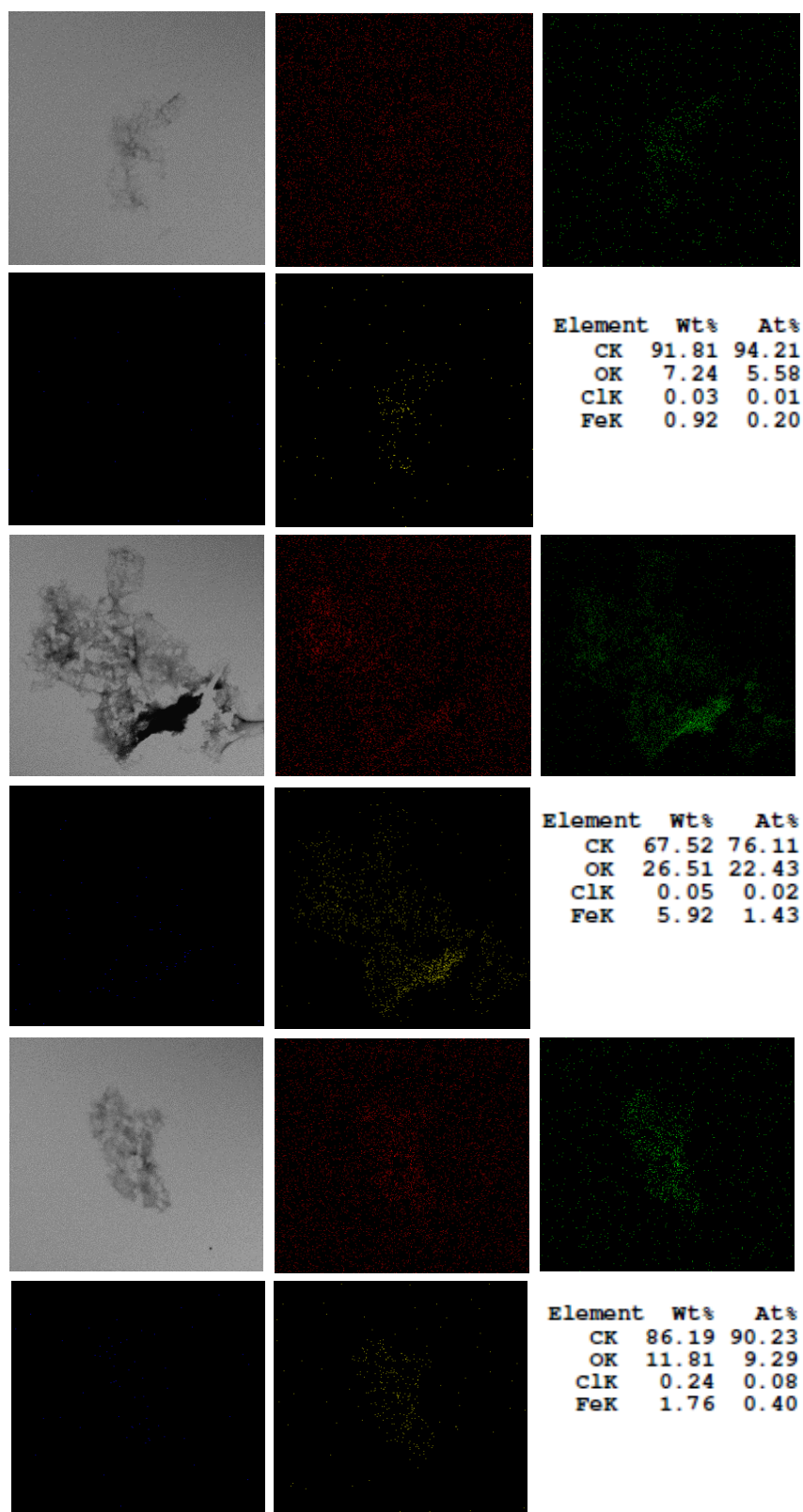


Figure 22. EDX mapping of Fc-GQD-HA agglomerates on the TEM grid.

Over 83 atopic % carbon is expected to project from the backbone of the GQDs, while oxygen/nitrogen can be attributed mainly to the functional groups left from glucosamine or formed/added in the synthesis. EDX analysis also ensures that the dichloromethane solvent is fully removed from the product as only 0.09% of Chlorine is detected, while the presence of ~2.8% iron indicates the successful incorporation of the ferrocene-COOH therapeutic. Thus, elements present in the mapping are consistent with the expected structure of the Fc-GQD-HA formulation.

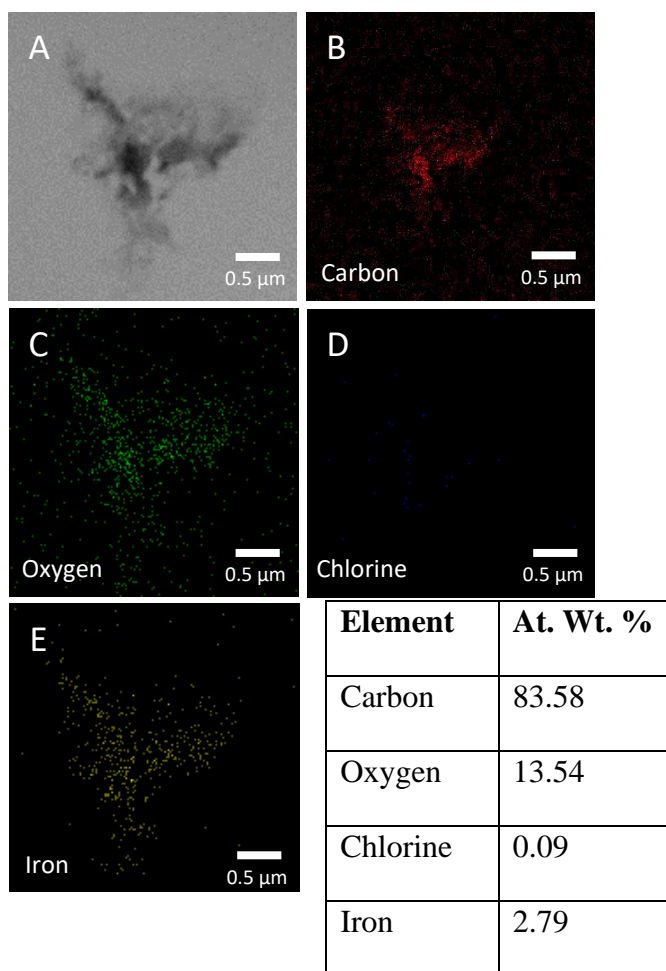


Figure 23. (a) TEM image of Fc-GQD-HA agglomerate. EDX elemental maps of the same area for (b) carbon, (c) oxygen, (d) chlorine, and (e) iron with their averaged atomic weight percentages listed in the table.

The presence of the expected functional groups is further assessed by the Fourier transform infrared spectroscopy. We expect an increase in COOH due to the addition of hyaluronic acid, containing an abundance of the carboxylic group, which is expected to affect the peak located at  $1410\text{ cm}^{-1}$ . Additionally, we expect the appearance of the amide peak at  $\sim 1600\text{ cm}^{-1}$  as the primary amines of the linker react with COOH groups of the HA forming amide. This feature can be indeed observed in Figure 24. Although structural characterization is suggesting successful formulation synthesis, its further utilization depends on the performance of 3 critical functions: the capability of fluorescence imaging, targeting, and redox-based cancer-specific treatment due to the reducing Fc moiety.

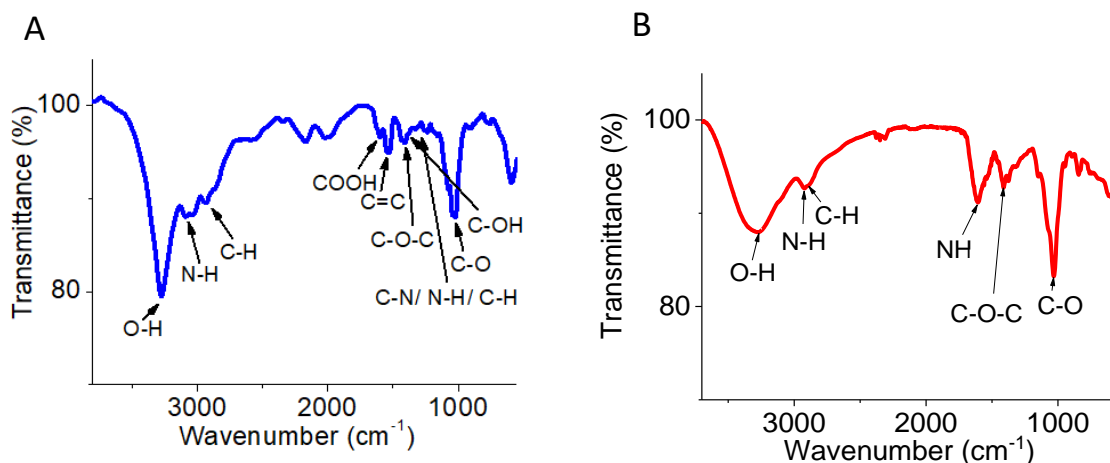


Figure 24. FTIR spectra of (a) pristine N-GQDs and (b) freeze-dried Fc-GQD-HA formulation.

### Summary

A targeting moiety (hyaluronic acid) and a redox treatment agent (ferrocene) are attached to the N-GQDs covalently in a 3-step procedure akin to peptide synthesis. TEM images of the Fc-GQD-HA formulation confirm the crystallinity of the product, while EDX mapping

indicates successful incorporation of the Fc ROS-generating unit. FTIR signifies toward the formation of amide groups and, therefore, also confirms successful synthetic attachment of the formulation.



## Chapter 7- Can the treatment formulation be used for imaging and delivery?

### Results and Discussion

#### Fluorescence

Absorbance spectrum of the Fc-GQD-HA formulation (Figure 25b) is different from that of pristine N-GQDs<sup>173</sup>, with a substantial increase in absorption peak located below 200 nm associated likely with HA absorption (Figure 25). The red shift of the ~300 nm feature potentially arises due to COOH functionalization affecting  $n \rightarrow \pi^*$  transitions. This also points to the successful formation of the Fc-GQD-HA formulation, while the preserved emission in the visible allows the N-GQDs to retain their capability as an imaging platform.

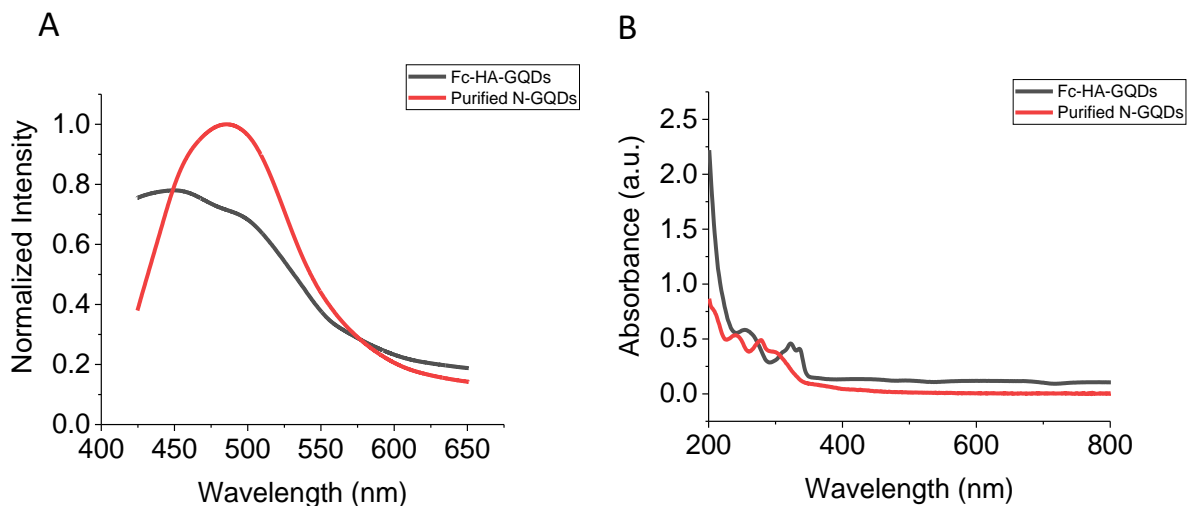


Figure 25. (a) Fluorescence spectrum of Fc-GQD-HA formulation (black) and purified N-GQDs (red) in the visible with excitation at 400 nm, measured in aqueous suspension; (b) absorbance spectra of Fc-GQD-HA formulation (black) and pristine N-GQDs (red).

Imaging and targeting capabilities of the synthesized hybrids are assessed *in vitro* via the analysis of their fluorescence emission in cancer versus non-cancer cells. The fluorescence of the GQD-Fc-HA appears stable in multiple media including complete medium, HeLa cell

medium, and mouse blood serum (Figure 26) for up to 48 hours suggesting sufficient for our experiments stability *in vitro* and giving the promise for their stability *in vivo*.

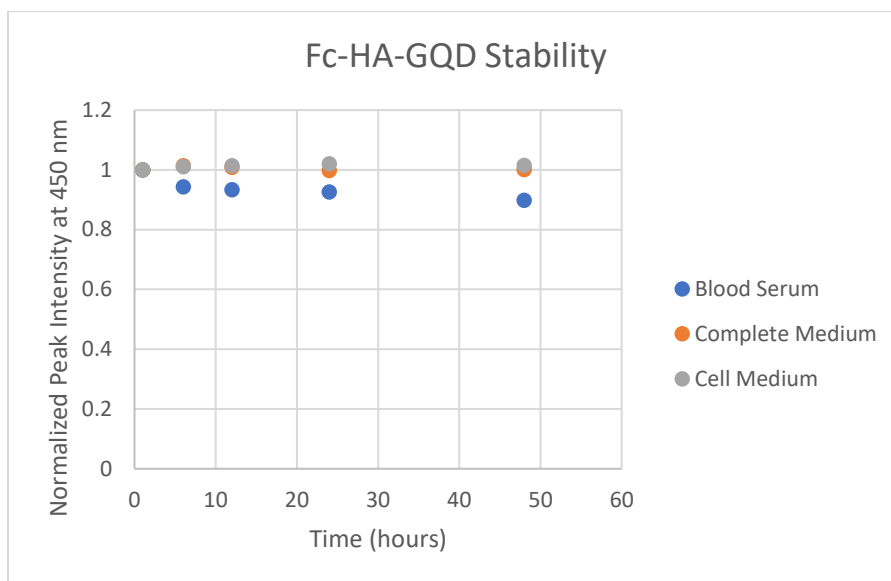
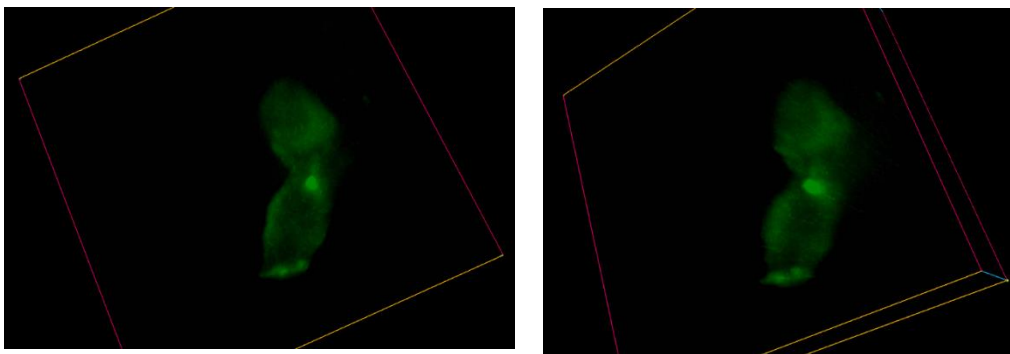


Figure 26. Normalized peak fluorescence at 450 nm with 350 nm excitation of Fc-HA-GQD formulation in blood serum (blue), complete medium (orange), and HeLa cell medium (gray) at 1, 6, 12, 24, and 48-hour timepoints indicating formulation stability.

A high temporal stability of GQD fluorescence<sup>159</sup> also permits the quantitative analysis of their presence in the cells (Figure 27) via assessing the fluorescence intensity per unit cell area as the measure of their concentration.



*Figure 27. 3D fluorescence images of Fc-GQD-HAs in HeLa cells built by z-stack accumulation of confocal microscopy images of GQD emission at different planes within the cells collected with 480 nm excitation and 535 nm emission. Right and left images are rendered at different angles of observation.*

This advantage over rapidly photobleaching molecular fluorophores is used to identify and quantify both the intracellular accumulation and targeting of the CD44 receptors by the attached HA. Cellular internalization of the formulation is first qualitatively verified by confocal fluorescence microscopy of Fc-GQD-HAs in HeLa cells. The 3D cell image created by z-stacking image planes indicates substantial GQD fluorescence signal originating from inside the cells (Figure 27).

### **Internalization**

Following quantitative analysis of internalization/ excretion is essential as it may allow determining a potential administration schedule to avoid adverse cytotoxic effects due to a build-up of therapeutic intracellularly.

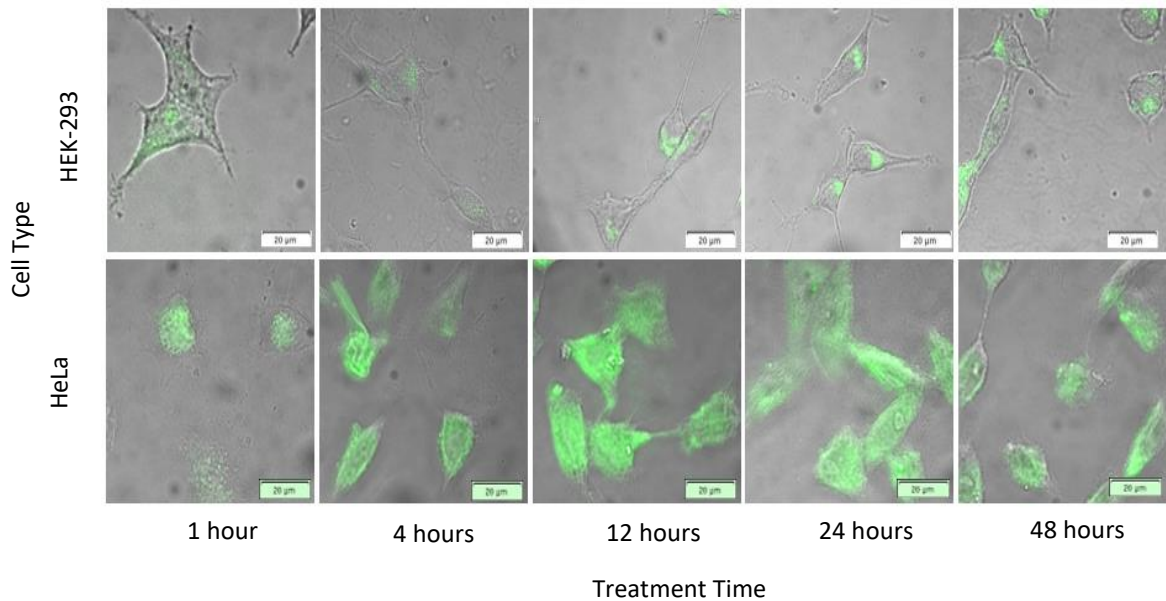


Figure 28. Fluorescence emission of 1 mg/mL of the Fc-GQD-HA formulation in HeLa cells and HEK-293 cells at 1, 4, 12, 24, 48-hour treatment time points.  $475 \pm 25$  nm excitation and  $535 \pm 20$  nm emission filters used. Scale bar = 20  $\mu$ m.

In order to accomplish this assessment, extracellular Fc-GQD-HAs are removed via an additional washing step prior to imaging using 0.5 mL of 1X PBS and the image settings are adjusted to the level at which autofluorescence is negligible, altogether allowing the detection of only internalized Fc-GQD-HA formulation fluorescence with 475 nm excitation. The integrated emission signal per unit area in this condition is expected to be proportional to the amount of product internalized by the cells (Figure 28). Similarly to previous assessments of GQD accumulation *in vitro*<sup>159</sup>, this analysis shows maximum internalization of the Fc-GQD-HA hybrids at 12 hours of incubation for both HeLa and HEK-293 cells followed by excretion and potential degradation, while *in vivo*, shorter timeframes could be expected.

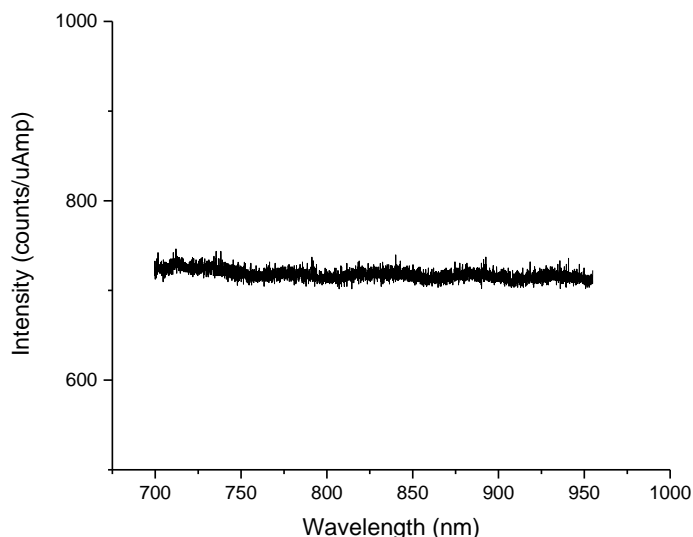
## Summary

The maintained fluorescence capabilities of the Fc-GQD-HA formulation *in-vitro* suggest that it can be used for successfully for imaging. The effective internalization of the Fc-GQD-HA formulation in cancer cells traced by its intracellular fluorescence is maximized at 12 hours with further potential excretion. The intracellular delivery of the therapeutic is imaged via confocal microscopy mapping of GQD accumulation throughout the cell and shows accumulation mainly in the cytoplasm. Thus, we verify both imaging and delivery capabilities of Fc-GQD-HA.

## Chapter 8- Does the treatment formulation offer sensing capabilities?

### Results and Discussion

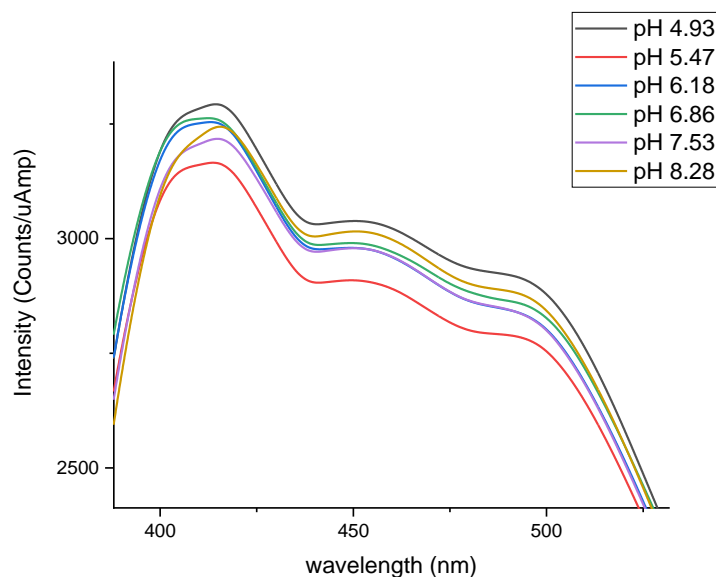
Fc-GQD-HA formulation successfully retains the visible emission of the GQD platform exhibiting a broad feature in the visible (Figure 25a) expected to be confinement-related<sup>173</sup> consisting of fluorescence peaks from a variety of different-sized GQD structures and carbon lattice substructures. The NIR fluorescence originating in the pristine N-GQDs from defect-related states at the functional groups<sup>173</sup> is diminished in the final Fc-GQD-HA formulation (Figure 29), suggesting that the majority of the functional groups of the N-GQD platform responsible for this emission are now passivated by the covalent attachment of HA and Fc-COOH.



*Figure 29. NIR fluorescence spectra of Fc-GQD-HA formulation*

pH-induced effects are inhibited likely for the same reason, while N-GQDs showed pH detection sensors *in vitro*<sup>159</sup> (Chapter 5), the Fc-GQD-HA formulation shows minimal to no change in the fluorescence spectra at varying pH levels (Figure 30) and only the intensity

change due to pH. Although pH sensitivity is present, without the variation in the spectral landscape, just the quenching of the emission spectra are not deterministic enough to serve as an optical pH sensing mechanism as the quenching of the GQD fluorescence can be facilitated by the means unrelated to pH change.



*Figure 30. Fluorescence spectra of Fc-GQD-HA Treatment formulation at varying pH levels.*

### **Summary**

According to the NIR fluorescence spectra, as well as the indeterminate visible fluorescence spectra at varying pH levels, the Fc-GQD-HA treatment formulation does not offer sensing capabilities. Sensing is potentially suppressed because the functional groups participating in protonation/deprotonation in acidic/basic environments in the GQDs are covalently altered in the Fc-GQD-HA treatment formulation upon its formation.

## **Chapter 9- How does developing combined imaging/targeting/treatment formulation affect treatment efficacy and targeted accumulation?**

### **Results and Discussion**

The development of the treatment formulation is intended to enhance both targeting and cancer treatment efficacy. In order to evaluate this hypothesis, cytotoxicity assays and fluorescence analysis must be conducted. The expectation is to observe preferential toxicity to cancer cells over non-cancer cell types, which can be observed through MTT cytotoxicity assays. Additionally, the use of the GQD platform in the treatment formulation will be evaluated to determine if there is any impact on the treatment formulation. Afterwards, fluorescence analysis of the Fc-GQD-HA formulation introduced to both cancer and non-cancer cell types will be evaluated to quantify the targeting capability of the treatment formulation.

### **Cytotoxicity**

Yet another important property of the engineered Fc-GQD-HA formulation is the selective cytotoxicity to cancer cells due to the generation of reactive oxygen species by ferrocene<sup>196</sup>. A selectivity of reduction-mediated toxic response is warranted by the difference between cancer and non-cancer cells, with cancer cells having a more negative, reducing environment due to the suppression of oxidative phosphorylation in the mitochondria<sup>197, 198</sup>. Fc conjugates<sup>199-201</sup> show cancer-specific toxicity with an increase in toxic response toward lower potentials tied to generation of reactive oxygen species (ROS) during the reduction cycle of the iron. The negative redox potential of iron is directly correlated to its increased cellular toxicity.<sup>200</sup> The Fc-GQD-HA formulation is, therefore, expected to generate more ROS in the reducing environment of cancer cells, suggesting that the ferrocene yields a cancer-selective therapeutic



effect. Non-cancer cells, on the other hand, are more likely to moderate ROS generation: as low levels of ROS are required for cell maintenance and renewal, those are mitigated throughout the life cycle<sup>165</sup> of the cell by cellular repair mechanisms. As a result, the ROS generation is likely to be mitigated in non-cancer cells as opposed to tumor-derived cells, which, together with HA targeting, is expected to generate cancer cell-specific therapeutic effect with little toxicity to normal cells. Cytotoxic anticancer effects of the Fc-GQD-HA formulation are therefore explored *in vitro*.

GQDs exhibit no substantial cytotoxic response on their own<sup>159</sup> at concentrations up to 1 mg/mL, suggesting that as a platform for the formulation they are not expected to affect therapeutic efficacy. The joint Fc-GQD-HA formulation, however (Figure 33a), exhibits a higher cytotoxic response in HeLa cells over the HEK 293 (Figure 33a) suggesting selective toxicity to cancer cells with up to 20% lower cancer cell viability. Comparison of the half maximum effective concentration ( $EC_{50}$ ) values, shows that the Fc-GQD-HA formulation is over 2 times more efficacious in HeLa cells ( $EC_{50}=2.630$  mg/mL) as opposed to the HEK-293 cells ( $EC_{50}= 6.004$  mg/mL) showing substantial redox selectivity. The ferrocene therapeutic when tested alone, however, shows the half maximum effective concentration in breast cancer MCF-7 cells ( $EC_{50}=0.89$  mM) to be nearly 4 times lower than in HEK-293 cells ( $EC_{50}= 3.33$ mM) (Figure 31).

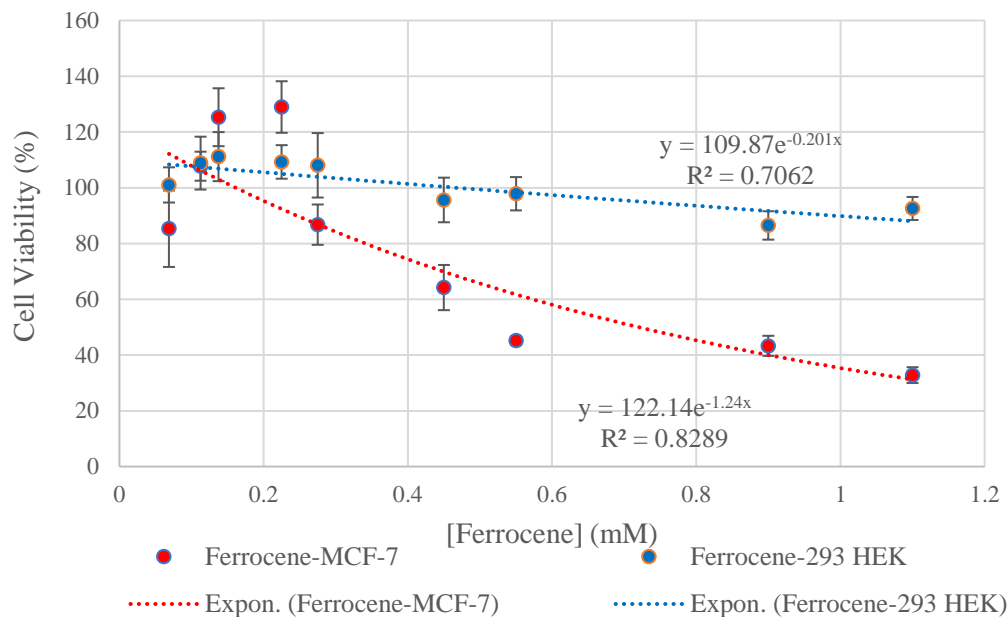
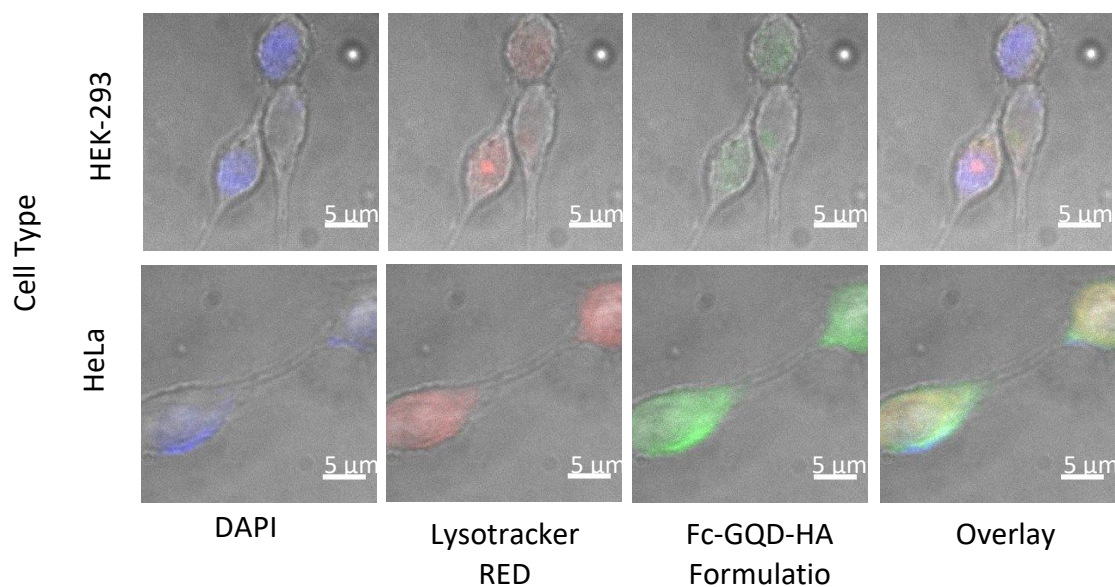


Figure 31. Cytotoxicity of ferrocene in MCF7 cells and HEK-293 cells.

The lower  $EC_{50}$  value of independent ferrocene indicates a stronger effect of the drug alone in part due to the encapsulation with the GQD-FC-HA platform as well as potential electron transfer to from/to the GQDs. However, it is most important to note that the toxicity of the Fc-GQD-HA formulation in non-cancer cells is substantially masked by the GQD platform having twice the  $EC_{50}$  of ferrocene in non-cancer cells. This gives promise to alleviating toxic effects of Fc therapeutics<sup>202</sup> in non-cancer cells.

Comparing the GQD emission intensities in cancer (HeLa) cells overexpressing CD44 receptor with those in HEK-293 cells that do not overexpress it shows a drastically (by over a factor of 6) enhanced accumulation in cancer cells (Figure 35) observable even from individual cell images (Figure 28). Such substantial enhancement in internalization indicates successful targeting capability with the HA functional group of the hybrid. The internalization pathways, due to targeting expected to be at least partly receptor-mediated<sup>203</sup>, lead to the further colocalization of the GQD emission with cell compartments. A colocalization study between

GQD emission in green, blue nuclear DAPI staining and cytoplasmic lysosomal lysotracker red performed via confocal microscopy locates Fc-GQD-HAs primarily in the cytoplasm (although with a lesser degree of lysosomal accumulation as compared to pristine GQDs<sup>159</sup>), and minimally in the nucleus (Figure 32). This altogether indicates the successful intracellular targeted delivery of the Fc redox agent by GQDs-HA allowing for its cancer-selective therapeutic effect.



*Figure 32. Fluorescence colocalization images of HeLa and HEK-293 cells stained with DAPI (blue), Lysotracker Red (Red) and introduced to Fc-GQD-HAs (green) for 12 h.*

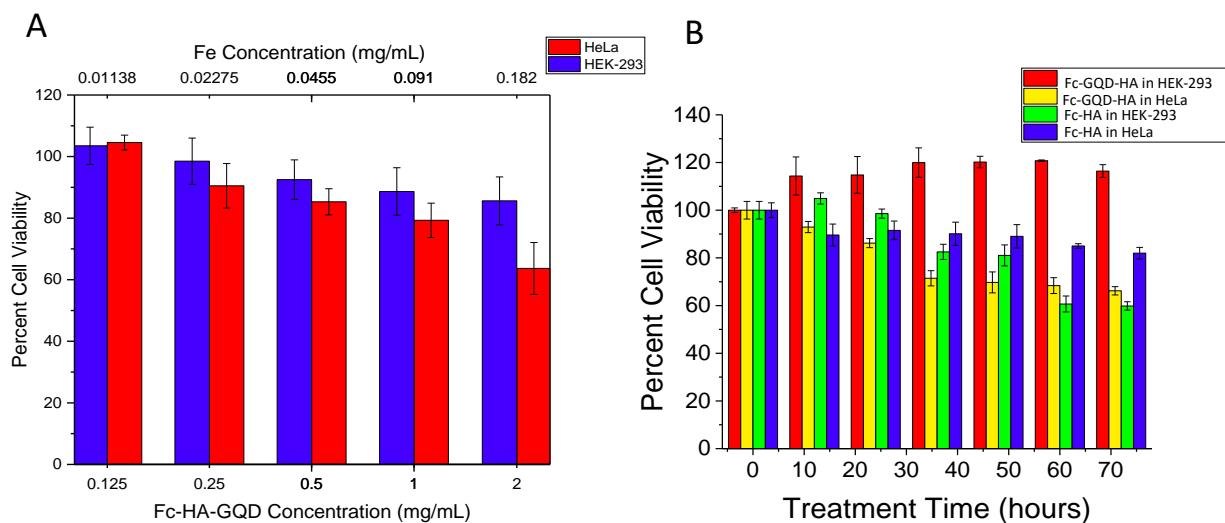
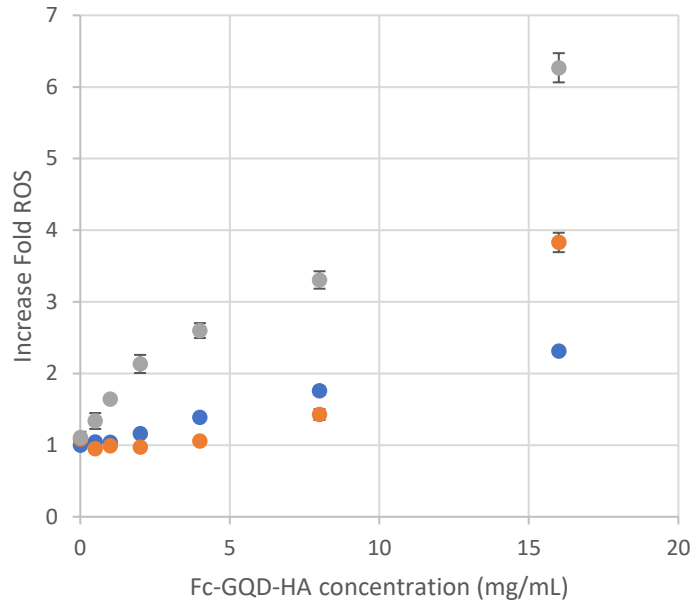


Figure 33. (a) MTT assay for the cytotoxicity of Fc-GQD-HA formulation at varying concentrations in HeLa (red) and HEK-293 (blue) cells. (b) MTT cell viability assay over a prolonged timeline. Fc-GQD-HA formulation in HEK-293 cells (red) and HeLa cells (yellow) compared to Fc-HA in HEK-293 cells (green) and HeLa cells (blue). Introduced at a concentration of 1 mg/mL.

While inducing toxic response in cancer cells, the synthesized formulation still exhibits substantial biocompatibility in the non-cancer (Figure 33), at high concentrations of 2 mg/mL yielding over 80% cell viability. Such cancer-selective treatment is highly desirable, although the difference between 80 and 60% cell viability for non-cancer and cancer cells at the 24h MTT time point is not substantial enough to claim highly effective cancer selective therapy. However, when evaluated at later time points, even the fully non-toxic 1 mg/mL concentrations of Fc-GQD-HA show substantial anti-cancer efficacy (Figure 33b) while not having any negative effects on the non-cancer cells. Increase in cell viability over 100% for the formulation in HEK-293 cells is similar to that observed for pure N-GQDs<sup>159</sup> and is attributed

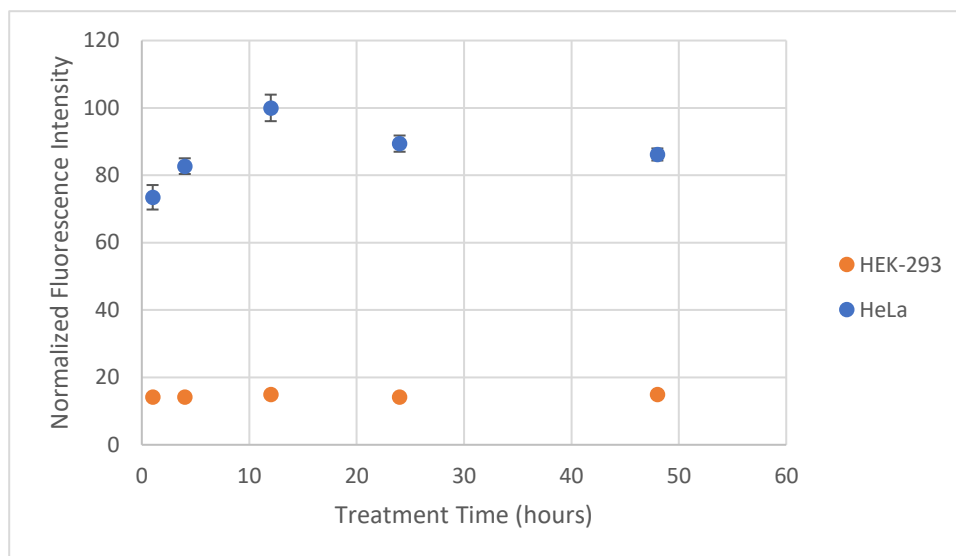
to their potential degradation by the cells into smaller consumable glucose-based structures. At the same time and concentration conditions, HA-Ferrocene conjugates (without the quantum dot delivery vehicle), (Figure 33b) show no selectivity indicating that GQD delivery does not only allow for tracking but may also aids the ROS generation in cancer cells via the electron-rich GQD platform and/or enhanced internalization in targeted cancer cells. According to the T-test with 95% confidence, the Fc-GQD-HA formulation produces statistically significant effect in cancer versus non-cancer cells, while this difference for HA-Fc introduced to the same cells was not statistically significant. This indicates that GQDs help enable the specificity of the treatment.

The observed cancer-selective response can be attributed both to targeting and to redox effect of Fc therapeutic. In order to assess the ROS generation<sup>204</sup> contribution to the enhanced anticancer efficacy we evaluate this capability of the Fc-GQD-HA hybrid over the drug alone via the dichloro-dihydro-fluorescein diacetate (DCFH-DA) assay. In this evaluation of the direct expected therapeutic effect, the Fc-GQD-HA formulation shows nearly a 3-fold increase in ROS at non-toxic to the non-cancer cells 1 mg/mL concentrations as compared to the same amounts of Fc-COOH (derived from the atomic percentage of the iron in the Fc-GQD-HA formulation given by the EDX) (Figure 34). This increase in the ROS contributes to the cytotoxic response observed *in vitro*, and, therefore, shows the Fc-GQD-HA formulation to be a more effective than its therapeutic constituents. It also resolves the drawbacks of Fc-based therapeutics<sup>205-207</sup> that do not offer high cancer selectivity being thus restricted by the non-specific toxicity. Additionally, as mentioned above GQDs having an electron-rich platform may positively contribute to the therapeutic redox effect of the formulation<sup>208</sup>.



*Figure 34. DCFH-DA assay of Fc-GQD-HA formulation (grey) as compared to ferrocene (orange) and N-GQDs (blue) in HeLa cells.*

To analyze the impact of targeting, Fc-GQD-HA formulation was introduced into both HEK-293 and HeLa cell lines for treatment times ranging from 1 hour to 48 hours (Figure 35).



*Figure 35. Cell internalization/excretion timeline assessed through the normalized intracellular Fc-GQD-HA emission intensity per unit area in HeLa (blue) and HEK-293 (orange) cells at different time points. Error bars for some points are within their size.*

Here, it is clear that the fluorescence intensity is relatively consistent and extremely low at all time points in non-cancer HEK-293 cells. The peak in fluorescence intensity, and therefore cellular internalization, occurs at 12 hours in HeLa cells, which maintains the trends observed in both independent N-GQDs as well as imaging observations of the Fc-GQD-HA treatment formulation. This specifically highlights how targeting with HA provides advantageous accumulation in cancer cells and that the treatment formulation is successful in targeting.

### **Summary**

Fc-GQD-HA treatment formulation, which combines imaging, targeting and treatment modalities, facilitates an enhancement to the redox treatment efficacy as compared to Fc therapeutic alone. MTT cytotoxicity analysis of the treatment formulation in both cancer versus

non-cancer cell types show a higher cytotoxic effect within cancer cells. The addition of the N-GQD platform to the treatment formulation also appears to positively impact the treatment efficacy potentially through improved delivery. Finally, the use of HA as the targeting agent increases the accumulation of the treatment formulation within cancerous HeLa cells, while minimizing the accumulation in non-cancerous HEK-293 cells. This suggests the improvement of the targeting and treatment capabilities as compared to the Fc treatment agent as was predicted for this targeted GQD-delivered therapeutic formulation.



## Chapter 10 Conclusions

In this work we have tested a novel nanomaterial, glucose-based graphene quantum dots, as a multifunctional platform for imaging, sensing and intracellular transport. Doped GQDs provide unique capabilities advantageous to a number of their counterparts including multicolor visible/near-IR fluorescence imaging, efficient internalization, and cancer detection. They are synthesized via 1-step scalable hydrothermal route and show high biocompatibility, small 3-5 nm sizes suitable for cell internalization, and apparent biodegradability after 36h in cell culture. Toxicity analyses indicate that high concentrations of up to 1 mg/mL of N-GQDs and NS-GQDs are essentially non-toxic to the cells, while BN-GQDs offer some cytotoxic response and should be restricted to lower concentrations of ~0.1 mg/mL. GQDs internalize with maximum intracellular fluorescence occurring at 12 hours and further potential excretion and/or degradation post 24 hours which lowers the risk of accumulation-derived toxicity. Additionally, all N-GQDs, NS-GQDs and BN-GQDs successfully exhibit in vitro fluorescence imaging in the visible and near-IR leading to versatile multicolor tracking in cells as well as near-IR in vivo imaging capabilities. In order to improve the modality of GQDs as NIR absorbers for photothermal therapy, further incorporation of metal dopants<sup>209</sup> or GQD structure alteration through additional oxidation, breaking the graphitic platform into smaller islands, could be beneficial. pH-dependence of GQD fluorescence spectral signatures allows for the deterministic ratiometric detection of cancerous (HeLa and MCF-7 cell) versus healthy (HEK-293 cell) environments with substantial differences between green/blue emission ratios of 1.6 to 8 in cancer versus healthy cells. This spectral technique, less prone to quenching discrepancies, provides a useful tool for

microscopic pH-sensing. GQDs developed and tested in this work, therefore, facilitate a novel single approach to critical biomedical needs of imaging in cells and tissues, sensing, and therapeutic delivery. Affordable and scalable in production, GQDs provide a fully multifunctional biocompatible and biodegradable platform for intracellular transport, multicolor imaging suggesting both in vitro and in vivo capabilities as well as pH-based detection of cancerous environments. Utilizing this platform, we have effectively synthesized a novel multifunctional Fc-GQD-HA formulation for image-tracked targeted cancer-selective therapeutics. Nitrogen-doped graphene quantum dots offer the most advantageous capabilities as the delivery platform including visible fluorescence imaging, effective cellular internalization, and, essentially, no added toxicity, furthermore, masking the toxic effects of the drug in non-cancer cells. Hyaluronic acid and ferrocene were attached to the N-GQDs covalently in a procedure akin to peptide synthesis. TEM images of the Fc-GQD-HA formulation confirm the crystallinity of the product, while EDX mapping indicates successful incorporation of the Fc ROS-generating unit. The effective internalization of the Fc-GQD-HA formulation in cancer cells traced by its intracellular fluorescence is maximized at 12 hours with further potential excretion. The intracellular delivery of the therapeutic imaged via confocal microscopy mapping GQD accumulation throughout the cell via their intrinsic fluorescence shows mainly accumulation in the cytoplasm. The substantially increased fluorescence from HA-targeted HeLa cancer cells over the non-targeted HEK 293 cells verifies the successful targeting of the CD44 receptors by the HA addend of the formulation. The enhanced efficacy of the Fc-GQD-HA formulation is assessed via 3 methods: MTT cytotoxicity assay, time-dependent cell viability study (both in non-cancer and cancer cells), and DCFH-DA assay for ROS generation in cancer cells evaluating the direct ROS generation

efficacy of the hybrid over the drug alone. These assays indicate an enhanced therapeutic effect of Fc-GQD-HA formulation in cancer cells with complete cancer selectivity over time together with 3-fold increase in ROS generation over the drug/targeting agent combination. This work aims to address the needs of cancer therapeutics for a multimodal treatment with minimal off-site accumulation and non-specific toxicity verifies that the pre-engineered essential capabilities of the synthesized Fc-GQD-HA formulation enable such potential. This therapeutic formulation is further expected to facilitate image-guided cancer-selective targeted treatment essential for the advancement of cancer nanotherapeutics and help to ultimately enhance the therapeutics and diagnostics of cancer.

### **Questions Answered**

1. Are graphene quantum dots suitable for biomedical applications?

Graphene quantum dots have shown that they can be used for biomedical applications. GQDs are very small (3-5 nm) allowing for effective cellular internalization and are non-toxic at high concentrations of over 1 mg/mL. Additionally, GQDs show degradation in cell culture after 36h which is beneficial as they are not expected to accumulate in the body for a long time constantly adding to the toxicity profile. This complements the biocompatibility of GQDs suggesting that they can be effectively used for biomedical applications. GQDs can be also scalably produced via green synthetic methods at low cost, which is uncommon for modern drug delivery and imaging agents.

2. Can these nanomaterials be used for imaging and delivery?

Graphene quantum dots can be imaged in both visible and near-IR, with emission well above autofluorescence levels at non-toxic concentrations. *In vitro* imaging studies

show that the doped nanomaterials are successfully internalized into cells with peak treatment times of 12 hours, with successive potential excretion. Lastly, N-GQDs and NS-GQDs appeared to localize primarily with the lysosomes and some in the nucleus as assessed during the colocalization study. This suggests potential cellular entry through endocytosis. As a result, we infer that GQDs can be used for image-guided delivery with tracking in the visible and in the near-IR, suggesting their further potential for low depth *in vivo* or *ex vivo* imaging.

3. Do they offer sensing capabilities?

The spectra for NS-GQDs and N-GQDs suggest that they can be used to sense a difference in pH between acidic cancerous and regular healthy environments. BN-GQDs do not show the same result, and therefore cannot be used as a sensing agent. When introduced to cancer versus healthy cell cultures, NS-GQDs and N-GQDs show a significant difference in their green to blue emission ratios associated with the acidity of the environment. This way they allow to distinguish between acidic and regular environments in cancer and healthy extracellular regions. Therefore, it is concluded that GQDs in general do offer sensing capabilities for biomedical applications.

4. Can these nanomaterials be used to create a targeted cancer treatment formulation?

As the structure of the N-GQDs is generally maintained during the synthesis process of the targeted treatment formulation, they can be successfully used as the platform for such formulation. A targeting moiety (hyaluronic acid) and a redox treatment agent (ferrocene) are attached to the N-GQDs covalently in a 3-step procedure similar to peptide synthesis. TEM images of the Fc-GQD-HA formulation confirm the crystallinity of the product, while EDX mapping indicates successful incorporation of

the Fc ROS-generating unit. FTIR suggests the successful attachment of the HA via the appearance of the minor amide feature.

5. Is the targeted cancer treatment formulation suitable for biomedical applications?

Nitrogen-doped graphene quantum dots offer advantageous capabilities as the delivery platform including visible fluorescence imaging, effective cellular internalization, and, essentially, no added toxicity, furthermore, masking the toxic effects of the drug in non-cancer cells.

6. Can the targeted cancer treatment formulation be used for imaging and delivery?

The Fc-GQD-HA formulation can be used for imaging and delivery as it is successfully internalized within HeLa cells with intracellular fluorescence maximized at 12 hours, followed by potential excretion. The intracellular delivery of the therapeutic imaged via confocal microscopy mapping GQD accumulation throughout the cell via their intrinsic fluorescence shows mainly accumulation in the cytoplasm.

7. Does the targeted cancer treatment formulation offer sensing capabilities?

Due to the indistinct fluorescence signal difference at varying pH levels, the Fc-GQD-HA treatment formulation does not offer sensing capabilities.

8. How does developing combined imaging/targeting/treatment formulation affect treatment efficacy and targeted accumulation?

The development of the Fc-GQD-HA treatment formulation, which combines the imaging, targeting, and treatment functionalities, improves the treatment efficacy for cancer versus healthy cells and targeted accumulation within cancer cell types over the noncancerous ones.

## Future Works

Our next step is to show that GQDs may not only improve the therapeutic efficacy of affect redox drugs but can also do so for conventional cancer therapeutics. We will non-covalently combine our tested GQD delivery agents with a variety of currently used anticancer drugs, including doxorubicin, gemcitabine, paclitaxel<sup>210, 211</sup> expecting improvement in their efficacy and decrease of their toxic profile, and then test the efficacy of such drug delivery *in vitro*. Upon non-covalent attachment of cancer therapeutics, we will repeat previous steps to assess how different cell types react to the different formulations. We are also currently studying the effect of using combinations of drugs delivered concomitantly by the nanocarriers as those are known to produce significantly improved anticancer effect<sup>212, 213, 214</sup>. Thus, we will assess the efficacy of the aforementioned common therapies when delivered by nanomaterials alone and in combination. Upon the analysis, the most effective formulations will be selected for the use in animal studies.

Prior to further animal work we would need to verify the capability of cancer detection via multiple GQD platform-based treatment formulations via their NIR emission that has a potential to be used *in vivo* due to its higher tissue penetration depth. It is critical to further test the functionality of the treatment formulation *in vivo*, as this is where current nanoparticles often fall short of revolutionizing treatment plans. We will first conduct a toxicity study with our formulations with less expensive BL-6 mice testing the maximum dose to be administered. Further we will treat tumor-bearing mice with subcutaneous tumors. The study will test the following groups for each formulation: non-treatment control, therapeutic alone, nanomaterial vehicle control, and the combinations of these, referred to as the treatment formulation. The efficacy of the formulation will be assessed via measuring tumor volume with a caliper.

Finally, we will test the organ tissues in a biodistribution study with BL-6 mice imaging the presence of the therapeutic formulation and assessing its sensing capabilities and its efficacy in organs including liver, spleen, kidneys and tumor via NIR intrinsic fluorescence of the nanomaterials. On the basis of tumor volume analyses, we will select the most efficacious formulation.

An *in vivo* study provides more information as to how the formulation would hold up as a treatment formulation for human patients. Successful results, analyzed using the methods and assessments listed above, could improve cancer treatment and diagnostics, as well as improving the efficacy of treatment of a number of diseases/conditions with a variety of payloads delivered via an innovative multifunctional nanomaterials-based approach.

## References

1. What Is Cancer? - National Cancer Institute. **2018**.
2. Peer, D.; Karp, J. M.; Hong, S.; Farokhzad, O. C.; Margalit, R.; Langer, R., Nanocarriers as an emerging platform for cancer therapy. *Nature Nanotechnology* **2007**, *2* (12), 751.
3. Haley, B.; barbara.haley@utsouthwestern.edu; Frenkel, E., Nanoparticles for drug delivery in cancer treatment. *Urologic Oncology: Seminars and Original Investigations* **2008**, *26* (1), 57-64.
4. Srikanth, M.; Kessler, J. A., Nanotechnology—novel therapeutics for CNS disorders. *Nat Rev Neurol* *8* (6), 307-18.
5. Kumar, M.; Guo, Y.; Zhang, P., Highly sensitive and selective oligonucleotide sensor for sickle cell disease gene using photon upconverting nanoparticles. *Biosensors and Bioelectronics* **2009**, *24* (5), 1522-1526.
6. Zolnik, B. S.; González-Fernández, Á.; Sadrieh, N.; Dobrovolskaia, M. A., Nanoparticles and the Immune System. *Endocrinology* **2010**, *151* (2), 458-65.
7. Qin, W.; Liu, D. D. J.; Yuan, W. Z.; Hu, Y.; Liu, B.; Tang, B. Z., Biocompatible Nanoparticles with Aggregation-Induced Emission Characteristics as Far-Red/Near-Infrared Fluorescent Bioprobes for In Vitro and In Vivo Imaging Applications - Qin - 2012 - Advanced Functional Materials - Wiley Online Library. **2011**.
8. Singh, R.; Lillard, J. W., Nanoparticle-based targeted drug delivery. *Exp Mol Pathol* **2009**, *86* (3), 215-23.
9. Chung, C.; Kim, Y.-K.; Shin, D.; Ryoo, S.-R.; Hong, B. H.; Min, D.-H., Biomedical Applications of Graphene and Graphene Oxide. **2013**.



10. Jung, H. S.; Kong, W. H.; Sung, D. K.; Lee, M.-Y.; Beack, S. E.; Keum, D. H.; Kim, K. S.; Yun, S. H.; Hahn, S. K., Nanographene Oxide–Hyaluronic Acid Conjugate for Photothermal Ablation Therapy of Skin Cancer. **2014**.
11. Sun, X.; Liu, Z.; Welsher, K.; Robinson, J. T.; Goodwin, A.; Zaric, S.; Dai, H., Nano-Graphene Oxide for Cellular Imaging and Drug Delivery. *Nano Res* **2008**, *1* (3), 203-12.
12. Graphene based materials for biomedical applications - ScienceDirect. **2017**.
13. Eda, G.; Lin, Y. Y.; Mattevi, C.; Yamaguchi, H.; Chen, H. A.; Chen, I. S.; Chen, C. W.; Chhowalla, M., Blue photoluminescence from chemically derived graphene oxide. *Adv Mater* **2010**, *22* (4), 505-9.
14. Feng, L.; Zhang, S.; Liu, Z., Graphene based gene transfection. **2011**.
15. Lu, C.-H.; Zhu, C.-L.; Li, J.; Liu, J.-J.; Chen, X.; Yang, H.-H., Using graphene to protect DNA from cleavage during cellular delivery. **2010**.
16. Shen, H.; Zhang, L.; Liu, M.; Zhang, Z., Biomedical Applications of Graphene. In *Theranostics*, 2012; Vol. 2, pp 283-94.
17. Chang, H.; Tang, L.; Wang, Y.; Jiang, J.; Li, J., Graphene Fluorescence Resonance Energy Transfer Aptasensor for the Thrombin Detection. **2010**.
18. Zhang, C.; Yuan, Y.; Zhang, S.; Wang, Y.; Liu, P. Z., Biosensing Platform Based on Fluorescence Resonance Energy Transfer from Upconverting Nanocrystals to Graphene Oxide - Zhang - 2011 - *Angewandte Chemie International Edition* - Wiley Online Library. **2018**.
19. Yang, K.; Feng, L.; Shi, X.; Liu, Z., Nano-graphene in biomedicine: theranostic applications. **2012**.

20. Martin, N.; Ros, T. D.; Nierengarten, J.-F., Carbon nanostructures in biology and medicine. **2017**.
21. Dong, Y.; Pang, H.; Yang, H. B.; Guo, C.; Shao, J.; Chi, Y.; Li, C. M.; Yu, T., Carbon-Based Dots Co-doped with Nitrogen and Sulfur for High Quantum Yield and Excitation-Independent Emission - Dong - 2013 - Angewandte Chemie International Edition - Wiley Online Library. **2013**.
22. Ivo Mekis; Dmitri V. Talapin; Andreas Kornowski; Markus Haase, a.; Weller\*, H., One-Pot Synthesis of Highly Luminescent CdSe/CdS Core-Shell Nanocrystals via Organometallic and "Greener" Chemical Approaches†. **2003**.
23. Kim, S.; Lim, Y. T.; Soltesz, E. G.; Grand, A. M. D.; Lee, J.; Nakayama, A.; Parker, J. A.; Mihaljevic, T.; Laurence, R. G.; Dor, D. M.; Cohn, L. H.; Bawendi, M. G.; Frangioni, J. V., Near-infrared fluorescent type II quantum dots for sentinel lymph node mapping. *Nature Biotechnology* **2003**, 22 (1), 93.
24. Wang, D.; Chen, J.-F.; Dai, L., Recent Advances in Graphene Quantum Dots for Fluorescence Bioimaging from Cells through Tissues to Animals - Wang - 2015 - Particle & Particle Systems Characterization - Wiley Online Library. **2014**.
25. Wenhao Liu; Mark Howarth, ‡; Andrew B. Greytak; Yi Zheng; Daniel G. Nocera, †; Alice Y. Ting, † and; Mounji G. Bawendi\*, Compact Biocompatible Quantum Dots Functionalized for Cellular Imaging. **2008**.
26. Rosenthal, S. J.; Chang, J. C.; Kovtun, O.; McBride, J. R.; Tomlinson, I. D., Biocompatible Quantum Dots for Biological Applications. *Chemistry & Biology* **2011**, 18 (1), 10-24.

27. Kukowska-Latallo, J. F.; Candido, K. A.; Cao, Z.; Nigavekar, S. S.; Majoros, I. J.; Thomas, T. P.; Balogh, L. P.; Khan, M. K.; Baker, J. R., Nanoparticle Targeting of Anticancer Drug Improves Therapeutic Response in Animal Model of Human Epithelial Cancer. **2005**.
28. Chen, J.; Chen, S.; Zhao, X.; Kuznetsova, L. V.; Wong, S. S.; Ojima, I., Functionalized Single-Walled Carbon Nanotubes as Rationally Designed Vehicles for Tumor-Targeted Drug Delivery. **2008**.
29. Zhang, X. Q.; Lam, R.; Xu, X.; Chow, E. K.; Kim, H. J.; Ho, D.; Lurie, R. H., Multimodal Nanodiamond Drug Delivery Carriers for Selective Targeting, Imaging, and Enhanced Chemotherapeutic Efficacy. *Advanced Materials* **2017**, *23* (41), 4770-4775.
30. Gu, Q.; Xing, J. Z.; Huang, M.; Zhang, X.; Chen, J., Nanoformulation of paclitaxel to enhance cancer therapy. <http://dx.doi.org/10.1177/0885328212446822> **2012**.
31. Bharali, D. J.; Khalil, M.; Gurbuz, M.; Simone, T. M.; Mousa, S. A., Nanoparticles and cancer therapy: A concise review with emphasis on dendrimers. In *Int J Nanomedicine*, 2009; Vol. 4, pp 1-7.
32. *Drug Delivery Nanoparticles Formulation and Characterization*. 2009; Vol. 191.
33. Tzakos, A. G.; Briasoulis, E.; Thalhammer, T.; Jäger, W.; Apostolopoulos, V., Novel Oncology Therapeutics: Targeted Drug Delivery for Cancer. *J Drug Deliv* **2013**, *2013*.
34. Rodzinski, A.; Guduru, R.; Liang, P.; Hadjikhani, A.; Stewart, T.; Stimphil, E.; Runowicz, C.; Cote, R.; Altman, N.; Datar, R.; Khizroev, S., Targeted and controlled anticancer drug delivery and release with magnetoelectric nanoparticles. *Scientific Reports* **2016**, *6*.
35. Liu, Z.; Robinson, J. T.; Sun, X.; Dai, H., PEGylated Nanographene Oxide for Delivery of Water-Insoluble Cancer Drugs. **2008**.

36. Galande, C.; Mohite, A. D.; Naumov, A. V.; Gao, W.; Ci, L.; Ajayan, A.; Gao, H.; Srivastava, A.; Weisman, R. B.; Ajayan, P. M., Quasi-Molecular Fluorescence from Graphene Oxide. In *Sci Rep*, 2011; Vol. 1.
37. Kumawat, M. K.; Thakur, M.; Gurung, R. B.; Srivastava, R., Graphene Quantum Dots for Cell Proliferation, Nucleus Imaging, and Photoluminescent Sensing Applications. *Scientific Reports* **2017**, 7 (1), 15858.
38. Gao, T.; Wang, X.; Yang, L.-Y.; He, H.; Ba, X.-X.; Zhao, J.; Jiang, F.-L.; Liu, Y. Red, Yellow, and Blue Luminescence by Graphene Quantum Dots - PDF Free Download. <https://datapdf.com/red-yellow-and-blue-luminescence-by-graphene-quantum-dots.html>.
39. Weinberg, R. A., *The Biology of Cancer*. W. W. Norton & Company; 2nd edition: 2013.
40. DiGiacomo, V.; Maziarz, M.; Luebbbers, A.; Norris, J. M.; Laksono, P.; Garcia-Marcos, M., Probing the mutational landscape of regulators of G protein signaling proteins in cancer. **2020**.
41. Types of Cancer Treatment - National Cancer Institute. <https://www.cancer.gov/about-cancer/treatment/types>.
42. Treatment for Cancer - National Cancer Institute. <https://www.cancer.gov/about-cancer/treatment>.
43. Immunotherapy for Cancer - National Cancer Institute. <https://www.cancer.gov/about-cancer/treatment/types/immunotherapy>.

44. Limonta, P.; Manea, M., Gonadotropin-releasing hormone receptors as molecular therapeutic targets in prostate cancer: Current options and emerging strategies. *Cancer Treatment Reviews* **2013**, *39* (6), 647-663.
45. Xing Chen, W.-J. T., Jing Bo Shi, Ming Ming Liu, Xin-Hua Liu, Therapeutic strategies for targeting telomerase in cancer - Chen - 2020 - Medicinal Research Reviews - Wiley Online Library. *Medicinal Research Reviews* **2021**.
46. Hosein, A. N.; Brekken, R. A.; Maitra, A., Pancreatic cancer stroma: an update on therapeutic targeting strategies. *Nature Reviews Gastroenterology & Hepatology* **2020**, *17* (8), 487-505.
47. Shen, S.; Xu, X.; Lin, S.; Zhang, Y.; Liu, H.; Zhang, C.; Mo, R., A nanotherapeutic strategy to overcome chemotherapeutic resistance of cancer stem-like cells. *Nature Nanotechnology* **2021**, *16* (1), 104-113.
48. Beg, S.; Alharbi, K. S.; Alruwaili, N. K.; Alotaibi, N. H.; Almalki, W. H.; Alenezi, S. K.; Altowayan, W. M.; Alshammari, M. S.; Rahman, M., Nanotherapeutic systems for delivering cancer vaccines: recent advances. <https://doi.org/10.2217/nnm-2020-0046> **2020**.
49. Gryczynski, Z., Fluorescence and Spectroscopy Course. 2018.
50. Fery-Forgues, S.; Lavabre, D., Are Fluorescence Quantum Yields So Tricky to Measure? A Demonstration Using Familiar Stationery Products. **1999**.
51. Terpetschnig, E.; Jameson, D. M. Fluorescence Lifetime (FLT).
52. Rich, R. M.; Stankowska, D. L.; Maliwal, B. P.; Sørensen, T. J.; Laursen, B. W.; Krishnamoorthy, R. R.; Gryczynski, Z.; Borejdo, J.; Gryczynski, I.; Fudala, R., Elimination of autofluorescence background from fluorescence tissue images by use of time-gated

detection and the AzaDiOxaTriAngulenium (ADOTA) fluorophore. *Analytical and Bioanalytical Chemistry* **2012**, 405 (6), 2065-2075.

53. Ehrat, F.; Bhattacharyya, S.; Schneider, J.; Löf, A.; Wyrwich, R.; Rogach, A. L.; Stolarczyk, J. K.; Urban, A. S.; Feldmann, J., Tracking the Source of Carbon Dot Photoluminescence: Aromatic Domains versus Molecular Fluorophores. **2017**.

54. Wang, S.; Li, B.; Zhang, F., Molecular Fluorophores for Deep-Tissue Bioimaging. **2020**.

55. Hofferber, E.; Meier, J.; Herrera, N.; Stapleton, J.; Ney, K.; Francis, B.; Calkins, C.; Iverson, N., Novel methods to extract and quantify sensors based on single wall carbon nanotube fluorescence from animal tissue and hydrogel-based platforms - IOPscience. **2021**.

56. Hartschuh, A.; Pedrosa, H. N.; Novotny, L.; Krauss, T. D., Simultaneous Fluorescence and Raman Scattering from Single Carbon Nanotubes. **2003**.

57. Esmaeili, Y.; Zarrabi, A.; Mirahmadi-Zare, S. Z.; Bidram, E., Hierarchical multifunctional graphene oxide cancer nanotheranostics agent for synchronous switchable fluorescence imaging and chemical therapy. *Microchimica Acta* **2020**, 187 (10), 1-15.

58. Masteri-Farahani, M.; Mashhadi-Ramezani, S.; Mosleh, N., Molecularly imprinted polymer containing fluorescent graphene quantum dots as a new fluorescent nanosensor for detection of methamphetamine. *Spectrochimica Acta Part A: Molecular and Biomolecular Spectroscopy* **2020**, 229, 118021.

59. Ren, H.; Shen, X.; Dai, J.; Peng, G.; Liang, L.; Shen, J.-W.; Zhang, L., On the mechanism of graphene quantum dot encapsulation by chitosan: A molecular dynamics study. *Journal of Molecular Liquids* **2020**, 320, 113453.

60. Mukherjee, S.; Bytesnikova, Z.; Ashrafi, A. M.; Adam, V.; Richtera, L., Graphene Oxide as a Nanocarrier for Biochemical Molecules: Current Understanding and Trends. *Processes* **2020**, *8* (12), 1636.
61. Cohen-Tanugi, D.; Grossman, J. C., Water Desalination across Nanoporous Graphene. **2012**.
62. Schwierz, F., Graphene transistors. *Nature Nanotechnology* **2010**, *5*, 487-496.
63. Randviir, E. P.; Brownson, D. A. C.; Banks, C. E., A decade of graphene research: production, applications and outlook. *Materials Today* **2014**, *17* (9), 426-432.
64. Kim, Y.-K.; Min, D.-H., Preparation of the Hybrid Film of Poly(allylamine hydrochloride)-Functionalized Graphene Oxide and Gold Nanoparticle and Its Application for Laser-Induced Desorption/Ionization of Small Molecules. **2012**.
65. Yuk, J. M.; Park, J.; Ercius, P.; Kim, K.; Hellebusch, D. J.; Crommie, M. F.; Lee, J. Y.; Zettl, A.; Alivisatos, A. P., High-Resolution EM of Colloidal Nanocrystal Growth Using Graphene Liquid Cells. **2012**.
66. Wu, Z.-S.; Ren, W.; Gao, L.; Zhao, J.; Chen, Z.; Liu, B.; Tang, D.; Yu, B.; Jiang, C.; Cheng, H.-M., Synthesis of Graphene Sheets with High Electrical Conductivity and Good Thermal Stability by Hydrogen Arc Discharge Exfoliation. **2009**.
67. Ghosh, S.; Calizo, I.; Teweldebrhan, D.; Pokatilov, E. P.; Nika, D. L.; Balandin, A. A.; Bao, W.; Miao, F.; Lau, C. N., Extremely high thermal conductivity of graphene: Prospects for thermal management applications in nanoelectronic circuits. **2008**.

68. Rafiee, M. A.; Rafiee, J.; Srivastava, I.; Wang, Z.; Song, H.; Yu, Z.-Z.; Koratkar, N., Fracture and Fatigue in Graphene Nanocomposites - Rafiee - 2010 - Small - Wiley Online Library. **2010**.
69. Nair, R. R.; Blake, P.; Grigorenko, A. N.; Novoselov, K. S.; Booth, T. J.; Stauber, T.; Peres, N. M. R.; Geim, A. K., Fine Structure Constant Defines Visual Transparency of Graphene. **2008**.
70. Min, S. K.; Kim, W. Y.; Cho, Y.; Kim, K. S., Fast DNA sequencing with a graphene-based nanochannel device. *Nature Nanotechnology* **2011**, *6*, 162-165.
71. Wang, Y.; Li, Z.; Wang, J.; Li, J.; Lin, Y., Graphene and graphene oxide: biofunctionalization and applications in biotechnology. *Trends in biotechnology* **2011**, *29* (5), 205-12.
72. Azizighannad, S.; Mitra, S., Stepwise Reduction of Graphene Oxide (GO) and Its Effects on Chemical and Colloidal Properties. *Scientific Reports* **2018**, *8* (1), 1-8.
73. Kozawa, D.; Zhu, X.; Miyauchi, Y.; Mouri, S.; Ichida, M.; Su, H.; Matsuda, K., Excitonic Photoluminescence from Nanodisc States in Graphene Oxides. **2014**.
74. Gokus, T.; Nair, R. R.; Bonetti, A.; Böhmler, M.; Lombardo, A.; Novoselov, K. S.; Geim, A. K.; Ferrari, A. C.; Hartschuh, A., Making Graphene Luminescent by Oxygen Plasma Treatment. **2009**.
75. Cuong, T. V.; Pham, V. H.; Shin, E. W.; Chung, J. S.; Hur, S. H.; Kim, E. J.; Tran, Q. T.; Nguyen, H. H.; Kohl, P. A., Temperature-dependent photoluminescence from chemically and thermally reduced graphene oxide. **2011**.



76. Hasan, M. T.; Senger, B. J.; Ryan, C.; Culp, M.; Gonzalez-Rodriguez, R.; Coffey, J. L.; Naumov, A. V., Optical Band Gap Alteration of Graphene Oxide via Ozone Treatment. *Scientific Reports* **2017**, *7* (1), 6411.
77. Zhang, M.; Bai, L.; Shang, W.; Xie, W.; Ma, H.; Fu, Y.; Fang, D.; Sun, H.; Fan, L.; Han, M.; Liu, C.; Yang, S., Facile synthesis of water-soluble, highly fluorescent graphene quantum dots as a robust biological label for stem cells. **2012**.
78. Liu, Q.; Guo, B.; Rao, Z.; Zhang, B.; Gong, J. R., Strong Two-Photon-Induced Fluorescence from Photostable, Biocompatible Nitrogen-Doped Graphene Quantum Dots for Cellular and Deep-Tissue Imaging. **2013**.
79. Markovic, Z. M.; Ristic, B. Z.; Arsić, K. M.; Klisic, D. G.; Harhaji-Trajkovic, L. M.; Todorovic-Markovic, B. M.; Kepic, D. P.; Kravic-Stevovic, T. K.; Jovanovic, S. P.; Milenkovic, M. M.; Milivojevic, D. D.; Bumbasirevic, V. Z.; Dramicanin, M. D.; Trajkovic, V. S., Graphene quantum dots as autophagy-inducing photodynamic agents. *Biomaterials* **2012**, *33* (29), 7084-7092.
80. Michalet, X.; Pinaud, F. F.; Bentolila, L. A.; Tsay, J. M.; Doose, S.; Li, J. J.; Sundaresan, G.; Wu, A. M.; Gambhir, S. S.; Weiss, S., Quantum Dots for Live Cells, in Vivo Imaging, and Diagnostics. **2005**.
81. Ya-Ping Sun; Bing Zhou; Yi Lin; Wei Wang; K. A. Shiral Fernando; Pankaj Pathak; Mohammed Jaouad Meziani; Barbara A. Harruff; Xin Wang; Haifang Wang; Pengju G. Luo; Hua Yang; Muhammet Erkan Kose; Bailin Chen; L. Monica Veca, a.; Xie, S.-Y., Quantum-Sized Carbon Dots for Bright and Colorful Photoluminescence. **2006**.

82. Hasan, M. T.; Gonzalez-Rodriguez, R.; Ryan, C.; Faerber, N.; Coffey, J. L.; Naumov, A. V., Photo-and Electroluminescence from Nitrogen-Doped and Nitrogen–Sulfur Codoped Graphene Quantum Dots - Hasan - 2018 - *Advanced Functional Materials* - Wiley Online Library. *Advanced Functional Materials* **2018**.
83. Kim, S.; Lim, Y. T.; Soltesz, E. G.; De Grand, A. M.; Lee, J.; Nakayama, A.; Parker, J. A.; Mihaljevic, T.; Laurence, R. G.; Dor, D. M.; Cohn, L. H.; Bawendi, M. G.; Frangioni, J. V., Near-infrared fluorescent type II quantum dots for sentinel lymph node mapping. *Nat Biotechnol* **2004**, *22* (1), 93-7.
84. Qu, D.; Sun, Z.; Zheng, M.; Li, J.; Zhang, Y.; Zhang, G.; Zhao, H.; Liu, X.; Xie, Z., Three Colors Emission from S,N Co-doped Graphene Quantum Dots for Visible Light H<sub>2</sub> Production and Bioimaging - Qu - 2015 - *Advanced Optical Materials* - Wiley Online Library. *Advanced Optical Materials* **2015**, 360-367.
85. Sun, J.; Yang, S.; Wang, Z.; Shen, H.; Xu, T.; Sun, L.; Li, H.; Chen, W.; Jiang, X.; Ding, G.; Kang, Z.; Xie, X.; Jiang, M., Ultra-High Quantum Yield of Graphene Quantum Dots: Aromatic-Nitrogen Doping and Photoluminescence Mechanism. *Particle & Particle Systems Characterization* **2015**, *32* (4), 434-440.
86. Zheng, B.; Chen, Y.; Li, P.; Wang, Z.; Cao, B.; Qi, F.; Liu, J.; Qiu, Z.; Zhang, W., Ultrafast ammonia-driven, microwave-assisted synthesis of nitrogen-doped graphene quantum dots and their optical properties. **2016**, *6* (1), 259-267.
87. Sun, H.; Wu, L.; Gao, N.; Ren, J.; Qu, X., Improvement of Photoluminescence of Graphene Quantum Dots with a Biocompatible Photochemical Reduction Pathway and Its Bioimaging Application. **2013**.

88. Cancer statistics, 2018 - Siegel - 2018 - CA: A Cancer Journal for Clinicians - Wiley Online Library. **2018**.
89. Cancer Statistics - National Cancer Institute. <https://www.cancer.gov/about-cancer/understanding/statistics>.
90. Nurgali, K.; Jagoe, R. T.; Abalo, R., Editorial: Adverse Effects of Cancer Chemotherapy: Anything New to Improve Tolerance and Reduce Sequelae? *Front Pharmacol* **2018**, *9*.
91. Kim, S. M.; Faix, P. H.; Schnitzer, J. E., Overcoming key biological barriers to cancer drug delivery and efficacy. *Journal of Controlled Release* **2017**, *267*, 15-30.
92. Singh, A.; Neupane, Y. R.; Mangla, B.; Shafi, S.; Kohli, K., PEGylated Nanoliposomes Potentiated Oral Combination Therapy for Effective Cancer Treatment. **2020**.
93. Mahalunkar, S.; Kundu, G. C.; Gosavi, S. W., Folated curcumin-gold nanoformulations: A nanotherapeutic strategy for breast cancer therapy. **2020**.
94. Persidis, A., Cancer multidrug resistance. *Nature Biotechnology* **1999**, *17* (1), 94-95.
95. Christopher W. Schultz, R. P., Teena Dhir, Dan A. Dixon, Jonathan R. Brody, Understanding and targeting the disease-related RNA binding protein human antigen R (HuR) - Schultz - 2020 - WIREs RNA - Wiley Online Library. **2021**.
96. Marques, A. C.; Costa, P. J.; Velho, S.; Amaral, M. H., Functionalizing nanoparticles with cancer-targeting antibodies: A comparison of strategies. *Journal of Controlled Release* **2020**, *320*, 180-200.
97. Vasir, J. K.; Labhasetwar, V., Targeted Drug Delivery in Cancer Therapy:. <http://dx.doi.org/10.1177/153303460500400405> **2016**.

98. Jie Cao, R. G., Min Zhang, Junfei Xia, Shangcong Han, Wei Lu, Yan Liang; Zhang, T.; Sun, Y., A triple modality BSA-coated dendritic nanoplatfom for NIR imaging, enhanced tumor penetration and anticancer therapy. **2018**.
99. Chow, E. K.-H.; Gu, M.; Xu, J., Carbon nanomaterials: fundamental concepts, biological interactions, and clinical applications. *Nanoparticles for Biomedical Applications* **2020**, 223-242.
100. Huang, S.; Jiang, G.; Wu, X.; Zhang, H.; Chen, Z.; Chen, A.; Zhang, J., Scalable synthesis of heterostructure of Fe<sub>2</sub>O<sub>3</sub>-Au nanomaterials for application in biological detection. *Materials Research Express* **2019**.
101. Yuan, Y.; Gu, Z.; Yao, C.; Luo, D.; Yang, D., Nucleic Acid-Based Functional Nanomaterials as Advanced Cancer Therapeutics. *Small* **2019**.
102. Mukherjee, S.; Liang, L.; Veisoh, O., Recent Advancements of Magnetic Nanomaterials in Cancer Therapy. *Pharmaceutics* **2019**, 12 (2), 147.
103. Shuang Liu, X. P., Prof. Huiyu Liu, Two-Dimensional Nanomaterials for Photothermal Therapy - Liu - 2020 - Angewandte Chemie - Wiley Online Library. **2021**.
104. Dreaden, E. C.; Austin, L. A.; Mackey, M. A.; El-Sayed, M. A., Size matters: gold nanoparticles in targeted cancer drug delivery. *Ther Deliv* **2012**, 3 (4), 457-78.
105. Markiewski, M. M.; DeAngelis, R. A.; Benencia, F.; Ricklin-Lichtsteiner, S. K.; Koutoulaki, A.; Gerard, C.; Coukos, G.; Lambris, J. D., Modulation of the anti-tumor immune response by complement. *Nat Immunol* **2008**, 9 (11), 1225-35.

106. Mitchell, L. A.; Lauer, F. T.; Burchiel, S. W.; McDonald, J. D., Mechanisms for how Inhaled Multiwalled Carbon Nanotubes Suppress Systemic Immune Function in Mice. *Nat Nanotechnol* **2009**, *4* (7), 451-6.
107. Ilinskaya, A. N.; Dobrovolskaia, M. A., Immunosuppressive and anti-inflammatory properties of engineered nanomaterials. *British Journal of Pharmacology* **2014**, *171* (17), 3988-4000.
108. Sahoo, N. G.; Bao, H.; Pan, Y.; Pal, M.; Kakran, M.; Cheng, H. K. F.; Li, L.; Tan, L. P., Functionalized carbon nanomaterials as nanocarriers for loading and delivery of a poorly water-soluble anticancer drug: a comparative study. *Chemical Communications* **2011**, *47* (18), 5235-5237.
109. Weissleder, R.; Kelly, K.; Sun, E. Y.; Shtatland, T.; Josephson, L., Cell-specific targeting of nanoparticles by multivalent attachment of small molecules. *Nature Biotechnology* **2005**, *23* (11), 1418-1423.
110. Pinheiro, P. C.; Sousa, C. T.; Araujo, J. P.; Guiomar, A. J.; Trindade, T., Functionalization of nickel nanowires with a fluorophore aiming at new probes for multimodal bioanalysis - ScienceDirect. *Journal of Colloid and Interface Science* **2013**, *410*.
111. Ghosh, K. S.; Sharma, A., Fluorescent Nanomaterials for Cellular Imaging. **2020**.
112. Li, S.-D.; Chen, Y.-C.; Hackett, M. J.; Huang, L., Tumor-targeted Delivery of siRNA by Self-assembled Nanoparticles. *Molecular Therapy* **2008**, *16* (1), 163-169.
113. Cheng, J.; Teply, B. A.; Sherifi, I.; Sung, J.; Luther, G.; Gu, F. X.; Levy-Nissenbaum, E.; Radovic-Moreno, A. F.; Langer, R.; Farokhzad, O. C., Formulation of functionalized PLGA-PEG nanoparticles for in vivo targeted drug delivery. *Biomaterials* **2007**, *28* (5), 869-876.

114. Banerjee, S. S.; Chen, D.-H., Multifunctional pH-sensitive magnetic nanoparticles for simultaneous imaging, sensing and targeted intracellular anticancer drug delivery - IOPscience. *Nanotechnology* **2008**, *19*.
115. Sanchez, V. C.; Jachak, A.; Hurt, R. H.; Kane, A. B., Biological Interactions of Graphene-Family Nanomaterials: An Interdisciplinary Review. **2011**.
116. Biju, V., Chemical modifications and bioconjugate reactions of nanomaterials for sensing, imaging, drug delivery and therapy. **2014**, *43*, 744-764.
117. Liu, W.; Zhu, Y.; Wang, F.; Li, X.; Liu, X.; Pang, J.; Pan, W., Galactosylated chitosan-functionalized mesoporous silica nanoparticles for efficient colon cancer cell-targeted drug delivery. **2018**.
118. Blanco, E.; Shen, H.; Ferrari, M., Principles of nanoparticle design for overcoming biological barriers to drug delivery. *Nature Biotechnology* **2015**, *33* (9), 941.
119. Yuan, X.; Zhang, X.; Sun, L.; Wei, Y.; Wei, X., Cellular Toxicity and Immunological Effects of Carbon-based Nanomaterials. *Particle and Fibre Toxicology* **2019**, *16* (1), 1-27.
120. Gu, Q.; Xing, J. Z.; Huang, M.; Zhang, X.; Chen, J., Nanoformulation of paclitaxel to enhance cancer therapy. *J Biomater Appl* **2013**, *28* (2), 298-307.
121. Biju, V., Chemical modifications and bioconjugate reactions of nanomaterials for sensing, imaging, drug delivery and therapy. *Chemical Society Reviews* **2014**, *43*, 744-764.
122. Liu, W.; Zhu, Y.; Wang, F.; Li, X.; Liu, X.; Pang, J.; Pan, W., Galactosylated chitosan-functionalized mesoporous silica nanoparticles for efficient colon cancer cell-targeted drug delivery. In *R Soc Open Sci*, 2018; Vol. 5.

123. Byrne, J. D.; Betancourt, T.; Brannon-Peppas, L., Active targeting schemes for nanoparticle systems in cancer therapeutics. *Advanced Drug Delivery Reviews* **2008**, *60* (15), 1615-1626.
124. Schrama, D.; Reisfeld, R. A.; Becker, J. C., Antibody targeted drugs as cancer therapeutics. *Nat Rev Drug Discov* **2006**, *5* (2), 147-159.
125. Zhu, M.; Bristol, J. A.; Xie, Y.; Mina, M.; Ji, H.; Forry-Schaudies, S.; Ennist, D. L., Linked Tumor-Selective Virus Replication and Transgene Expression from E3-Containing Oncolytic Adenoviruses. *Journal of Virology* **2005**, *79* (9), 5455-5465.
126. Khazi-Syed, A.; Hasan, M. T.; Campbell, E.; Gonzalez-Rodriguez, R.; Naumov, A. V., Single-Walled Carbon Nanotube-Assisted Antibiotic Delivery and Imaging in *S. epidermidis* Strains Addressing Antibiotic Resistance. *Nanomaterials* **2019**, *9* (12), 1685.
127. Yoosefian, M.; Sabaei, S.; Etminan, N., Encapsulation efficiency of single-walled carbon nanotube for Ifosfamide anti-cancer drug - ScienceDirect. *Computers in Biology and Medicine* **2019**, *114*.
128. Raphey, V. R.; Henna, T. K.; Nivitha, K. P.; Mufeedha, P.; Sabu, C.; Pramod, K., Advanced biomedical applications of carbon nanotube. *Materials Science and Engineering: C* **2019**, *100*, 616-630.
129. Rao, H.; Zhang, Z.; Ge, H.; Liu, X.; Zou, P.; Wang, X.; Wang, Y., Enhanced amperometric sensing using a NiCo<sub>2</sub>O<sub>4</sub>/nitrogen-doped reduced graphene oxide/ionic liquid ternary composite for enzyme-free detection of glucose. *New Journal of Chemistry* **2017**, *41* (9).

130. Qian, R.; Maiti, D.; Zhong, J.; Xiong, S.; Zhou, H.; Zhu, R.; Wan, J.; Yang, K., Multifunctional nano-graphene based nanocomposites for multimodal imaging guided combined radioisotope therapy and chemotherapy. *Carbon* **2019**, *149*, 55-62.
131. Mohajeri, M.; Behnam, B.; Sahebkar, A., Biomedical applications of carbon nanomaterials: Drug and gene delivery potentials. *Journal of Cellular Physiology* **2018**, *234* (1), 298-319.
132. Zhang, X.-Q.; Lam, R.; Xu, X.; Chow, E. K.; Kim, H.-J.; Ho, D., Multimodal Nanodiamond Drug Delivery Carriers for Selective Targeting, Imaging, and Enhanced Chemotherapeutic Efficacy - Zhang - 2011 - *Advanced Materials* - Wiley Online Library. **2011**.
133. Ren, J.; Shen, S.; Wang, D.; Xi, Z.; Guo, L.; Pang, Z.; Qian, Y.; Sun, X.; Jiang, X., The targeted delivery of anticancer drugs to brain glioma by PEGylated oxidized multi-walled carbon nanotubes modified with angiopep-2. **2012**.
134. Zhou, M.; Zhai, Y.; Dong, S., Electrochemical Sensing and Biosensing Platform Based on Chemically Reduced Graphene Oxide. **2009**.
135. Liu, Y.; Dong, X.; Chen, P., Biological and chemical sensors based on graphene materials. **2011**.
136. Karlsson, H. L.; Cronholm, P.; Gustafsson, J.; Möller, L., Copper Oxide Nanoparticles Are Highly Toxic: A Comparison between Metal Oxide Nanoparticles and Carbon Nanotubes. **2008**.



137. Zhu, Y.; Murali, S.; Cai, W.; Li, X.; Suk, J. W.; Potts, J. R.; Ruoff, R. S., Graphene and Graphene Oxide: Synthesis, Properties, and Applications - Zhu - 2010 - Advanced Materials - Wiley Online Library. **2010**.
138. Allen, M. J.; Tung, V. C.; Kaner, R. B., Honeycomb Carbon: A Review of Graphene. **2009**.
139. Si, Y.; Samulski, E. T., Synthesis of Water Soluble Graphene. **2008**.
140. Peng, C.; Hu, W.; Zhou, Y.; Fan, C.; Huang, Q., Intracellular Imaging with a Graphene-Based Fluorescent Probe - Peng - 2010 - Small - Wiley Online Library. **2010**.
141. Campbell, E.; Hasan, M. T.; Pho, C.; Callaghan, K.; Akkaraju, G. R.; Naumov, A. V., Graphene Oxide as a Multifunctional Platform for Intracellular Delivery, Imaging, and Cancer Sensing. *Scientific Reports* **2019**, 9 (1), 416.
142. Qu, Y.; He, F.; Yu, C.; Liang, Z.; Liang, D.; Ma, L.; Zhang, Q.; Lv, J.; Wu, J., Advances on graphene-based nanomaterials for biomedical applications. **2018**.
143. Shareena, T. P. D.; McShan, D.; Dasmahapatra, A. K.; Tchounwou, P. B., A Review on Graphene-Based Nanomaterials in Biomedical Applications and Risks in Environment and Health | SpringerLink. **2019**.
144. Vaishali Bagalkot; Liangfang Zhang; Etgar Levy-Nissenbaum; Sangyong Jon; Philip W. Kantoff; Robert Langer, a.; Farokhzad, O. C., Quantum Dot–Aptamer Conjugates for Synchronous Cancer Imaging, Therapy, and Sensing of Drug Delivery Based on Bi-Fluorescence Resonance Energy Transfer. **2007**.
145. Kim, D.; Jeong, Y. Y.; Jon, S., A Drug-Loaded Aptamer–Gold Nanoparticle Bioconjugate for Combined CT Imaging and Therapy of Prostate Cancer. **2010**.

146. Jang, J.; Ha, J.; Cho, J., Fabrication of Water-Dispersible Polyaniline-Poly(4-styrenesulfonate) Nanoparticles For Inkjet-Printed Chemical-Sensor Applications - Jang - 2007 - *Advanced Materials* - Wiley Online Library. *Advanced Materials* **2007**, 1772-1775.
147. Jokerst, J. V.; Lobovkina, T.; Zare, R. N.; Gambhir, S. S., Nanoparticle PEGylation for imaging and therapy. *Nanomedicine (Lond)* **2011**, 6 (4), 715-28.
148. Bae, Y. H.; Park, K., Targeted drug delivery to tumors: Myths, reality and possibility. *J Control Release* **2011**, 153 (3), 198-205.
149. Karchemski, F.; Zucker, D.; Barenholz, Y.; Regev, O., Carbon nanotubes-liposomes conjugate as a platform for drug delivery into cells. *Journal of Controlled Release* **2012**, 160 (2), 339-345.
150. Munoz, R.; Singh, D. P.; Kumar, R.; Matsuda, A., *Graphene Oxide for Drug Delivery and Cancer Therapy*. 2019; p 552.
151. Prabakaran, S.; Jeyaraj, M.; Nagaraj, A.; Sadasivuni, K. K.; Rajan, M., Polymethyl methacrylate–ovalbumin @ graphene oxide drug carrier system for high anti-proliferative cancer drug delivery | SpringerLink. *Applied Nanoscience* **2019**.
152. Suresh, R.; Mangalaraja, R. V.; Mansilla, H. D.; Santander, P.; Yáñez, J., Reduced Graphene Oxide-Based Photocatalysis. In *Green Photocatalysts*, Springer, Cham: 2019.
153. Gonzalez-Rodriguez, R.; Granitzer, P.; Rumpf, K.; Coffey, J. L., New MRI contrast agents based on silicon nanotubes loaded with superparamagnetic iron oxide nanoparticles. **2018**.

154. Galande, C.; Mohite, A. D.; Naumov, A. V.; Gao, W.; Ci, L.; Ajayan, A.; Gao, H.; Srivastava, A.; Weisman, R. B.; Ajayan, P. M., Quasi-Molecular Fluorescence from Graphene Oxide. *Scientific Reports* **2011**, *1*, 85.
155. Frontiers | Lactate Contribution to the Tumor Microenvironment: Mechanisms, Effects on Immune Cells and Therapeutic Relevance | Immunology. **2016**.
156. Fan, T.; Zeng, W.; Tang, W.; Yuan, C.; Tong, S.; Cai, K.; Liu, Y.; Huang, W.; Min, Y.; Epstein, A. J., Controllable size-selective method to prepare graphene quantum dots from graphene oxide | SpringerLink. *Nanoscale Research Letters* **2015**.
157. Liu, Q.; Guo, B.; Rao, Z.; Zhang, B.; Gong, J. R., Strong Two-Photon-Induced Fluorescence from Photostable, Biocompatible Nitrogen-Doped Graphene Quantum Dots for Cellular and Deep-Tissue Imaging. *Nano Letters* **2013**, *13* (6), 2436-2441.
158. Sun, Y.; Wang, S.; Li, C.; Luo, P.; Tao, L.; Wei, Y.; Shi, G., Large scale preparation of graphene quantum dots from graphite with tunable fluorescence properties. *Physical Chemistry Chemical Physics* **2013**, *15* (24), 9907-9913.
159. Campbell, E.; Hasan, M. T.; Gonzalez Rodriguez, R.; Akkaraju, G. R.; Naumov, A. V., Doped Graphene Quantum Dots for Intracellular Multicolor Imaging and Cancer Detection. *ACS Biomaterials Science & Engineering* **2019**, *5* (9), 4671-4682.
160. Yan, C.; Hu, X.; Guan, P.; Hou, T.; Chen, P.; Wan, D.; Zhang, X.; Wang, J.; Wang, C., Highly biocompatible graphene quantum dots: green synthesis, toxicity comparison and fluorescence imaging. *Journal of Materials Science* **2019**, *55* (3), 1198-1215.
161. Wang, S.; Cole, I. S.; Li, Q., The toxicity of graphene quantum dots. *RSC Advances* **2016**, *6* (92), 89867-89878.

162. Zhu, C.; Yang, S.; Wang, G.; Mo, R.; He, P.; Sun, J.; Di, Z.; Kang, Z.; Yuan, N.; Ding, J.; Ding, G.; Xie, X., A new mild, clean and highly efficient method for the preparation of graphene quantum dots without by-products. *Journal of Materials Chemistry B* **2015**, *3* (34), 6871-6876.
163. Zheng, B.; Chen, Y.; Li, P.; Wang, Z.; Cao, B.; Qi, F.; Liu, J.; Qiu, Z.; Zhang, W., Ultrafast ammonia-driven, microwave-assisted synthesis of nitrogen-doped graphene quantum dots and their optical properties. *Nanophotonics* **2016**, *6* (1), 259-267.
164. Hegedűs, C.; Kovács, K.; Polgár, Z.; Regdon, Z.; Szabó, É.; Robaszkiewicz, A.; Forman, H. J.; Martner, A.; Virág, L., Redox control of cancer cell destruction. *Redox Biology* **2018**, *16*, 59-74.
165. Zhou, D.; Shao, L.; Spitz, D. R., Reactive Oxygen Species in Normal and Tumor Stem Cells. *Adv Cancer Res* **2014**, *122*, 1-67.
166. Poillet-Perez, L.; Despouy, G.; Delage-Mourroux, R.; Boyer-Guittaut, M., Interplay between ROS and autophagy in cancer cells, from tumor initiation to cancer therapy. *Redox Biology* **2015**, *4*, 184-192.
167. Płażuk, D.; Zakrzewski, J.; Salmain, M.; Błaż, A.; Rychlik, B.; Strzelczyk, P.; Bujacz, A.; Bujacz, G., Ferrocene–Biotin Conjugates Targeting Cancer Cells: Synthesis, Interaction with Avidin, Cytotoxic Properties and the Crystal Structure of the Complex of Avidin with a Biotin–Linker–Ferrocene Conjugate. *Organometallics* **2013**, *32* (20), 5774-5783.
168. Lincoln, K. M.; Gonzalez, P.; Richardson, T. E.; Julovich, D. A.; Saunders, R.; Simpkins, J. W.; Green, K. N., A potent antioxidant small molecule aimed at targeting metal-based

- oxidative stress in neurodegenerative disorders. *Chemical communications (Cambridge, England)* **2013**, 49 (26), 2712-2714.
169. Misra, S.; Hascall, V. C.; Markwald, R. R.; Ghatak, S., Interactions between Hyaluronan and Its Receptors (CD44, RHAMM) Regulate the Activities of Inflammation and Cancer. *Front Immunol* **2015**, 6.
170. Basakran, N. S., CD44 as a potential diagnostic tumor marker. *Saudi medical journal* **2015**, 36 (3), 273-279.
171. Chen, C.; Zhao, S.; Karnad, A.; Freeman, J. W., The biology and role of CD44 in cancer progression: therapeutic implications. In *J Hematol Oncol*, 2018; Vol. 11.
172. Riss, T. L.; Moravec, R. A.; Niles, A. L.; Duellman, S.; Benink, H. A.; Worzella, T. J.; Minor, L., Cell Viability Assays. **2016**, 1-25.
173. Hasan, M. T.; Gonzalez-Rodriguez, R.; Ryan, C.; Faerber, N.; Coffey, J. L.; Naumov, A. V., Photo-and Electroluminescence from Nitrogen-Doped and Nitrogen–Sulfur Codoped Graphene Quantum Dots. *Advanced Functional Materials* **2018**, 28 (42), 1804337.
174. DCFDA / H2DCFDA - Cellular Reactive Oxygen Species Detection Assay Kit.  
<https://www.abcam.com/dcfda--h2dcfda-cellular-ros-assay-kit-ab113851.html>.
175. Hasan, M. T.; Gonzalez-Rodriguez, R.; Ryan, C.; Pota, K.; Green, K.; Coffey, J. L.; Naumov, A. V., Nitrogen-doped graphene quantum dots: Optical properties modification and photovoltaic applications | SpringerLink. **2019**.
176. Smith, A. M.; Mancini, M. C.; Nie, S., Second window for in vivo imaging. *Nat Nanotechnol* **2009**, 4 (11), 710-1.

177. Faraji, A. H.; Wipf, P., Nanoparticles in cellular drug delivery. **2009**, *17* (8), 2950-2962.
178. Lin, K. L. T. A. N. G. R. W. W., Nanoscale Metal–Organic Frameworks for Therapeutic, Imaging, and Sensing Applications - Lu - 2018 - Advanced Materials - Wiley Online Library. **2018**.
179. Altinoğlu, E. I.; Russin, T. J.; Kaiser, J. M.; Barth, B. M.; Eklund, P. C.; Kester, M.; Adair, J. H., Near-Infrared Emitting Fluorophore-Doped Calcium Phosphate Nanoparticles for In Vivo Imaging of Human Breast Cancer. **2008**.
180. Zane, A.; McCracken, C.; Knight, D. A.; Young, T.; Lutton, A. D.; Olesik, J. W.; Waldman, W. J.; Dutta, P. K., Uptake of bright fluorophore core-silica shell nanoparticles by biological systems. *Int J Nanomedicine* **2015**, *10*, 1547-67.
181. Albini, A.; Pagani, A.; Pulze, L.; Bruno, A.; Principi, E.; Congiu, T.; Gini, E.; Grimaldi, A.; Bassani, B.; De Flora, S.; de Eguileor, M.; Noonan, D. M., Environmental impact of multi-wall carbon nanotubes in a novel model of exposure: systemic distribution, macrophage accumulation, and amyloid deposition. *Int J Nanomedicine* **2015**, *10*, 6133-45.
182. Dan Qu, M. Z., Peng Du, Yue Zhou, Ligong Zhang, Di Li, Huaqiao Tan, Zhao Zhao , Zhigang Xie and Zaicheng Sun, Highly luminescent S, N co-doped graphene quantum dots with broad visible absorption bands for visible light photocatalysts. **2013**.
183. Shoujun Zhu, J. Z., Chunyan Qiao, Shijia Tang, Yunfeng Li, Wenjing Yuan, Bo Li, Lu Tian, Fang Liu, Rui Hu, Hainan Gao, Haotong Wei, Hao Zhang, Hongchen Sun and Bai Yang, Strongly green-photoluminescent graphene quantum dots for bioimaging applications. **2011**.

184. Swietach, P.; Vaughan-Jones, R. D.; Harris, A. L.; Hulikova, A., The chemistry, physiology and pathology of pH in cancer. *Philos Trans R Soc Lond B Biol Sci* **2014**, *369* (1638).
185. Gerweck, L. E.; Seetharaman, K., Cellular pH Gradient in Tumor versus Normal Tissue: Potential Exploitation for the Treatment of Cancer. **1996**.
186. Romero-Garcia, S.; Moreno-Altamirano, M. M. B.; Prado-Garcia, H.; Sánchez-García, F. J., Lactate Contribution to the Tumor Microenvironment: Mechanisms, Effects on Immune Cells and Therapeutic Relevance. *Front Immunol* **2016**, *7*.
187. Han, J.; Burgess, K., Fluorescent Indicators for Intracellular pH. **2009**.
188. Grabowski, J.; Ke-Cheng, H.; Baker, P. R.; Bornman, C. H., Fluorogenic compound hydrolysis as a measure of toxicity-induced cytoplasmic viscosity and pH changes.
189. Casey, J. R.; Grinstein, S.; Orlowski, J., Sensors and regulators of intracellular pH. *Nature Reviews Molecular Cell Biology* **2009**, *11* (1), 50-61.
190. Damaghi, M.; Wojtkowiak, J. W.; Gillies, R. J., pH sensing and regulation in cancer. *Front Physiol* **2013**, *4*.
191. Jiang, B., Aerobic glycolysis and high level of lactate in cancer metabolism and microenvironment.
192. Gottfried, E.; Kunz-Schughart, L. A.; Ebner, S.; Mueller-Klieser, W.; Hoves, S.; Andreesen, R.; Mackensen, A.; Kreutz, M., Tumor-derived lactic acid modulates dendritic cell activation and antigen expression. *Blood* **2006**, *107*.

193. Abdullah Al, N.; Lee, J.-E.; In, I.; Lee, H.; Lee, K. D.; Jeong, J. H.; Park, S. Y., Target Delivery and Cell Imaging Using Hyaluronic Acid-Functionalized Graphene Quantum Dots. *Molecular Pharmaceutics* **2013**, *10* (10), 3736-3744.
194. Khayrani, A. C.; Mahmud, H.; Oo, A. K. K.; Zahra, M. H.; Oze, M.; Du, J.; Alam, M. J.; Afify, S. M.; Quora, H. A. A.; Shigehiro, T.; Calle, A. S.; Okada, N.; Seno, A.; Fujita, K.; Hamada, H.; Seno, Y.; Mandai, T.; Seno, M., Targeting Ovarian Cancer Cells Overexpressing CD44 with Immunoliposomes Encapsulating Glycosylated Paclitaxel. *International Journal of Molecular Sciences* **2019**, *20* (5), 1042.
195. Scarborough, J. H.; Gonzalez, P.; Rodich, S.; Green, K. N., Synthetic Methodology for Asymmetric Ferrocene Derived Bio-conjugate Systems via Solid Phase Resin-based Methodology. *JoVE (Journal of Visualized Experiments)* **2015**, (97).
196. Acevedo-Moreantes, C. Y.; Melendez, E.; Singh, S. P.; Ramirez-Vick, J. E., Cytotoxicity and Reactive Oxygen Species Generated by Ferrocenium and Ferrocene on MCF7 and MCF10A Cell Lines. *Journal of Cancer Science & Therapy* **2012**, *4* (9), 271-275.
197. Ho, M.-W., Cancer a redox disease. *ACNEM* **2013**, *32*, 12-18.
198. MENCALHA, A.; VICTORINO, V. J.; CECCHINI, R.; PANIS, C., Mapping Oxidative Changes in Breast Cancer: Understanding the Basic to Reach the Clinics. *Anticancer Research* **2014**.
199. Duivenvoorden, W. C. M.; Liu, Y.-n.; Schatte, G.; Kraatz, H.-B., Synthesis of redox-active ferrocene pyrazole conjugates and their cytotoxicity in human mammary adenocarcinoma MCF-7 cells. *Inorganica Chimica Acta* **2005**, *358* (11), 3183-3189.



200. Workentine, M. L.; Harrison, J. J.; Stenroos, P. U.; Ceri, H.; Turner, R. J., Pseudomonas fluorescens' view of the periodic table. *Environmental microbiology* **2008**, *10* (1), 238-50.
201. Harrison, J. J.; Ceri, H.; Turner, R. J., Multimetal resistance and tolerance in microbial biofilms. *Nature reviews. Microbiology* **2007**, *5* (12), 928-38.
202. Reid, E., Testing the Specificity and Cytotoxicity of Biotin-Ferrocene Compounds on Cancer Cells. **2017**.
203. Jiang, H.; Peterson, R. S.; Wang, W.; Bartnik, E.; Knudson, C. B.; Knudson, W., A Requirement for the CD44 Cytoplasmic Domain for Hyaluronan Binding, Pericellular Matrix Assembly, and Receptor-mediated Endocytosis in COS-7 Cells. *Journal of Biological Chemistry* **2002**, 10531-10538.
204. NavaneethaKrishnan, S.; Rosales, J. L.; Lee, K.-Y., ROS-Mediated Cancer Cell Killing through Dietary Phytochemicals. *Oxidative Medicine and Cellular Longevity* **2019**, 2019.
205. Peter, S.; Aderibigbe, B. A., Ferrocene-Based Compounds with Antimalaria/Anticancer Activity. *Molecules* **2019**, *24* (19), 3604.
206. Wang, R.; Chen, H.; Yan, W.; Zheng, M.; Zhang, T.; Zhang, Y., Ferrocene-containing hybrids as potential anticancer agents: Current developments, mechanisms of action and structure-activity relationships. *European Journal of Medicinal Chemistry* **2020**, *190*, 112109.
207. Noyhouzer, T.; L'Homme, C.; Beaulieu, I.; Mazurkiewicz, S.; Kuss, S.; Kraatz, H.-B.; Canesi, S.; Mauzeroll, J., Ferrocene-Modified Phospholipid: An Innovative Precursor for

Redox-Triggered Drug Delivery Vesicles Selective to Cancer Cells. *Langmuir* **2016**, *32* (17), 4169-4178.

208. Yan, X.; Li, B.; Cui, X.; Wei, Q.; Tajima, K.; Li, L.-s., Independent Tuning of the Band Gap and Redox Potential of Graphene Quantum Dots. *The Journal of Physical Chemistry Letters* **2011**, *2* (10), 1119-1124.

209. Li, Y.; Lu, W.; Huang, Q.; Li, C.; Chen, W., Copper sulfide nanoparticles for photothermal ablation of tumor cells. <https://doi.org/10.2217/nnm.10.85> **2010**.

210. Zhang, L.; Xia, J.; Zhao, Q.; Liu, L.; Zhang, Z., Functional Graphene Oxide as a Nanocarrier for Controlled Loading and Targeted Delivery of Mixed Anticancer Drugs - Zhang - 2010 - Small - Wiley Online Library. **2010**.

211. Ihle, N. T.; Williams, R.; Chow, S.; Chew, W.; Berggren, M. I.; Paine-Murrieta, G.; Minion, D. J.; Halter, R. J.; Wipf, P.; Abraham, R.; Kirkpatrick, L.; Powis, G., Molecular pharmacology and antitumor activity of PX-866, a novel inhibitor of phosphoinositide-3-kinase signaling. **2004**.

212. Wiradharma, N.; Tong, Y. W.; Yang, Y.-Y., Self-assembled oligopeptide nanostructures for co-delivery of drug and gene with synergistic therapeutic effect. *Biomaterials* **2009**, *30* (17), 3100-3109.

213. Liu, Y.; Miyoshi, H.; Nakamura, M., Nanomedicine for drug delivery and imaging: A promising avenue for cancer therapy and diagnosis using targeted functional nanoparticles - Liu - 2007 - International Journal of Cancer - Wiley Online Library. **2007**.

214. Sun, D. T.; Zhang, D. Y. S.; Pang, B.; Hyun, D. D. C.; Yang, M.; Xia, P. Y., Engineered Nanoparticles for Drug Delivery in Cancer Therapy - Sun - 2014 - Angewandte Chemie International Edition - Wiley Online Library. **2014**.

## VITA

### PERSONAL BACKGROUND

Elizabeth Campbell  
Fort Worth, Texas

### EDUCATION

Ph.D. Candidate, Texas Christian University, 2021  
Master of Science, Texas Christian University, 2018  
Bachelor of Science, University of Dallas, 2014

### PROFESSIONAL EXPERIENCE

2016-Present Graduate Teaching Assistant, Texas Christian University  
2014-2016 Teacher, Fort Worth ISD

### PUBLICATIONS

1. *Afeefah Khazi-Syed, Md. Tanvir Hasan, E. Campbell, Anton V. Naumov* “Single-Walled Carbon Nanotube-Assisted Antibiotic Delivery and Imaging in *S. Epidermidis* Strains Addressing Antibiotic Resistance” *Nanomaterials*, <https://doi.org/10.3390/nano9121685> (2019).
2. *E. Campbell, Md. Tanvir Hasan, C. Pho, K. Callaghan, G.R. Akkaraju, and A. V. Naumov* “Graphene Oxide as a Multifunctional Platform for Intracellular Delivery, Imaging, and Cancer Sensing” *Scientific Reports*, 9:416, doi:10.1038/s41598-018-36617-4 (2019).
3. *Roberto Gonzalez-Rodriguez, Elizabeth Campbell, Anton Naumov* “Multifunctional Graphene oxide/Iron oxide Nanoparticles for Magnetic Targeted Drug Delivery Dual Magnetic Resonance/Fluorescence Imaging and Cancer Sensing” *PLoS ONE*, <https://doi.org/10.1371/journal.pone.0217072> (2019).
4. *Md. Tanvir Hasan, E. Campbell, V. Lyle, G. R. Akkaraju, L. Kirkpatrick, A. V. Naumov* “Multi-Drug/Gene NASH Therapy Delivery and Selective Hyperspectral Near-IR Imaging Using Chirality-Sorted Single-Walled Carbon Nanotubes.” *Cancers*, doi:10.3390/cancers11081175 (2019).
5. *E. Campbell, Md. Tanvir Hasan, R. Gonzalez-Rodriguez, G.R. Akkaraju, and A. V. Naumov* “Doped Graphene Quantum Dots for Intracellular Multicolor Imaging, and Cancer Detection” *ACS Biomaterials Science and Engineering*, doi:10.1021/acsbomaterials.9b00603 (2019).
6. *Md. Tanvir Hasan, Roberto Gonzalez-Rodriguez, Ching-Wei Lin, Elizabeth Campbell, Satvik Vasireddy, Uyanga Tsedev, Angela M. Belcher, Anton V. Naumov* “Rare-Earth Metal Ions Doped Graphene Quantum Dots for Near-IR In Vitro/In Vivo/Ex Vivo Imaging Applications” *Advanced Optical Materials*, <https://doi.org/10.1002/adom.202000897> (2020).
7. *Anne E. D’Achille, Roberto Gonzalez-Rodriguez, Elizabeth Campbell, Bong Han Lee, Jeffery L. Coffey, and Anton V. Naumov* “Rare-Earth-Doped Cerium Oxide Nanocubes for Biomedical Near-Infrared and Magnetic Resonance Imaging” *ACS Biomaterials Science and Engineering*, <https://doi.org/10.1021/acsbomaterials.0c01193> (2020)
8. *Elizabeth Campbell, Tanvir Hasan, Roberto Gonzalez-Rodriguez, Tate Truly, Bong Han Lee, Kayla N. Green, Giridhar Akkaraju, Anton V. Naumov* “Graphene quantum dot formulation for cancer imaging and redox-based drug delivery” *Nanomedicine: Nanotechnology, Biology and Medicine*, <https://doi.org/10.1016/j.nano.2021.102408> (2021).

## ABSTRACT

### Graphene Quantum Dots as Imaging, Sensing, and Targeted Delivery Platform for Cancer Therapeutics

By: Elizabeth Campbell, Ph.D., 2021  
Department of Physics & Astronomy  
Texas Christian University

Advisor: Anton V. Naumov, Assistant Professor of Physics

The objective of this research is to develop, optimize and test graphene quantum dots (GQDs) as imaging, sensing, and drug delivery platform. GQDs possess properties beneficial for molecular drug delivery/imaging/sensing applications. GQDs exhibit pH-dependent fluorescence in the visible, is water soluble and has a substantial platform for functionalization with multiple therapeutics. GQDs are beneficial for their biocompatibility, small size ( $< 5$  nm), ease in synthesis, and high yield fluorescence in the visible and near-infrared. We explore the imaging and sensing capabilities of GQDs *in vitro* via their intrinsic fluorescence, pH-dependence of their emission for detection of acidic cancerous environments, and capabilities for *in vitro* transport of therapeutics. As a result, we expect GQDs to be successful multifunctional agents for imaging, sensing, and drug delivery advancing scientific approach to cancer treatment and therapeutics. This work then develops a new multifunctional biocompatible anticancer nanoformulation to provide targeted image-guided cancer-selective therapeutics. It consists of three active covalently bound components: (1) biocompatible nitrogen-doped graphene quantum dots (GQDs) as a multifunctional delivery and imaging platform, (2) hyaluronic acid (HA) unit targeted to the CD44 receptors on a variety of cancer cells, and (3) oxidative stress-based cancer-selective ferrocene (Fc) therapeutic. The

biocompatible GQD platform synthesized from glucosamine exhibits high-yield intrinsic fluorescence. It is utilized for tracking Fc-GQD-HA formulation *in vitro* indicating internalization enhancement in HeLa cells targeted by the HA over non-cancer HEK-293 cells not overexpressing CD44 receptor. Fc-GQD-HA, non-toxic at 1 mg/mL to HEK-293 cells, induces cytotoxic response in HeLa enhanced over time, while therapeutic ROS generation by Fc-GQD-HA is ~3 times greater than that of Fc alone. This outlines the targeted delivery, imaging, and cancer-specific treatment capabilities of the new Fc-GQD-HA formulation enabling desired cancer-focused nanotherapeutic approach.